UNIVERSITY OF SOUTHAMPTON

Faculty of Natural and Environmental Sciences

Quinones as Redox Mediators for the Lithium-Oxygen Battery

by

William Andrew Richardson

Thesis for the degree of Doctor of Philosophy

March 2017

UNIVERSITY OF SOUTHAMPTON

ABSTRACT

FACULTY OF NATURAL AND ENVIRONMENTAL SCIENCES

Chemistry

Doctor of Philosophy

Quinones as Redox Mediators for the Lithium-Oxygen Battery

by William Andrew Richardson

Increasing demand for lighter and more powerful batteries has driven research beyond lithium-ion batteries. One system that has received significant attention is lithium-oxygen. This system exploits the reduction of oxygen to lithium peroxide, to provide a theoretical specific energy of 3500 Wh kg^{-1}. One of the major problems facing the lithium-oxygen battery is the passivation of the air electrode caused by insoluble lithium oxides and lithium carbonate formed from unstable electrolytes. These products are not fully oxidized during the charge step and accumulate within the electrode, causing the capacity to fade with each cycle.

This work focuses on the use of quinones as solution based catalysts in non-aqueous electrolytes to facilitate the electron transfer of both the oxygen reduction reaction (ORR) and the oxygen evolution reaction (OER). The required overpotential for the ORR is shown to decrease by 400 mV and the discharge capacity increase by 100% by incorporating quinones into the electrolyte. Analysis of the carbon electrode by X-ray diffraction confirms lithium peroxide as the discharge product. Furthermore the evolution and consumption of oxygen during cycling has been demonstrated to require only two electrons per mole of oxygen using on-line mass spectrometry indicating that the dominant reaction is the formation of lithium peroxide.

Table of Contents

Academic Thesis: Declaration of Authorship

I, William Andrew Richardson

declare that this thesis and the work presented in it are my own and has been generated by me as the result of my own original research.

Quinones as Redox Mediators for the Lithium-Oxygen Battery

I confirm that:

1. This work was done wholly or mainly while in candidature for a research degree at this University;

2. Where any part of this thesis has previously been submitted for a degree or any other qualification at this University or any other institution, this has been clearly stated;

3. Where I have consulted the published work of others, this is always clearly attributed;

4. Where I have quoted from the work of others, the source is always given. With the exception of such quotations, this thesis is entirely my own work;

5. I have acknowledged all main sources of help;

6. Where the thesis is based on work done by myself jointly with others, I have made clear exactly what was done by others and what I have contributed myself;

7. Either none of this work has been published before submission, or parts of this work have been published as: [please list references below]:

Signed: ……

Date: ……

Acknowledgements

I would like to give special thanks to my supervisor Dr. Nuria Garcia-Araez for her continued support and for her guidance throughout my studies. In addition I would like to thank both Professor John Owen for always being on hand as a wealth of information and new ideas and Professor Andrew Hector for all his help in the early days of my PhD.

A huge thank you must go to the old guard of level 7, Jake, Mike, Jimmy, Andy, Nora, Roy, Tom F, Doug and Jack for all their help in making this thesis possible. While an equally big thanks must go to, James, Tom H, Nina, Dan, Rinaldo, Liam, Vivek and the members of Level 6 for all the Thursday crosswords and drinks on a Friday. I also would like to mention the 5-a-side football and T20 cricket teams for providing some much appreciated midweek competition.

Finally I would offer my deepest thanks to my parents, who have always supported me and continue to provide encouragement in all aspects of my life, and to my brother who I can at last agree with in that it is probably about time I got a job.

Chapter 1: Introduction

1.1 Fundamentals of Batteries

A battery is a device that converts the chemical energy contained in its active materials directly into electrical energy.[1] While the term "battery" is often used, the basic electrochemical unit is referred to as the "cell". A battery consists of one or more of these cells connected together in series or parallel or both to generate the required voltage and capacity. Each cell consists of electrodes separated by an ionically conducting electrolyte shown below in Figure 1.1.1. The anode gives up electrons to the external circuit causing it to be oxidised by the electrochemical reaction. The cathode accepts electrons from the external circuit and is in turn reduced. Finally the electrolyte insulates against the conduction of electrons, forcing them around the external circuit while acting as a good ionic conductor to allow the transfer of charge between the two electrodes.

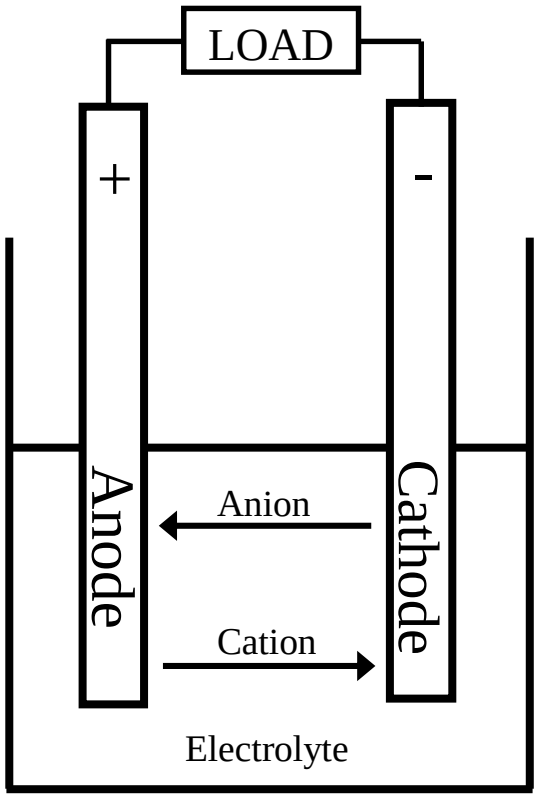

Figure 1.1.1 Schematic of a battery during discharge.

1.2 Lithium-Ion Batteries

Early lithium batteries relied upon using a lithium metal negative electrode, a positive electrode material and a non-aqueous ion conducting electrolyte.[2] An example of these systems is lithium/carbon monofluoride. The discharge reaction is shown below in Equation 1.2.1.

$$nLi + (CF)_n \xrightarrow{\text{discharge}} nLiF + nC$$

Equation 1.2.1

In this system, it was proposed by Whittingham *et al.* that the lithium initially intercalates into the carbon monofluoride lattice and subsequently the lithium fluoride is formed.[3] This reaction occurs outside the electrolyte stability window and is only possible due to the presence of the solid electrolyte interface (SEI). This layer is formed from the reaction of lithium with the electrolyte to form a protective layer guarding against further reaction while enabling lithium ion transport between the electrolyte and the electrode.[4,5]

The use of lithium metal offered significant advantages due to its light weight and high energy density. However, there were safety issues on long term cycling as dendrite formation at the lithium electrode could cause short circuits and battery fires as a result of thermal runaway.[2,6,7] In order to solve this problem a second intercalation material was used for the negative electrode. The first commercially successful example of this was graphite.[2,8] This enabled a maximum of one lithium atom per every six carbon atoms to be stored within the carbon electrode. An example of this reaction is shown below using lithium cobalt oxide as the positive electrode material.

$$0.5LiC_6 + Li_{0.5}CoO_2 \underset{\text{charge}}{\overset{\text{discharge}}{\rightleftharpoons}} LiCoO_2 + 3C$$

Equation 1.2.2

Here the negative carbon electrode acts as a lithium ion store, accepting lithium ions during charging and releasing them during discharge. This effect led to the name 'rocking chair battery', or more generally 'lithium-ion battery'. A schematic of the lithium-ion battery is shown in Figure 1.2.1. Lithium cobalt oxide was first recognised as an intercalating material by Goodenough in 1980.[9] Upon the complete removal of lithium from $LiCoO_2$ the oxygen atoms would rearrange themselves from cubic close packed to a hexagonal structure.[2] For this reason the lithium extraction was limited to 50%. Beyond this phase, changes in the material occur resulting is capacity loss. This combination of lithium cobalt oxide and an intercalating carbon electrode formed the first commercially successful lithium-ion battery introduced by Sony® in 1991.[10] The use of intercalating materials avoided the safety concerns of using lithium metal by preventing dendrite formation. However, as the negative electrodes are now heavier than lithium metal the overall specific energy of the system is lower.

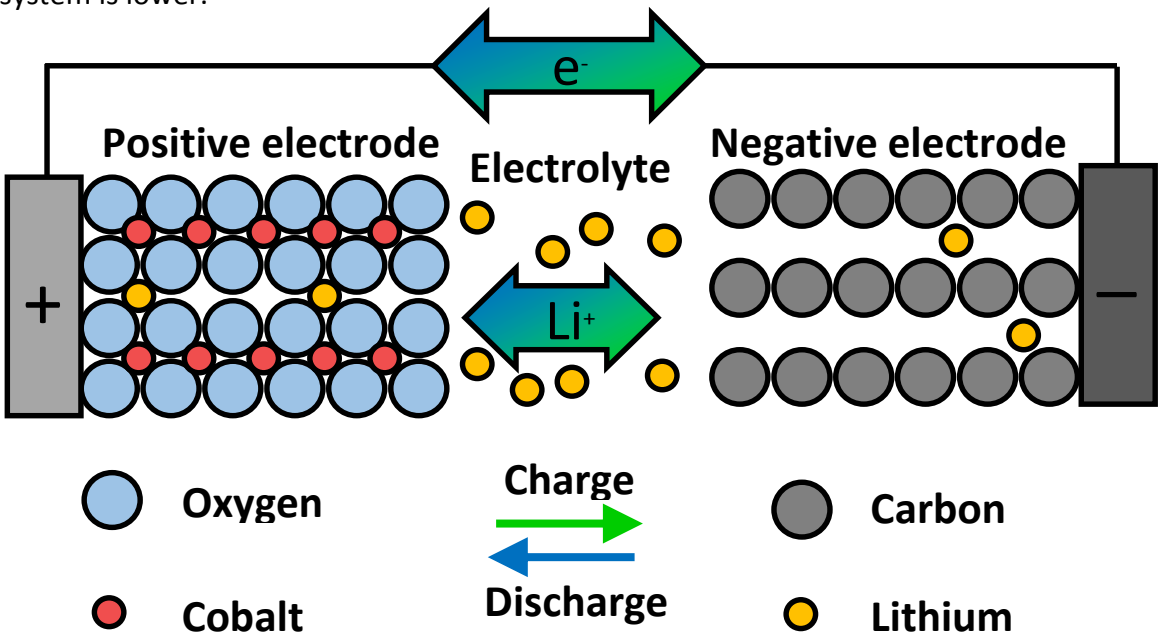

Figure 1.2.1 Schematic of a lithium-ion battery showing how lithium ions move between electrodes as the cell is charged and discharged.

1.3 Beyond Lithium-Ion Batteries

There has been continuous improvement in lithium-ion battery technology as new electrode materials have provided ever increasing energy densities. There is a renewed drive to find improved energy storage technologies thanks in part to the growing market in electric vehicles. New negative electrode materials such as silicon have been shown to achieve capacities of up to 1000 mAh g^{-1}.[11,12] While high voltage cathode materials based on the formula $LiMPO_4$, where M = Mn, Mn and Fe or Co, can offer cell voltages up to 5 V.[13] Figure 1.3.1 below illustrates the potential for development of lithium-ion and metal-air batteries alongside existing systems. Moving back towards the use of lithium metal in combination with an air electrode offers some of the highest theoretical energy densities available. Research into metal-air batteries as a result has been increasingly popular in recent years. Some examples of these are discussed further.

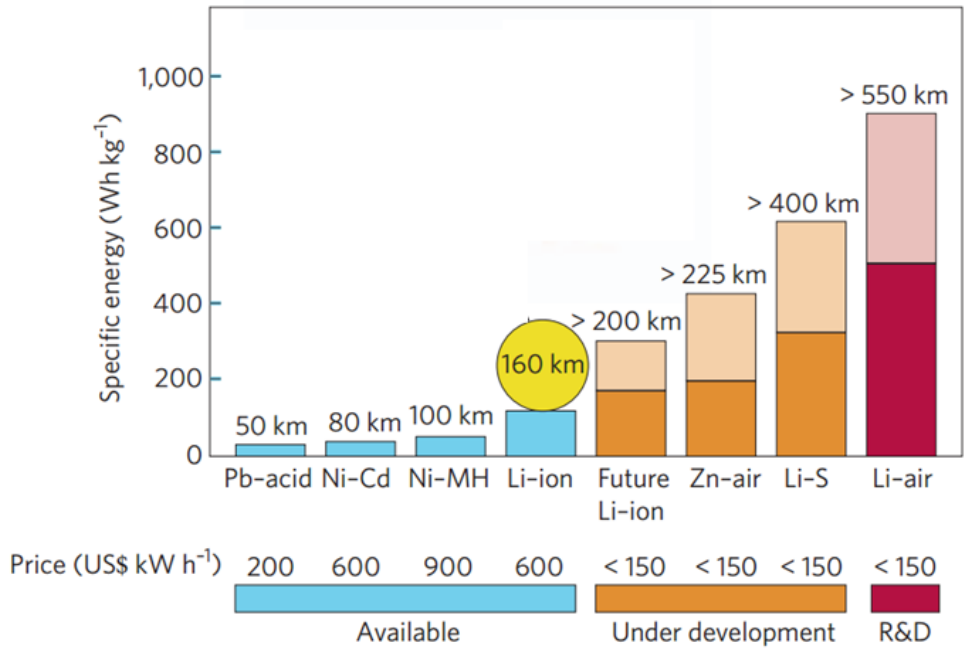

Figure 1.3.1 Theoretical and practical specific energies for rechargeable batteries. Estimated driving distances with cost per unit of electricity are also shown based on a Nissan leaf with 140 Wh kg^{-1} lithium-ion battery and a driving distance of 160 km. Lighter regions indicate the highest achievable specific energy. Reproduced with permission from reference.[14]

1.3.1 Zinc-Air Batteries

The zinc-air battery is a rechargeable battery system comprised of a negative zinc electrode and a positive air electrode using an alkaline electrolyte. Upon battery discharge the oxidation of zinc occurs giving rise to soluble zincate ions ($Zn(OH)_4^{2-}$). This process continues until these ions are supersaturated in the electrolyte resulting in the formation of insoluble zinc oxide. The reactions at the positive and negative electrodes are shown below.

$$\text{Negative Electrode} \quad Zn + 4OH^- \longrightarrow Zn(OH)_4^{2-} + 2e^-$$

$$Zn(OH)_4^{2-} \longrightarrow ZnO + H_2O + 2OH^-$$

Equation 1.3.1

$$\text{Positive Electrode} \quad O_2 + 4e^- + 2H_2O \longrightarrow 4OH^-$$

Equation 1.3.2

$$\text{Parasitic Reaction} \quad Zn + 2H_2O \longrightarrow Zn(OH)_2 + H_2$$

Equation 1.3.3

This system provides a high theoretical specific energy of 1086 Wh kg^{-1} (including the mass of oxygen) using cheap and readily available materials.[15] The high solubility of the discharge product leads to the loss of active material into the electrolyte, decreasing the cycle life of the cell. Attempts have been made to mechanically recharge each cell by replacing the zinc electrode, including a battery module developed by Arotech used to power a mini-jeep. The module was capable of delivering 191 Wh kg^{-1} with manually exchangeable zinc cassettes.[16] Zinc air suffers from a parasitic reaction also found in other aqueous metal-air technologies such as aluminium-air and magnesium-air. The zinc electrode reacts with water, evolving hydrogen gas, causing a gradual self-corrosion of the zinc metal.

1.3.2 Sodium-Oxygen Batteries

Another popular secondary battery system is sodium-oxygen. This system relies upon reacting sodium metal in a non-aqueous electrolyte with oxygen to form either Na_2O_2 or NaO_2. The energy densities of the sodium-oxygen cell are 1600 and 1100 Wh kg^{-1} based on the mass of NaO_2 and Na_2O_2 respectively. Controlling the nature of the discharge product has been shown to be dependent on the physical and chemical conditions within the cell such as the electrolyte donor number and the oxygen concentration.[17,18] The formation of NaO_2 leads to a lower overpotential when charging the cell whereas the formation of Na_2O_2 provides a higher energy density.[17,19] The discharge reactions for sodium-oxygen are shown in Equation 1.3.4 and Equation 1.3.5 below.

Equation 1.3.4

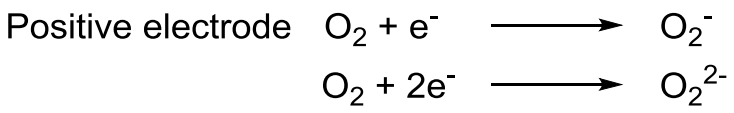

Equation 1.3.5

One of the key problems facing sodium-oxygen battery development is the severe dendrite, and subsequent SEI formation upon cycling which is reportedly worse than what is observed in lithium metal batteries.[17] The dendrite formation leads to continuous SEI formation which consumes both the sodium metal and the electrolyte as well as increasing the risk of cell failure and fires due to a short circuit. One solution to this problem was proposed by Peled *et al.* where the sodium metal was heated to above its melting point (98 ^{o}C) to 110 ^{o}C so dendrite formation can no longer occur. This prevented dendrite formation but the cell was still found to only operate with 85% faradaic efficiency.[20]

1.3.3 Lithium-Sulfur Batteries

While not technically a metal-air battery, lithium-sulfur batteries have received a growing interest in recent years as a promising alternative to lithium-oxygen batteries. The system uses a non-aqueous electrolyte with a metallic lithium negative electrode and an elemental sulfur positive electrode. They offer an identical theoretical capacity to lithium-oxygen due to the reduction of sulfur to lithium sulfide.[14,21,22] Overall the specific energy of lithium sulfur is lower than lithium-oxygen at 2600 Wh kg^{-1} due to a lower cell voltage.[21] The discharge reactions at each electrode for the lithium-sulfur cell are shown below in Equation 1.3.6 and Equation 1.3.7.

$$\text{Negative electrode} \qquad Li \longrightarrow Li^{+} + e^{-}$$

Equation 1.3.6

$$\text{Positive electrode} \qquad S_8 + 16e^{-} \longrightarrow 8S^{2-}$$

Equation 1.3.7

Although the intermediate stages of sulfur reduction from S_8 through to Li_2S are not fully understood, the various polysulfides (Li_2S_x, x = 2 to 8) are known to diffuse away from the sulfur electrode during cycling. These are then chemically reduced at the lithium electrode resulting in capacity loss. Upon charge this mechanism is also a problem as the polysulfides are continuously reduced to provide an ongoing charge step. This is known as the shuttle mechanism and is a widely accepted problem in lithium-sulfur.[21,23] The use of solid-state electrolytes are a possible solution to this problem as they are able to isolate the two electrodes while mitigating dendrite growth.[24]

For comparison, some of the key properties of these battery systems have been collated in Table 1.3.1 including values for the lithium-oxygen system. The table highlights the cost of using lithium metal over the cheaper more abundant alternatives. But also displays the far superior theoretical specific energy that lithium metal offers. Dendrite formation and poor cycle life is a problem in all of these systems and is a consistent problem that must be addressed throughout metal-air battery research. This work focuses on improving the discharge and charging reactions of the lithium-oxygen battery in an attempt to improve both the rate capability and cycle life of the system. For that reason the lithium-oxygen system is discussed in more detail below.

Table 1.3.1 A comparison of different types of beyond lithium-ion batteries.

	Zn-air	**Na-O_2**	**Li-S**	**Li-O_2**
Cost of metal / $ kg^{-1}	1.85	1.7	68	68
Theoretical voltage / V	1.7	2.3	2.2	3.0
Theoretical specific energy / Wh kg^{-1}	1090	1100	2570	3500
Electrolyte	Alkaline	Non-aqueous	Non-aqueous	Non-aqueous
Primary or secondary	Secondary	Secondary	Secondary	Secondary

1.4 Lithium-Oxygen Batteries

Lithium-oxygen batteries have received significant interest as they have the potential to greatly surpass the specific energy of lithium-ion batteries. The limited energy density of current battery systems is a major struggle facing the development of electric vehicles as demonstrated by Figure 1.3.1. While lithium-ion cells may one day reach 400 Wh kg^{-1} they are limited by the capacity of the materials used in the cell. The use of materials with higher specific energies such as lithium peroxide in lithium-oxygen could achieve theoretical specific energies of 3500 Wh kg^{-1} based on the mass of the lithium peroxide discharge product.[14] The high specific energy comes from combining lithium metal, 11,680 Wh kg^{-1} at the anode with Li_2O_2 at the cathode providing a cell voltage of 2.96 V vs. Li/Li^+.[22,25] The two electron reduction forming lithium peroxide stores considerably more charge per unit mass than the transition metal oxides currently used.[14] However, allowances must be made for the incorporation of a porous cathode framework (typically carbon) along with current collectors and packaging. Using the Li-S system as a comparison, the practical specific energy could be expected to be between 500-900 Wh kg^{-1}.[14] Despite it being a severe reduction from the theoretical specific energy, it remains between two to three times greater than that of current lithium-ion technology.

The desired reaction on discharge in non-aqueous systems involves the combination of lithium and oxygen at the positive electrode surface resulting in the formation of Li_2O_2, as shown in Equation 1.4.1.[26]

$$2Li + O_2 \longrightarrow Li_2O_2 \quad 2.96\ V\ vs.\ Li/Li^+$$

Equation 1.4.1

$$4Li + O_2 \longrightarrow 2Li_2O \quad 2.91\ V\ vs.\ Li/Li^+$$

Equation 1.4.2

However, lithium peroxide is both insoluble and electrically insulating and therefore forms a passivating layer on the porous electrode surface that clogs the pores and prevents further discharge. As a result, the capacity delivered by the battery is limited by the available pores within the air electrode. The reaction leading to the formation of lithium oxide, shown in Equation 1.4.2, is theoretically preferable as the specific energy is higher due to the additional reduction reaction taking place. Practically it has been suggested that this is difficult to decompose on charge which would reduce the reversibility of the cell.[14,27]

1.4.1 Oxygen Reduction Reaction

The oxygen reduction reaction may proceed via a mixture of two different mechanisms as shown in the equations below. Equation 1.4.3 represents the electrochemical one electron reduction of oxygen to form lithium superoxide. Laoire and Peng have suggested that this disproportionates to form lithium peroxide and oxygen in step 2.[28–30] Equation 1.4.4 represents two consecutive electrochemical steps as oxygen is first reduced to the superoxide then further reduced to form the lithium peroxide. These reactions are known to occur with significant overpotentials due to the poor kinetics of the reduction reaction exhibiting overpotentials of between up to 800 mV.[26,30,31]

$$Li^+ + e^- + O_2 \longrightarrow LiO_2 \quad \text{step 1 electrochemical}$$

$$2LiO_2 \longrightarrow Li_2O_2 + O_2 \quad \text{step 2 chemical}$$

Equation 1.4.3

$$Li^+ + e^- + O_2 \longrightarrow LiO_2 \quad \text{step 1 electrochemical}$$

$$Li^+ + e^- + LiO_2 \longrightarrow Li_2O_2 \quad \text{step 2 electrochemical}$$

Equation 1.4.4

Water has been shown to have a significant effect on the oxygen reduction reaction. In 2011, Gasteiger *et al.* demonstrated how the discharge capacity of a lithium-oxygen cell is greatly enhanced by the presence of just 250 ppm of water. In their study the discharge capacity of a cell was shown to increase from 200 mAh g^{-1}_{carbon} to 400 mAh g^{-1}_{carbon}.[32] While more recently Aetukuri *et al.* observed that in concentrations > 500 ppm, water functions to encourage the toroidal growth of lithium peroxide particles instead of a thin film, which increases the capacity of the cell.[33] One downside of this method is that any addition of water will lead to corrosion of the lithium metal negative electrode.

1.4.2 Oxygen Evolution Reaction

The charge reaction in a lithium-oxygen cell is one of the factors limiting its development. The reaction is expected to proceed via the two electron oxidation of lithium peroxide therefore limiting the formation of superoxide in accordance with Equation 1.4.5. Evidence for this has come from the utilization of a propylene carbonate electrolyte which is known to be unstable in the presence of superoxide leading to the formation of CO_2.[34] The absence of CO_2 when oxidising Li_2O_2 in this electrolyte indicates that no superoxide is generated

during the charge reaction. In addition to this, *in situ* Raman spectroscopy shows no evidence of superoxide formation during the charging of Li_2O_2 on gold.[30]

$$Li_2O_2 \longrightarrow 2Li^+ + 2e^- + O_2$$

Equation 1.4.5

The oxidation of Li_2O_2 requires a large overpotential leading to the incomplete removal of lithium peroxide from the electrode surface. Gallant *et al.* demonstrated that lithium peroxide deposits with a clustered morphology resulted in charge plateaus above 3.5 V vs. Li/Li^+, while small lithium peroxide particles resulted in sloping charge profiles with lower average charging potentials.[35] These clusters were found to form as a result of protons present within the cell. At high potentials, protons are formed as a result of water oxidation, these protons are then able to solubilise small quantities of lithium peroxide through the formation of hydrogen peroxide. An equilibrium is formed between hydrogen peroxide, lithium hydroxide and lithium peroxide enabling the formation of toroidal lithium peroxide deposits according to Equation 1.4.6.[36]

$$2H_2O + Li_2O_2 \rightleftharpoons 2LiOH + H_2O_2$$

Equation 1.4.6

1.5 Development of the Air Electrode

1.5.1 Carbon Electrodes

Carbon has been widely used as a cathode material in the Li-O_2 battery. This is largely due to its low density, and low cost. On charging above 3.5 V vs. Li/Li^+ in the presence of Li_2O_2, carbon has been shown to be unstable in the presence of lithium peroxide.[37–39] This decomposition leads to the formation of Li_2CO_3 and lithium carboxylates (HCO_2Li and CH_3CO_2Li).[37] These decomposition products occur both from the breakdown of the electrolyte and direct reaction with the electrode although below 3.5 V vs. Li/Li^+ lithium carbonate formation occurs predominately from electrolyte breakdown. Upon charging above 3.5 V vs. Li/Li^+, this Li_2CO_3 is oxidised and evolved as CO_2.[38] The rate of decomposition from the electrolyte increases and the electrode itself also can be seen to decompose forming Li_2CO_3 which is then simultaneously oxidised forming CO_2.[37] These side reactions involve the consumption of the electrode, depletion of lithium peroxide and the formation of insoluble carbonates at the cathode surface.

Through the use of an isotopically labelled carbon electrode, the CO_2 arising from breakdown of the electrolyte and the electrode has been quantified using a tetraglyme electrolyte. The results for this are shown below in Figure 1.5.1. All of this contributes to reducing the cells overall capacity and cycle life. Therefore, this is a key problem facing the development of the Li-O_2 battery. The porosity of carbon electrodes has been shown to have an effect on the reversibility and rate capabilities in ionic liquids.[40] Smaller pores favour better charge-discharge reversibility, while larger pores facilitate higher rates and larger overall capacities. The pore size distribution can be related to the discharge capacity of a lithium-oxygen cell with pores smaller than 12 nm assumed not to offer any capacity.[41]

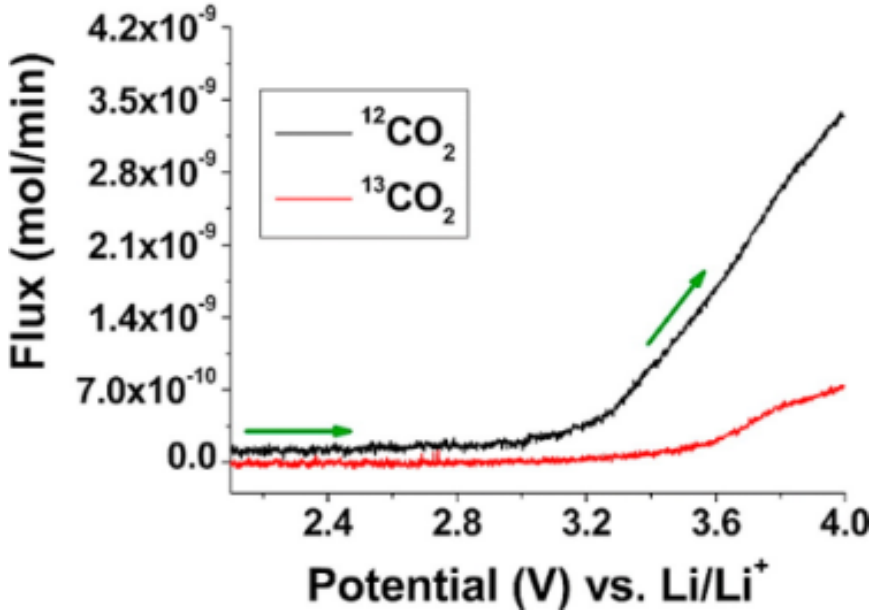

Figure 1.5.1 *In situ* differential electrochemical mass spectrometry (DEMS) data for CO_2 evolution from the decomposition of products formed from the electrolyte ($^{12}CO_2$) and the carbon cathode ($^{13}CO_2$) in a tetragylme based electrolyte during the first charge step. Figure reproduced with permission from reference.[37]

When using carbon electrodes, cells have been shown to exhibit a large overpotential during charging and when examined by cyclic voltammetry the peak current significantly decreases with progressive cycling.[22,28,37,38,42,43] This has led to the theory that the electrode is being passivated by a film formed on the surface of the electrode that is not completely oxidised during the charge step. It has been shown that reaction of the lithium peroxide with the carbon electrode accounts for approximately a monolayer of lithium carbonate at the electrode surface. While reactions between the peroxide and the electrolyte account for another monolayer at the peroxide electrolyte interface.[38] This lithium carbonate layer is not fully oxidised at 4 V vs. Li/Li^+ and therefore accumulates on cycling leading to electrode passivation and capacity fading.[37]

1.5.2 Oxygen Selectivity

Excluding other atmospheric gases is a major hurdle in designing a commercial lithium-oxygen cell, as the presence of water would cause rapid cell failure. While lithium is known to be reactive towards O_2 and N_2, the reaction with O_2 has been shown to be beneficial towards lithium cycling due to the formation of surface films.[44,45] The inclusion of CO_2 has also been shown to aid stability at the anode.[46] The incorporation of selective membranes for the exclusion of unwanted atmospheric gases will add extra weight to the cell reducing the attractive commercial nature of this system.

1.5.3 Alternative Electrode Materials

A stable system using a nano-porous gold electrode has been proposed with a DMSO based electrolyte.[43,47] While the gold electrode itself will never be a commercially viable option due to its high cost and high density, this does provide a system with a stable cathode from which alternative ideas can be proposed. More recently the use of titanium carbide (TiC) has been shown to outperform nanoporous gold in terms of reversible Li_2O_2 formation.[43] TiC is significantly lighter than gold and of lower cost. In this study, Fourier transform infrared spectroscopy (FTIR) and X-ray diffraction (XRD) were used to determine the composition of each electrode after charge and discharge. This spectroscopy gave good evidence of Li_2O_2 being the dominant discharge product with very little formation of carbonates.[43] However, this does not solve the lack of conductivity of the Li_2O_2 discharge product.

1.6 Electrolytes

The electrolyte is another key component in the cell that faces many challenges. A successful electrolyte must be stable to the highly reducing lithium metal at the negative electrode and a powerful oxidant in Li_2O_2 at the positive electrode. A high conductivity of Li^+ ions is required with high O_2 solubility and low viscosity to maintain good charge and discharge rates.[14,48] Efforts to increase the stability by removing the hazardous lithium metal anode with an intercalating silicon-carbon electrode have shown some success but at the expense of voltage and capacity.[25]

In the presence of lithium, the mechanism for the formation of lithium peroxide is dependent on the electrolyte. A high donor number solvent such as DMSO is more able to dissolve the superoxide species, increasing its lifetime, leading to more lithium peroxide being formed in solution.[49] A low donor number solvent such as acetonitrile encourages the immediate decomposition of superoxide to form the peroxide species at the electrode surface. One downside of using high donor number solvents is that they tend to be more susceptible to degradation by lithium superoxide due to their higher polarity.[50]

1.6.1 Dimethyl Sulfoxide

In much of the current work on lithium-oxygen batteries, DMSO is being used due to its relative stability towards the air electrode and the Li_2O_2 formed on discharge.[43,51–53] However, it is known that DMSO reacts when in contact with lithium metal. Carbonate electrolytes are also known to be reactive towards lithium metal, but further decomposition is limited by the formation of a layer of insoluble inorganic compounds at the electrode electrolyte interface known as the solid electrolyte interface (SEI).[4,5,54,55] In the case of DMSO, this SEI layer is not observed which is most likely due to the reduction

of DMSO by lithium yielding soluble dimethyl sulphide (DMS).[53] In previous studies this has been overcome by soaking the lithium metal in carbonate based solvents to allow an effective SEI layer to form prior to its emergence in dimethyl sulfoxide.[52]

1.6.2 Ionic Liquids

As an alternative to DMSO, ionic liquids have received growing interest for use in a lithium-oxygen cell.[42,47,56–62] The first study that looked at ionic liquids for the specific purpose of lithium-oxygen batteries compared five hydrophobic ionic liquids finding 1-ethyl-3-methylimidazolium bis(trifluorosulfonyl)imide (EMIMTFSI) to be the most effective due to its protection of the anode through the formation of LiF at the surface. The low volatility of the ionic liquid allowed the cell to be cycled at a range of temperatures from 20-100^{o}C with good cycle life.[63] However, EMIMTFSI was later shown to be unstable towards lithium superoxide whereas pyrrolidinium based ionic liquids, such as 1-butyl-1-methylpyrrolidinium bis(trifluoromethylsulfonyl)imide ($Pyr_{14}TFSI$) are more resistant towards superoxide.[64] There is a noticeable difference in the cyclic voltammetry of oxygen reduction and evolution in ionic liquids once lithium salt is introduced to the electrolyte. In the absence of Li^+ there is a soft acid (e.g. $EMIM^+$) soft base (O_2^{-*}) interaction, which stabilises the one electron reduction of oxygen.[47] Once Li^+ is added it is likely to outcompete the $EMIM^+$ due to its higher charge density providing a stronger acidity. However, due to the hard acid nature of the Li^+, its complex with the superoxide radical is unstable leading to its decomposition forming Li_2O_2. In a cyclic voltammogram, this gives rise to two additional oxidation peaks occurring at higher potentials than the EMIM-superoxide oxidation, the oxidation of the lithium superoxide and then the lithium peroxide.[47]

1.6.3 Ethers

Ethers are considered to be an attractive prospect for the Li-O_2 battery as they possess a range of key attributes. They are stable in contact with lithium metal and are not oxidised until potentials higher than 4.5 V vs. Li/Li^+.[65] They are relatively non-toxic and in the case of tetraglyme, possess low volatility. Early works suggested that dimethoxyethane (DME) was stable towards lithium peroxide since it was identified as the main discharge product by XRD and *in situ* spectroscopies such as Raman and FTIR.[65–67] This lead to increased interest in heavier, less volatile ethers such as diglyme and tetraglyme. However, more recent studies have indicated that the lithium peroxide that is formed on the first discharge is associated with subsequent electrolyte decomposition to give lithium carbonates and water.[65,68,69] The extent of this decomposition was seen to increase upon cycling.

Ether based electrolytes have been shown to have a higher stability towards the reduced O_2 species than carbonates due to the formation of lithium peroxide on the first discharge. The purity of these electrolytes has also been shown to be a key factor as water contamination can lead to an increase in cell capacity of an order of magnitude which could easily be greater than the effects attempting to be measured.[32] Freunberger *et al.* used X-ray diffraction of carbon electrodes after cycling in a tetraglyme electrolyte to demonstrate the formation of lithium peroxide on the first cycle. However, after several cycles no crystalline products could be detected.[65] Due to the demonstrated stability of glymes towards the superoxide radical as well as their high oxygen solubility and lower viscosity when compared with ionic liquids, diglyme was used as the electrolyte solvent throughout the work shown in this thesis.[39,70,71]

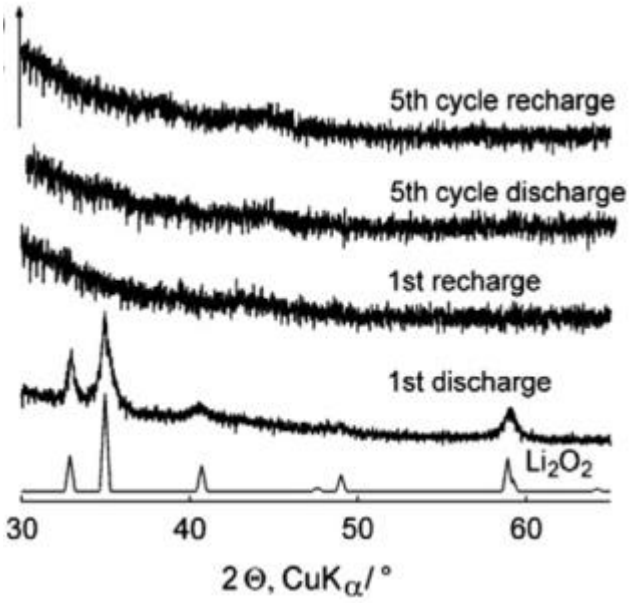

Figure 1.6.1 Powder X-ray diffraction patterns of the composite cathode (Super P/Kynar) cycled in 1 M $LiPF_6$ in tetraglyme under 1 atm O_2 between 2.0 and 4.6 V vs. Li/Li^+. Figure reproduced with permission from reference.[65]

1.7 Redox Mediators

Redox mediators are an elegant solution to electrode passivation by moving the reaction away from the electrode surface and have previously been used in a range of applications including biological sensors and lithium-ion batteries.[29–34] Taking the example of a charge mediator for lithium-oxygen batteries, the mediator would be electrochemically oxidised at a more positive potential than the formal potential of oxygen evolution (2.97 V vs. Li/Li^+). The oxidised form of the mediator would then react chemically with lithium peroxide to evolve oxygen while the mediator is in turn reduced. The mediator is then free to be re-oxidised electrochemically restarting the cycle. The major benefit of this system is that the large overpotentials required to oxidise lithium peroxide can be avoided. In their existing use as overcharge protection in Li-ion cells this prevents the reaction of battery components, mitigates temperature elevation and diminishes the risk of explosion[78–80]. These mediators could also be used to help solve the electrode passivation problem that is observed in the $Li\text{-}O_2$ cell.[81]

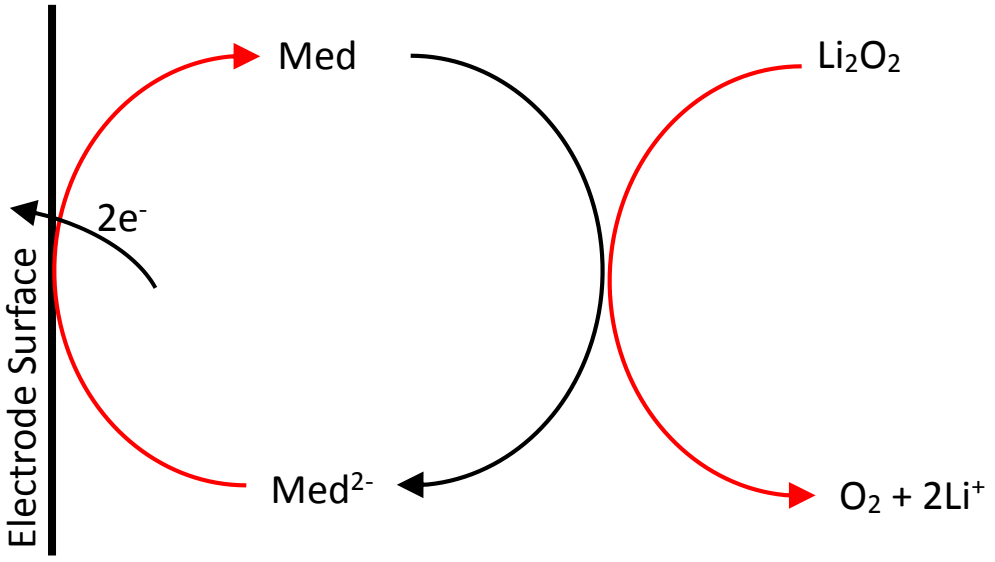

Figure 1.7.1 Oxidation of lithium peroxide via a solution based mediator.

By using mediators that are able to reversibly react with oxygen to form Li_2O_2 in a favourable chemical reaction, the formation of Li_2O_2 is moved away from the electrode interface and instead forms in solution. This idea was suggested by Lacey *et al.* who found ethyl viologen ditriflate could significantly improve the rate of oxygen reduction in an ionic liquid electrolyte.[82,83] Building on this, Bruce *et al.* studied several compounds for mediating the charge reaction of the lithium-oxygen cell. The reaction of these compounds with lithium peroxide was monitored by mass spectrometry and tetrathiafulvalene (TTF) was found to be the most effective. When using a 10 mM addition of TTF to a DMSO electrolyte, the charging voltage of a lithium-oxygen cell was maintained at 3.5 V vs. Li/Li^+ at rates of 1 mA cm^{-2}.[52]

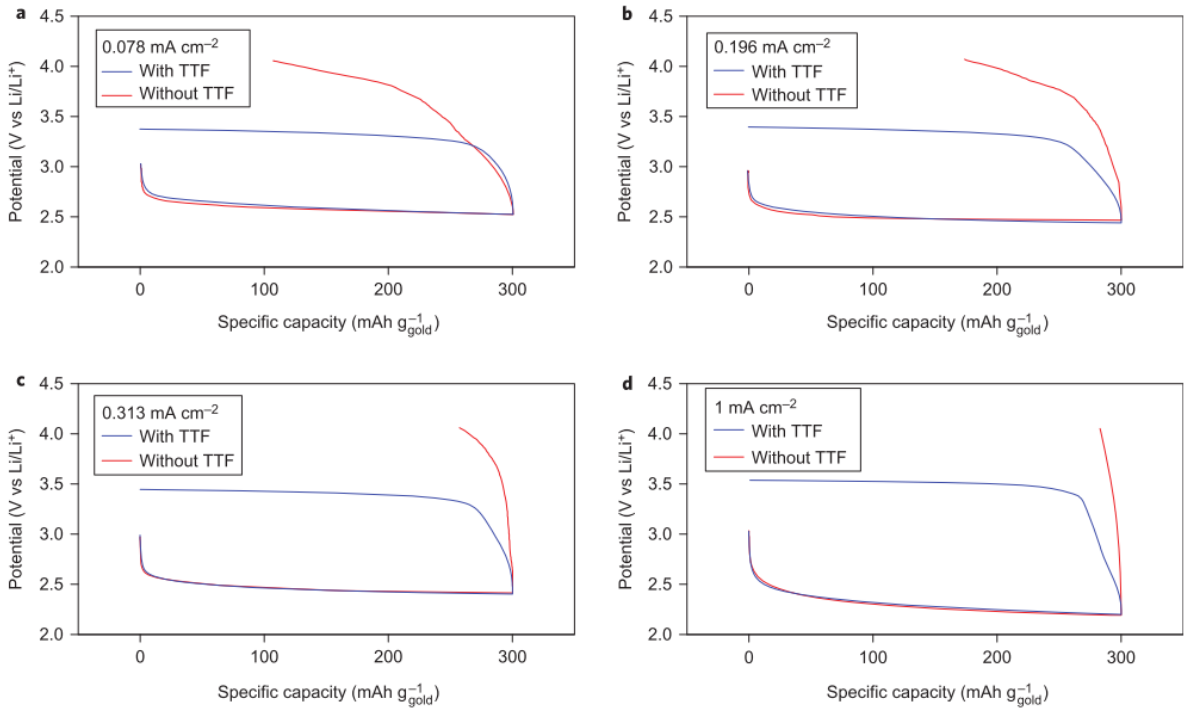

Figure 1.7.2 First cycle galvanostatic discharge/charge with and without the redox mediator at various rates. Cells consisted of 1 M $LiClO_4$ in DMSO with a nanoporous gold electrode under 1 atm O_2 with 10 mM TTF (blue) and without (red). Reproduced with permission from reference.[52]

The use of transition metal oxides incorporated into the carbon electrode has also been examined. The use of λ-MnO_2 in lithium-oxygen cells was first investigated by Read in 2002. Although the study did not focus on the effect of the surface bound catalyst it did note that the λ-MnO_2 did improve the reversibility of the air electrode reaction.[84] This work was continued by Débart *et al.* who found that α-MnO_2 nanowires resulted in the largest capacities on discharge. The discharge capacity was limited to ~ 50% which was found to greatly improve the cycling of the cell. This led to the belief that the electrode pores were becoming blocked by the discharge product.[85] One drawback of the solid cathode based catalysts is that they are limited to enhancing the electron transfer to areas in direct contact with the catalyst. This is an area where solution based mediators have an advantage.

Since these early publications, there have been several studies conducted in parallel to the work shown in this thesis. In 2014, Janek *et al.* demonstrated that TEMPO (2,2,6,6-tetramethylpiperidinyloxyl) was able to mediate the oxidation of lithium peroxide using a combination of galvanostatic and cell pressure measurements. Here it was shown that by electrochemically oxidising TEMPO it was possible to detect oxygen evolution from an electronically isolated carbon electrode.[86] Another interesting observation from this study was that upon the addition of 10 mM TEMPO to the electrolyte, the dissolved oxygen concentration was found to decrease. This led to an overall decrease in the discharge capacity of the cell. However, the benefits on the charge step were seen to outweigh this.

The use of iron pthalocyanine (FePc) dissolved in an organic electrolyte (DMSO or TEGDME) has been shown to improve the kinetics of both the ORR and the OER.[87] Sun *et al.* in 2014 demonstrated through the use of voltage plateaus that the incorporation of FePc at 2 mM

was sufficient to improve the discharge capacity from 800 mAh g^{-1} to 2400 mAh g^{-1}. The lithium peroxide discharge product was detected using XRD. While in 2015 Tonti *et al.* demonstrated the use of the inert carbon free radical tris(2,4,6-trichlorophenyl)methyl to enhance capacity and rate capability of the ORR in aprotic media.[88] The use of further functionalised structures are suggested to tune the redox voltage, solubility and diffusivity of these low toxic and oxygen stable compounds.

Lithium iodide has been considered as a possible redox mediator for the charge reaction in lithium-oxygen batteries.[89,90] The use of K^+ as a cation instead of lithium has been shown to increase the cycle life when using I^- as a redox mediator.[91] The I_3^- / I^- redox couple has also been suggested as an aqueous cathode for a lithium-iodine battery.[92] Taking a slightly different approach, in 2015 Grey *et al.* used small concentrations of water in a dimethyl ether (DME) electrolyte in combination with lithium-iodide as an additive. This led to the reversible cycling of a lithium-oxygen cell with lithium hydroxide as the dominant discharge product.[93] The discharge reactions proposed for this cell are given in Equation 1.7.1 while the charge reactions are given in Equation 1.7.2. These reaction products have also been confirmed by Zhu *et al.* in a more recent study.[94]

$$4Li^+ + 4O_2 + 4e^- \longrightarrow 4LiO_2 \qquad \text{step 1 electrochemical}$$

$$4LiO_2 + 2H_2O \xrightarrow{LiI} 4LiOH + 3O_2 \qquad \text{step 2 chemical}$$

Equation 1.7.1

$$6I^- \longrightarrow 2I_3^- + 4e^- \qquad \text{step 1 electrochemical}$$

$$4LiOH + 2I_3^- \longrightarrow 4Li^+ + 6I^- + 2H_2O + O_2 \qquad \text{step 2 chemical}$$

Equation 1.7.2

The cells assembled consisted of a reduced graphene oxide positive electrode and a lithium metal negative electrode. During discharge, a plateau at 2.7 V vs. Li/Li^+ was observed with the capacity limited to 8000 mAh g^{-1}. The charging plateau is observed at 3.0 V vs. Li/Li^+ for the entirety of the charge step. While the discharge products have been confirmed by NMR and XRD these impressive results have been met with scepticism about the true nature of the charge reaction. Shen *et al.* have proposed that the charge capacity is in fact solely due to the oxidation of LiI forming I_3^-.[95,96] The use of cell pressure testing or differential electrochemical mass spectrometry could be used to resolve this debate.

Building on the use of iodide as a charging mediator for lithium oxygen, bromine has also been suggested as a possible mediator.[97] Due to its high redox potential of 4.0 V vs. Li/Li^+, bromine is also capable of oxidising lithium carbonate at the electrode surface. The use of tris[4-(diethylamino)phenyl]amine (TDPA) has been shown by Nazar *et al.* to lower the charging voltage by as much as 0.8 V in a tetraglyme electrolyte.[98] The chemical reaction of the proposed mediator was monitored by mass spectrometry and found to require ~ 2.2 electrons per mole of oxygen evolved. This deviation from the desired 2 electrons per mole was attributed to experimental error. Utilising a mixed electrolyte of diglyme and $Pyr_{14}TFSI$, Yao *et al.* demonstrated that the redox potential of a cobalt bis(terpyridine) changed depending on the ratio of the solvents.[99] It was found that the redox potential of the cobalt complex decreased with an increasing ratio of $Pyr_{14}TFSI$. This was attributed to a weakening of the Li^+ solvation causing an upward shift in the Li/Li^+ couple used as a reference electrode in the measurements.

1.8 Quinones

There has been a great amount of research involving the redox behaviour of quinones due to their wide use in biological systems.[73,100–104] Research has been carried out in both aqueous and non-aqueous media including the use of quinones as electron transfer agents.[73,104] In non-aqueous electrochemistry, quinones typically show two distinct reductions, first to the radical anion and then to the di-anion as shown in Figure 1.8.1. The first reduction is considered to be completely reversible whereas the second is quasi-reversible.[104] While the exact potential for reduction is strongly dependant on the solvent, a typical formal potential for an unsubstituted quinone is approximately 2.5 V vs. Li/Li^+.[83,84] The incorporation of lithium ions into the electrolyte enables the dianion to form a complex, shifting the second reduction to more positive potentials.[104]

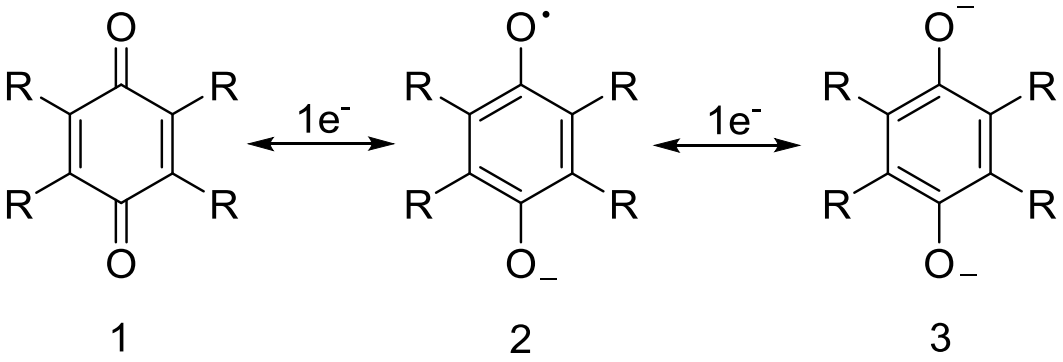

Figure 1.8.1 Two stage reduction of a quinone from the neutral quinone (1) to the semi-quinone (2) and finally to the dianion (3).

The potential of substituted quinones being in the region of 2.5 V vs. Li/ Li^+ initially suggests that they could be useful for catalysing the ORR in lithium-oxygen batteries. However, through the use of electron withdrawing groups (e.g. $R\text{-}NO_2$) the quinone can be made more electron deficient, resulting in a positive shift in the reduction potential. This allows the electrochemistry of the compound to be tuned enabling the oxidation of lithium peroxide via a quinone.

Quinones are good candidates for solution based catalysts as previous work has shown they are able to mediate the reduction of oxygen to superoxide in non-aqueous electrolytes.[105] In this work, Schiffer *et al.* grafted anthraquinone compounds onto glassy carbon electrodes using the electrochemical reduction of their corresponding diazonium salts. The reduction of the quinone to the semi-quinone was found to be up to 16 times faster with large functional groups able to stabilise the radical formed (e.g. sulphones).

The formal potentials of a range of substituted quinones in different non-aqueous electrolytes has been studied and their relative potential shifts are consistent across different non-aqueous systems. Figure 1.8.2 below by Sasaki *et al.* compares the first electron transfer potential of various quinones in an acetonitrile to a range of other non-aqueous electrolytes. Each of these quinones can be identified using Table 1.8.1.

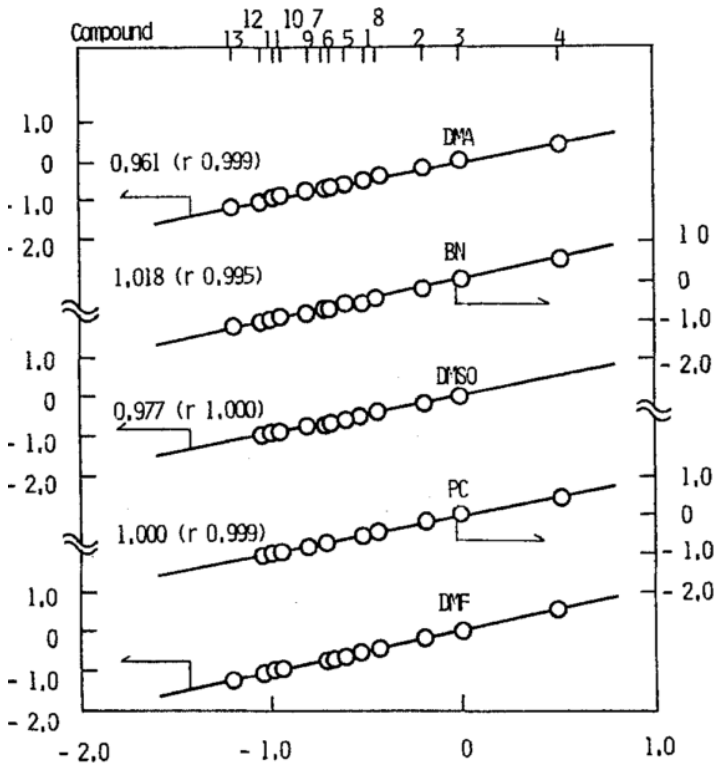

Figure 1.8.2 Electrode potential vs. SCE for the first electron transfer of various quinones in the specified non-aqueous electrolyte against the observed potential in acetonitrile. Numerical annotation represents the gradient with the associated correlation coefficient in parenthesis. Reproduced from reference with permission.[103]

Table 1.8.1 Reduction potential of quinones in various solvents. Reproduced from reference with permission.[103]

Compound	Solvent	E°_1	E°_2	ΔE°
1 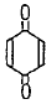	AN	−0.522	−1.210[b]	−0.69
	PC	−0.537	−1.007[c]	−0.47
	DMF	−0.507	−1.447	−0.94
	DMSO	−0.464[b]	−1.382[b]	−0.92
	BN	−0.513[c]	−1.161[c]	−0.65
	DMA	−0.507	—	—
2 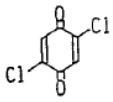	AN	−0.197	−0.980[b]	−0.79
	PC	−0.199	−0.830[c]	−0.63
	DMF	−0.168	−1.126	−0.96
	DMSO	−0.147	−1.028	−0.88
	BN	−0.217	−0.941	−0.72
	DMA	−0.158[b]	−1.141	−0.98
3 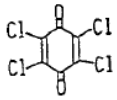	AN	−0.005	−0.792	−0.80
	PC	−0.014	−0.725[b]	−0.71
	DMF	+0.027	−0.880	−0.91
	DMSO	+0.032	−0.790	−0.82
	BN	−0.010	−0.779	−0.77
	DMA	+0.038	−0.899	−0.94
4 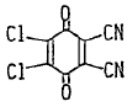	AN	+0.502	−0.320	−0.82
	PC	+0.456	−0.302[b]	−0.76
	DMF	+0.502[a]	−0.366[c]	−0.87
	DMSO	—	—	—
	BN	+0.509	−0.351	−0.86
	DMA	+0.492	—	—
5 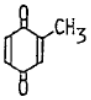	AN	−0.609	−1.348[b]	−0.74
	PC	−0.619[b,d]	−1.111[b]	−0.49[d]
	DMF	−0.583	−1.499	−0.92
	DMSO	−0.541	−1.438	0.90
	BN	−0.608[b]	−1.213[c]	−0.61
	DMA	−0.590	—	—
6 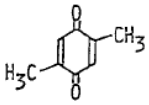	AN	−0.684	−1.332[c]	−0.65
	PC	—	—	—
	DMF	−0.661	−1.445[b]	−0.78
	DMSO	−0.626	−1.488	−0.86
	BN	−0.72[b]	−1.241[c]	−0.52
	DMA	−0.659	—	—
7 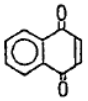	AN	−0.706	−1.343	−0.64
	PC	−0.71[b]	−1.119[c]	−0.41
	DMF	−0.682	−1.509	−0.83
	DMSO	−0.644	−1.465	−0.82
	BN	−0.721	−1.331	−0.61
	DMA	−0.675	−1.483[b]	−0.81
8 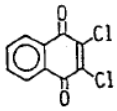	AN	−0.448	−1.134	−0.69
	PC	−0.462	−0.946[b]	−0.49
	DMF	−0.414[b]	−1.255[c]	−0.84
	DMSO	−0.380	−1.158	−0.78
	BN	−0.469	−1.099	−0.63
	DMA	−0.389	−1.249[b]	−0.86
9 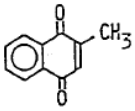	AN	−0.801	−1.466[b]	−0.67
	PC	−0.810	−1.277	−0.39
	DMF	−0.774[b]	−1.616[b]	−0.84
	DMSO	−0.726	−1.534	−0.81
	BN	−0.825	−1.343[b]	−0.52
	DMA	−0.746	−1.488[b]	−0.74
10 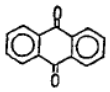	AN	−0.952	−1.498	−0.55
	PC	−0.965	−1.297[b]	−0.33
	DMF	−0.924	−1.661	−0.74
	DMSO	−0.875[b]	−1.594[b]	−0.72
	BN	−0.963	−1.403[b]	−0.44
	DMA	−0.897	−1.610[b]	−0.71
11 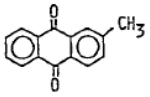	AN	−0.981	−1.579	−0.60
	PC	−0.996	−1.324[b]	−0.33
	DMF	−0.946	−1.681	−0.74
	DMSO	−0.907	−1.618	−0.71
	BN	−1.034	−1.547[b]	−0.51
	DMA	−0.932	−1.640	−0.71
12 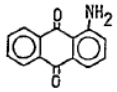	AN	−1.042	−1.571[b]	−0.53
	PC	−1.052	−1.391[b]	−0.34
	DMF	−1.013	−1.691	−0.68
	DMSO	−0.993	−1.642	−0.65
	BN	−1.050	−1.508[b]	−0.46
	DMA	−1.016	−1.653	−0.64
13 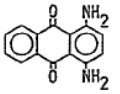	AN	−1.200	−1.623	−0.42
	PC	—	—	—
	DMF	−1.225	−1.748	−0.52
	DMSO	—	—	—
	BN	−1.218	−1.612[b]	−0.39
	DMA	−1.221	−1.738	−0.52

[a] Reference electrode: SCE in respective solvent, sweep rate: 0.1 V s^{-1}.
[b] 151 mV < ($E_{pc} - E_{pa}$) < 200 mV.
[c] 201 mV < ($E_{pc} - E_{pa}$).
[d] Cathodic peak potential.

Two papers have been published from other research groups detailing the use of quinones in lithium-oxygen batteries. The first by Nakanishi *et al.* in 2014 detailed the use of several quinones as mediators for the ORR.[106] Of all the quinones shown, benzoquinone was found to have the greatest improvement upon the ORR overpotential. The researchers suggested that it was the semi-quinone which catalysed the reduction of molecular oxygen to superoxide, which then went onto disproportionate forming lithium peroxide. This study used extremely low discharge rates of 1 μA cm^{-2} and limited the discharge capacity to 1 mC making it difficult to determine whether this effect was truly catalytic.

More recently, Bruce *et al.* published the use of 2,5-di-tert-butyl-1,4-benzoquinone (DBBQ) as an electrolyte additive in lithium-oxygen batteries.[50] Using cyclic voltammetry, a clear EC mechanism was demonstrated upon the addition of oxygen. The use of DBBQ was suggested as a means of encouraging the formation of lithium peroxide in solution when using low donor number solvents. Contrary to the previous study, Bruce *et al.* proposed that a complex forms involving the lithiated semi-quinone and oxygen. Two of these complexes then go onto react forming lithium peroxide and the neutral quinone. The advantage of this mechanism being the avoidance of any free superoxide radicals in solution. A 10 mM concentration of the quinone was shown to greatly enhance the discharge capacity of lithium-oxygen cells when discharging at high rates while Li_2O_2 was confirmed as the discharge product by SEM and XRD. The charge reaction is said to be unaffected by the DBBQ inclusion possibly due to the peroxide formation occurring far from the electrode surface. This could explain why there is no information about the DBBQ stability over multiple charge/discharge cycles.

1.9 Differential Electrochemical Mass Spectrometry

Much of the early work in lithium-oxygen batteries was performed in carbonate electrolytes since these were initially thought to be stable towards lithium peroxide.[84,107–110] However, it was later shown using differential electrochemical mass spectrometry (DEMS) that reactions taking place in these solvents are dominated by electrolyte degradation. The discharge product was shown to contain mostly lithium alkyl carbonates and lithium carbonate with very little lithium peroxide or oxide.[34,111–114] As a result of this it has become increasingly important to demonstrate with absolute certainty that the reactions during discharge or charge are not as a result of side reactions or decomposition.

On-line mass spectrometry has become a popular tool in confirming the reaction products for lithium-oxygen batteries.[14,38,43,52,67,69,115] It allows the user to demonstrate not only that certain mass fractions are present but also to calculate the moles formed during the reaction. However, gas flow rates of approximately 1 mL min^{-1} are required in order to provide continuous sampling. In closed systems like batteries this presents a problem as the typical electrolyte volume in a working battery cell is only between 10-100 µL. To resolve this, either a continuous gas stream is employed to purge the products of the cell, sometimes referred to as on-line electrochemical mass spectrometry (OEMS), or the head space is intermittently purged between cycles.[52,67,69] The disadvantage of these solutions is that there is no longer a sealed volume from which the sampling is performed but instead there is a continuous flow which is more prone to contamination.

This technique has been used effectively in identifying potential redox mediators by comparing their efficiency per mole in evolving oxygen.[52] Combining mass spectrometry with isotopically labelled carbon was used to evaluate the relative contributions of the

carbon electrode and tetraglyme electrolyte to the formation of CO_2 during the charge cycle. This study found that the increased rate of carbonate formation during charging overtakes the rate of carbonate decomposition leading to the accumulation of lithium carbonate at the electrode surface and the subsequent electrode passivation.[37] McCloskey *et al.* used isotopically labelled carbon and oxygen to examine the decomposition observed in carbonate solvents.[67] The carbonate based solvents were found to irreversibly decompose upon cell discharge. Whereas cells using a DME electrolyte produced mainly lithium peroxide on discharge.

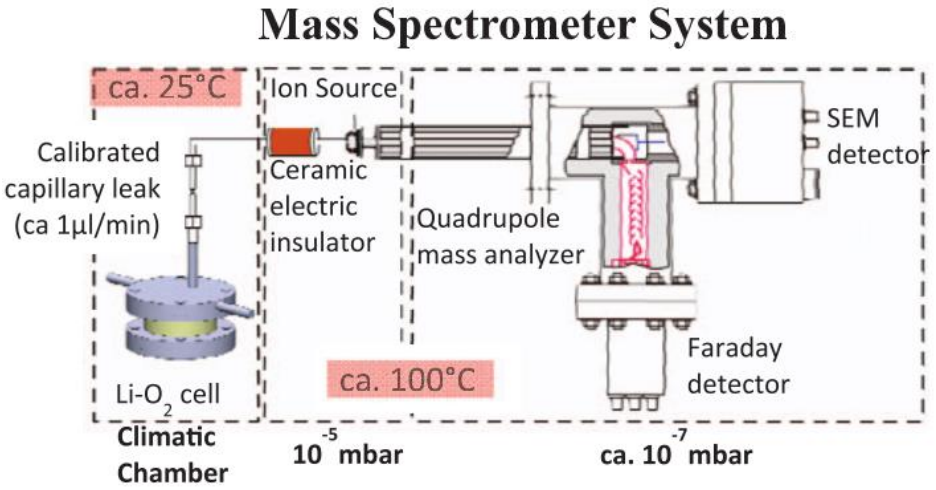

Figure 1.9.1 Example of an on-line electrochemical mass spectrometer (OEMS) system. Reproduced with permission from reference.[69]

Chapter 2: Experimental Techniques and Procedures

This chapter describes the majority of the experimental procedures and techniques which have been used throughout this thesis. This includes preparation of electrodes and electrolytes while also describing in detail the assembly of electrochemical cells. Any technique which applies only to a specific chapter will be discussed in the experimental section of that chapter.

2.1 Cell Assembly

2.1.1 Two Electrode Glass Cell (U-Cell)

All cyclic voltammetry measurements were collected using the two electrode set up shown in Figure 2.1.1. The cell consisted of two compartments separated by a glass frit. This was done to prevent chemical reaction of mediators dissolved in the electrolyte of the working electrode compartment with the lithium metal counter/reference electrode in the other compartment. The working electrode was a glassy carbon rod (Alfa-Aesar, Ø = 3mm) encased in a glass surround to provide a smooth disk shaped electrode. The counter/reference electrode was lithium metal (Lithium foil battery grade, Rockwood Lithium) pressed onto a stainless steel mesh. Into each compartment, 3 mL of electrolyte was added via auto pipette. Cells were assembled in an argon filled glove box (< 10 ppm H_2O, < 10 ppm O_2) atmosphere allowing measurements to be recorded first in an inert argon atmosphere before purging the cell with oxygen via the rubber septa shown. When purging the cell with oxygen a flow meter was set at 50 mL · min^{-1} to prevent any surging in the flow rate while molecular sieves (3 Å, 4 – 8 mesh, Sigma-Aldrich) were used to ensure the gas supply remained dry. Each cell was purged with oxygen for 10 minutes to saturate the electrolyte. Due to the possibility of cross contamination between the electrolyte chambers, all experiments were carried out on the same day as assembly.

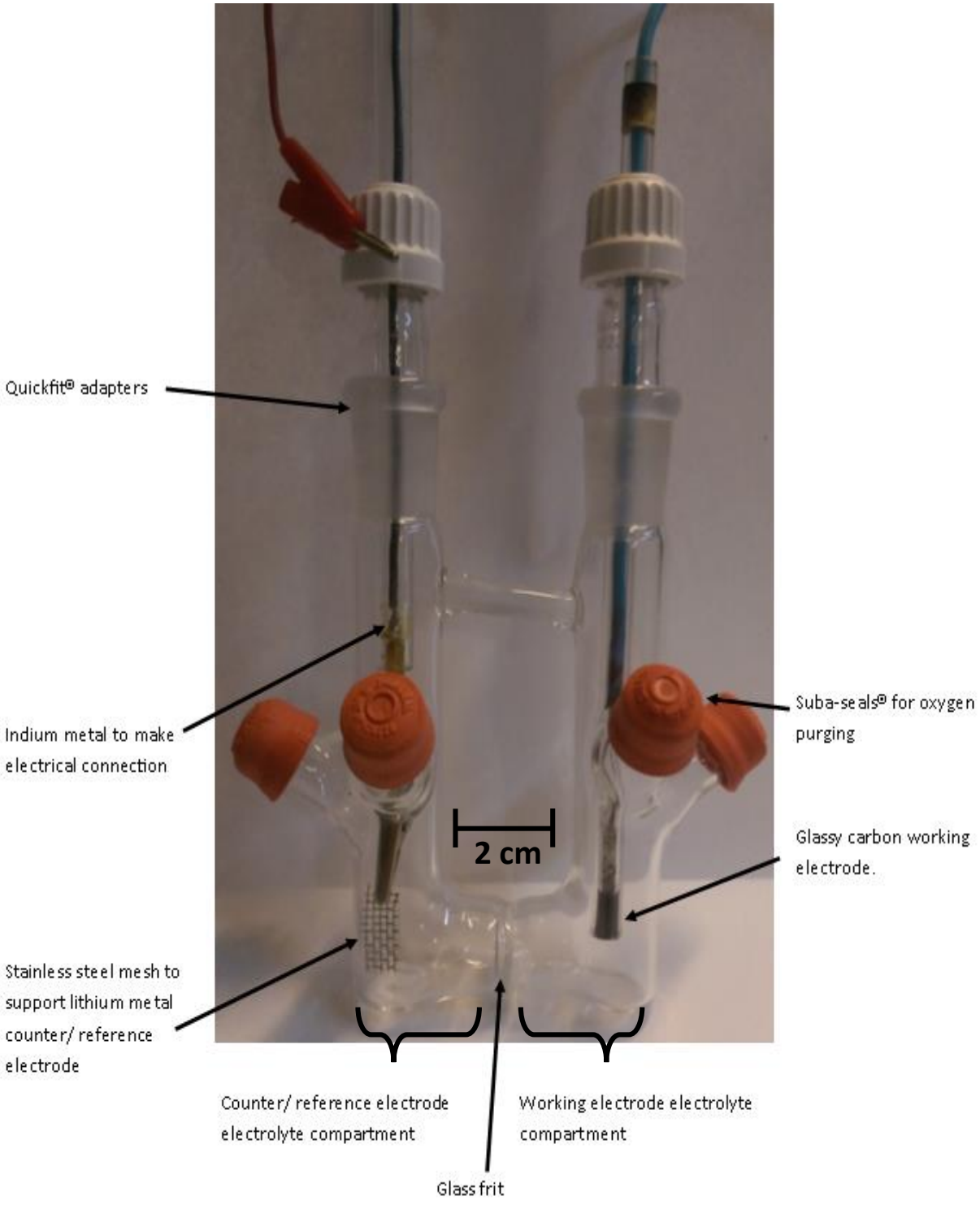

Figure 2.1.1 Labelled photograph of fully constructed U-Cell.

2.1.2 Swagelok Cells Adapted for Lithium-Oxygen

In order to carry out galvanostatic cycling experiments, a technique more in-line with conventional battery use, an alternative cell design was employed. This arrangement focussed on having stacked cells with high surface area carbons as the positive electrode to provide high specific capacities. The Swagelok cell still comprised of a lithium metal counter/reference electrode (Lithium foil battery grade, Rockwood lithium) cut into a disk (Ø = 24 mm). On top of this was a Celgard separator (Ø = 25.4 mm/1", Celgard 2320) wetted with 50 µL of electrolyte, followed by an Ohara glass separator (Ø = 25.4 mm) and another Celgard separator (Ø = 25.4 mm) wetted with 50 µL of electrolyte. The Ohara glass separator is a lithium ion conducting glass ceramic which allows the effective separation of the anode and cathode sides of the cell. This was done to prevent reactions between organic compounds contained in the electrolyte at the carbon electrode, with the highly reactive lithium electrode. The carbon electrode consisted of a Celgard disk (Ø = 13 mm) coated in an acetylene black – nafion carbon ink. The ink was prepared by mixing acetylene black (Chevron) with lithiated nafion dispersed in isopropyl alcohol (IPA) (LITHion, Ion Power) in a 2:1 by weight percent ratio. This mixture was diluted to contain 100 mg of carbon in 3 mL of IPA before homogenising (Whirlimixer, Fisher brand) and casting over a Celgard sheet. Disks were cut and then dried under vacuum for 24 hours at room temperature. No further electrolyte was added on top of the carbon electrode during cell as this was found to better preserve the electrodes for use in *ex situ* measurements. The Swagelok fitting itself was made of stainless steel and so required a chemically inert insulating film of fluorinated ethylene propylene (FEP, RS components, thickness = 0.127 mm) to electronically isolate each of the current collectors in order to prevent short circuiting the cell. Above the carbon electrode a steel spacer was used to maintain a

consistent head space of 3 cm^3. This was followed by a spring to ensure good conductivity by providing stack pressure and finally the current collector itself. At the lithium electrode, the current collector was a simple stainless steel cylinder (Ø = 1”). At the carbon electrode an inlet and an outlet had been drilled with a Swagelok needle valve to provide a seal and allow the atmosphere to be exchanged after the cells construction.

In order to exchange the atmosphere, the cell was connected to a specially constructed gas line. This would allow the lines to be evacuated and refilled with oxygen repeatedly, purging all contaminates. Once the purge was completed the cell was opened, allowing the head space to become saturated with oxygen. Purging was carried out for 10 minutes to ensure that the concentration of oxygen in the cell was close to 100%.

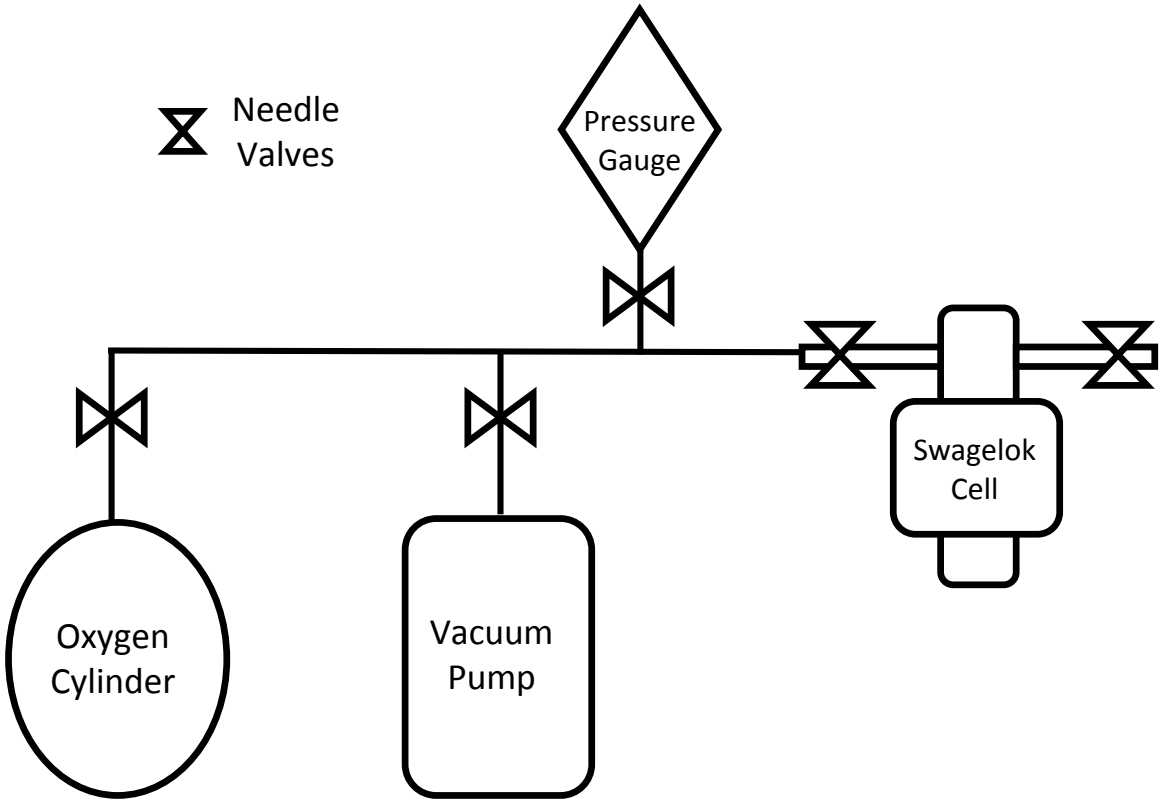

Diagram 2.1.1 Gas purging apparatus for use with Swagelok cells.

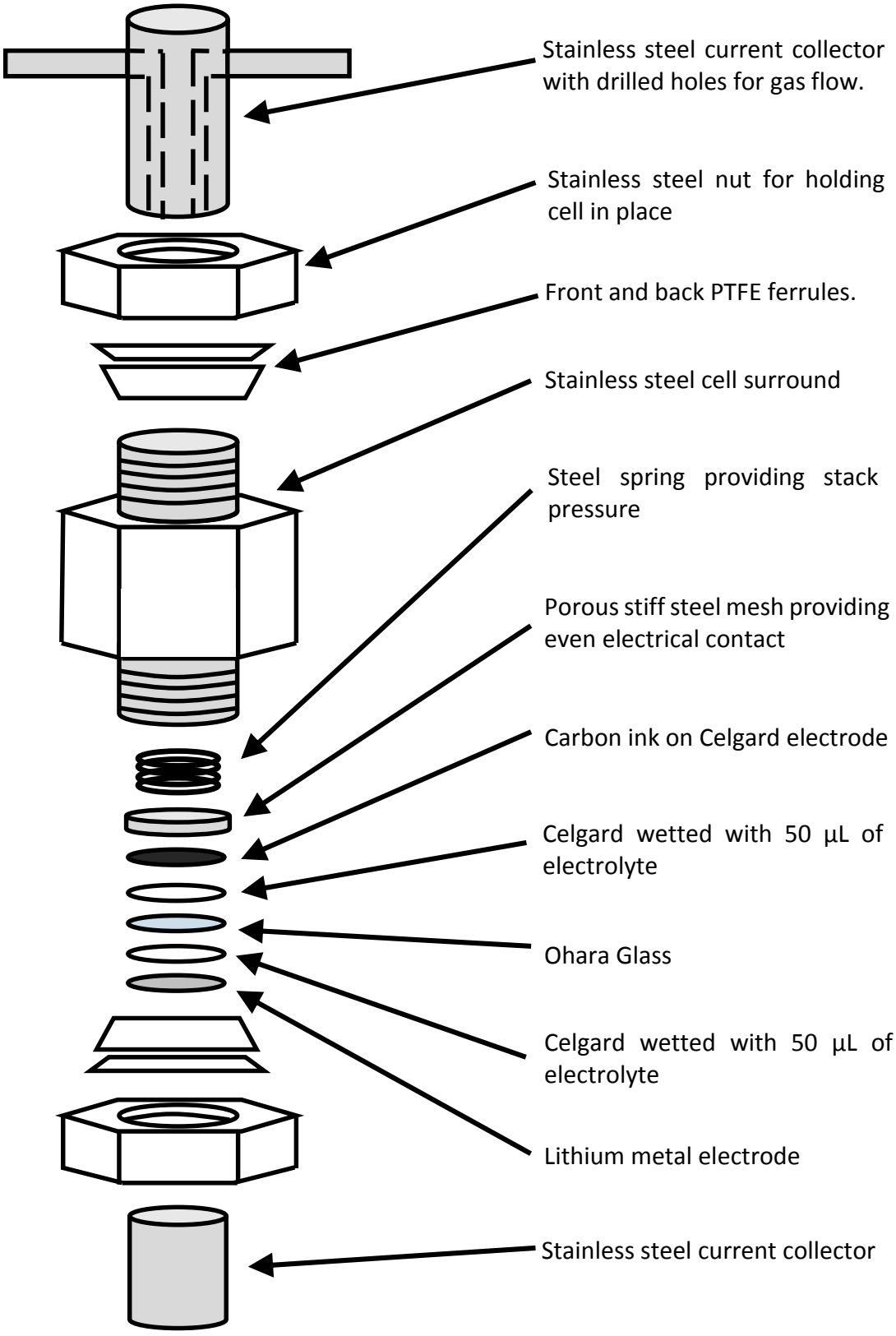

Diagram 2.1.2 Deconstructed Swagelok cell arrangement, including Ohara glass and adapted oxygen electrode current collector.

2.2 Electrolyte Preparation

Diglyme (anhydrous, 99.5%, Sigma-Aldrich) was dried over molecular sieves (3 Å, 4 – 8 mesh, Sigma-Aldrich). The water content of the dried solvent was found to be between 10 – 15 ppm. The sieves themselves were dried by heating to 120 °C under vacuum for 48 hours in a BUCHI furnace.

The lithium salt used throughout this work was lithium bis(trifluoromethylsulfonyl)imide (LiTFSI, Sigma Aldrich, 99.95%). The salt was dried under vacuum at 120 °C for 48 hours before being stored in an argon filled glove box (< 10 ppm H_2O, < 10 ppm O_2, MBraun).

All quinones were purchased at the highest available purity from Sigma Aldrich (See Table 2.2.1), dried under vacuum at room temperature for 24 hours to remove any residual water unless stated otherwise, before transferring to an argon filled glove box (< 10 ppm H_2O, < 10 ppm O_2, MBraun).

Electrolytes were prepared in an argon filled glove box (< 10 ppm H_2O, < 10 ppm O_2, MBraun) by first dissolving the required moles of lithium salt into the electrolyte. Low concentrations of mediator containing electrolytes were achieved by sequential dilution. Solutions of > 50 mM were first prepared then diluted down using the lithium salt containing solvent to form the desired electrolyte. To avoid the effect of any contamination, or decomposition of the quinones, electrolytes were prepared as required and not stored for longer than one week.

Table 2.2.1 List of quinones and their associated purity as received from Sigma Aldrich.

Quinone	Purity ($\geq x\,\%$)
1,4-Benzoquinone	98
Methyl-1,4-benzoquinone	98
2,5-Dimethyl-1,4-benzoquinone	98
1,4-Napthoquinone	97
2,3-Dichloro-1,4-napthoquinone	98
Anthraquinone	97
1,5-Dichloroanthraquinone	96
Tetrafluoro-1,4-benzoquinone	97
Tetrachloro-1,4-benzoquinone	99
Tetrabromo-1,4-benzoquinone	90
2,3-Dichloro-5,6-dicyano-1,4-benzoquinone	98

2.3 Electrochemical and Spectroscopic Techniques

All electrochemical measurements described in this work were carried out using a Bio-Logic variable multi-channel potentiostat (VMP2). These systems typically rely upon a three electrode arrangement; a working electrode, a counter electrode and a reference electrode. The working electrode is defined as the electrode under investigation. Potentials are applied across the working and counter electrode. The counter electrode balances the flow of charge at the working electrode. The reference electrode does not undergo any electrochemical changes but should have a stable and well-known redox couple. The potential between the reference and working electrode can then be measured with all changes ascribable to the working electrode.

The dependence of potential on the concentration of electroactive species can be determined by thermodynamics. Consider the reaction proposed below, where 'O' is the oxidised species, 'R' is the reduced species and 'n' is the number of electrons transferred.

$$O + ne^- \leftrightarrow R$$

Equation 2.3.1

The relationship between the activities of the oxidised and reduced species and the free energy 'Δ G' (J mol^{-1}) is given as

$$\Delta G = \Delta G^o + RT \cdot ln\frac{a_O}{a_R}$$

Equation 2.3.2

where 'R' is the gas constant (8.314 J K^{-1} mol^{-1}), 'T' (K) is the temperature and 'a' is the activity coefficient. An important thing to note in this equation is that the concentration of active species is related to the Gibbs free energy change, from which we can determine the potential 'E' (V).

$$\Delta G = -nFE$$

Equation 2.3.3

Here 'E' represents the equilibrium potential, and 'F' is the Faraday constant (96485 C mol^{-1}). Assuming the reactant and product have unit activities the equation can be written as below.

$$\Delta G^o = -nFE^o$$

Equation 2.3.4

In this case, the potential is referred to as the standard electrode potential and it is related to the standard Gibbs free energy change. Combining Equation 2.3.2 and Equation 2.3.4 yields the Nernst equation which describes the correlation of cell potential and concentration.

$$E = E^o + \frac{RT}{nF} \cdot ln\frac{a_O}{a_R}$$

Equation 2.3.5

For dilute solutions of reactant in the presence of a large excess of inert electrolyte it can be assumed that the activity coefficients tend to unity. The activities can then be replaced with concentrations and the standard potential (E^o) replaced with the formal potential (E'^o). Equation 2.3.5 can then be written as.

$$E = E'^o + \frac{RT}{nF} \cdot ln\frac{[O]}{[R]}$$

Equation 2.3.6

The potential of a system with equal concentrations of the oxidised and reduced form would therefore sit at the standard potential. If the potential at the electrode surface is changed the concentration of each species will change according to the Nernst equation.

2.3.1 Cyclic Voltammetry

Cyclic voltammetry is a very popular technique for the initial study of electrochemical systems and has proven very useful in obtaining information about complicated electrode reactions. During cyclic voltammetry, the potential of the working electrode is swept through the potential range where an electrode reaction occurs, then the direction of scan is reversed to determine whether the product of electron transfer is stable and if any other electroactive species are formed. The rate at which the potential is changed is described as the scan rate and has units of $V \cdot s^{-1}$. The current that flows through the system is measured and plotted against the potential. Figure 2.3.1 displays the change of voltage with time and the resulting measured current response in the case of a fast one electron transfer.

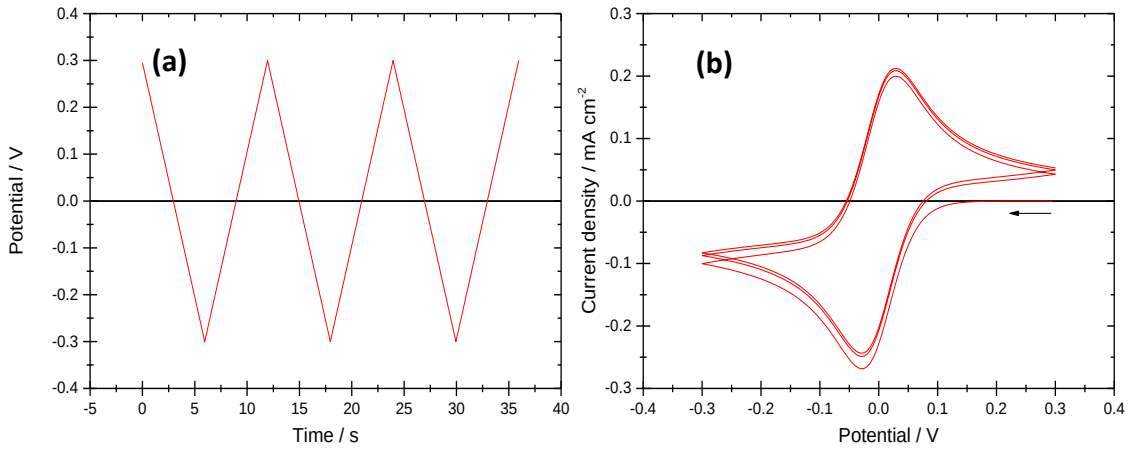

Figure 2.3.1 Simulation using Digielch software of cyclic voltammetry using 0.1 V s^{-1} sweep rate for three cycles with the formal potential at 0 V. A 1 mM concentration of the oxidised form of a 1 electron redox species was used with the diffusion coefficient set to 10^{-5} cm^2 s^{-1}. The arrow in (b) indicates the initial direction of the scan.

There are two types of peak shape which are dependent on whether the reaction rate is limited by non-steady state diffusion of the reactant to the electrode or by the surface coverage. In the first instance as the potential is swept towards the formal potential the surface concentration of reactant is rapidly decreased in accordance with the Nernst equation, resulting in a steep rise in the current density. At the standard potential, in this case 0 V, [O] and [R] are equal. As the potential continues to decrease the concentration of the reactant at the surface is lowered until it approaches zero. It is at this point the diffusion layer expands further into the bulk electrolyte resulting in a peak current, as shown in Figure 2.3.2. This decrease in current can be related to the changing concentration gradients and to the rate of the reaction as described by Fick's first and second law. These concentration profiles have been illustrated below in Figure 2.3.2.

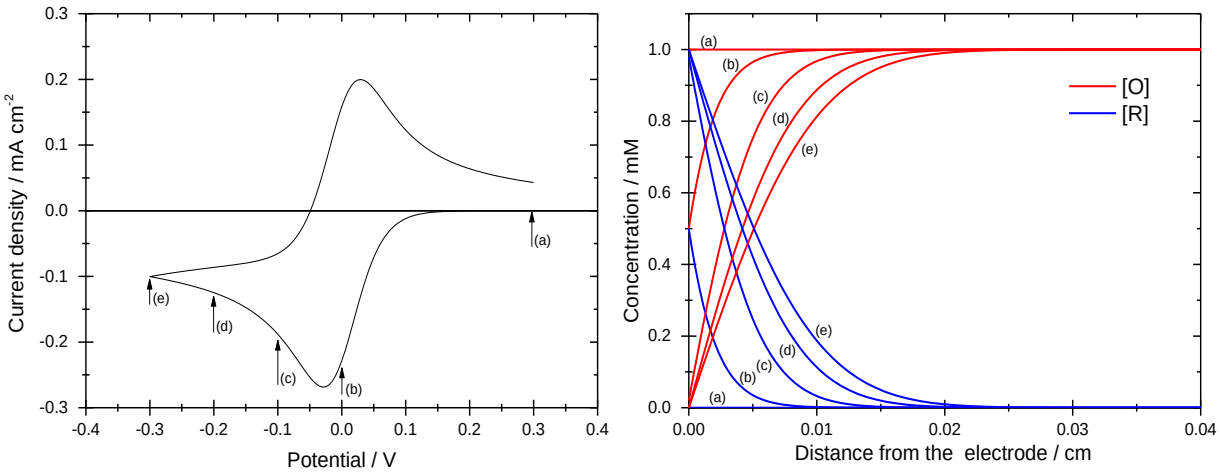

Figure 2.3.2 Cyclic voltammogram and concentration profiles simulated using Digielch software. The standard potential was set to 0 V while the sweep rate was 0.1 V s^{-1}. The initial concentration of 'O' was set to 1 mM with a diffusion coefficient of 10^{-5} cm^2 s^{-1}.

When the electrode reaction leads to the formation of a monolayer or involves the oxidation/ reduction of a layer on the surface, the peak has a different shape. The current density will again rise steeply as the scan approaches the formal potential for the reaction but once the surface is covered, or the amount of reactant consumed, the current will drop sharply decaying to zero. This provides a much more symmetrical peak shape as the current density is zero both before and after the peak. The surface coverage can be described using isotherms, the simplest of which is the Langmuir isotherm. The Langmuir isotherm assumes that the Gibbs free energy of adsorption is independent of coverage and can be written as

$$\frac{\theta}{1-\theta} = c \exp \frac{-\Delta G^{o}_{ads}}{RT}$$

Equation 2.3.7

where:

θ = Surface coverage

c = Concentration (M)

ΔG^{o}_{ads} = Gibbs free energy of adsorption (J mol^{-1})

Using this equation it is possible to produce an isotherm describing the surface coverage during an oxidative adsorption process. The associated current response can then also be calculated. Both are shown in Figure 2.3.3.

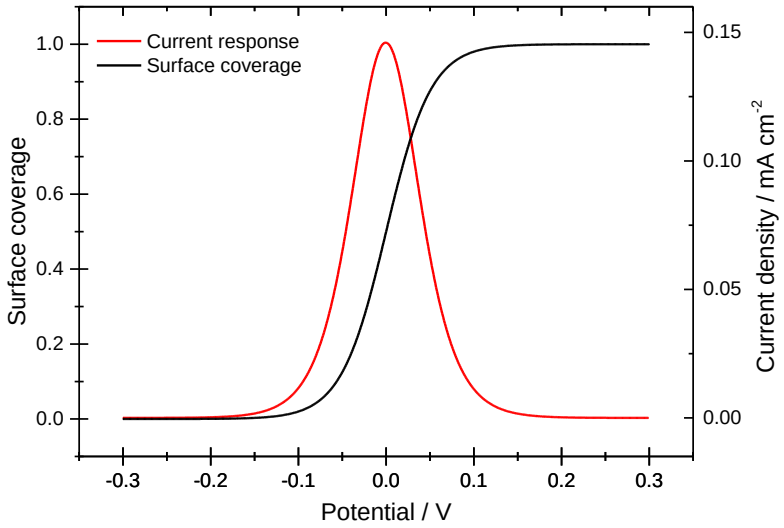

Figure 2.3.3 Langmuir isotherm and the associated current response of a surface absorbed species. Both curves produced using Equation 2.3.7 with a 100 mV s^{-1} sweep rate, and a 1 mM initial concentration.

The peak current of a solution phase reversible system using a macro electrode can be related to several factors in accordance with the Randles-Sevcik equation. Using this equation it is possible to calculate the diffusion coefficient of a species in a given electrolyte.

$$j_p = 2.69 \cdot 10^5 \cdot n^{3/2} D^{1/2} c v^{1/2}$$

Equation 2.3.8

Where:

j_p = Peak current density (A cm^{-2})

n = Number of moles of electrons transferred

c = Concentration of species (mol L^{-1})

v = Scan rate (V s^{-1})

D = Diffusion coefficient (cm^2 s^{-1})

From a plot of current vs. voltage it is possible to calculate the charge (q) by integrating under the area of the curve according to the equation:

$$q = \frac{i\Delta E}{v}$$

Equation 2.3.9

Where:

q = Charge (C)

i = Current (A)

ΔE = Change in voltage (V)

v = Scan rate (V s^{-1})

The charge can then be related to the number of moles of a given species being oxidised or reduced according to:

$$q = nFm$$

Equation 2.3.10

Where:

q = Charge (C)

n = Number of moles of electrons transferred

F = Faradays constant (96485 C mol^{-1})

m = number of moles

2.3.2 Galvanostatic Cycling

Galvanostatic cycling, sometimes called chronopotentiometry, involves the study of voltage transients at an electrode surface while applying a controlled current. In battery research it is common to alternate between positive and negative current many times in order to replicate the charging and discharging of a battery.

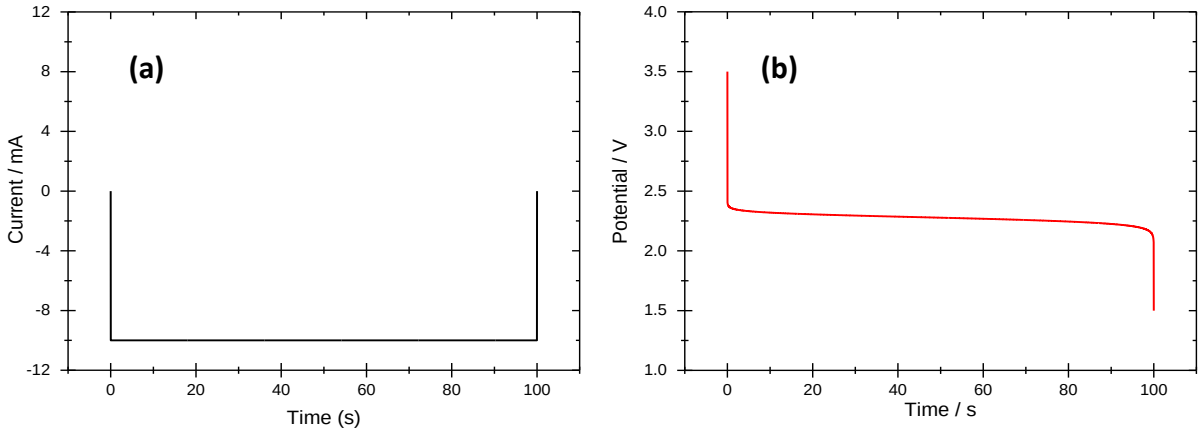

Figure 2.3.4 Galvanostatic discharge with a voltage cut off of 1.5 V modelled using the Sand equation. A transition time of 100 s was used with a quarter transition potential of 2.3 V. The applied current over time is plotted in part (a) while the measured voltage response is shown in (b).

The voltage response measured indicates the changes in the electrode processes occurring at the interface. As an example, if the oxidation of species 'R' to 'O' was being monitored by galvanostatic cycling a constant plateau would be observed at the formal potential for that oxidation. As the process continues the concentration of R at the electrode surface begins to deplete driving the diffusion of R towards the electrode surface from the bulk electrolyte. Once the surface concentration of R reaches zero the constant current can no longer be supported by the oxidation of R to O causing the voltage to increase. This can be seen by a sharp change in potential and is referred to as the transition time τ. The transition time for the electrochemical reduction or oxidation of a species for diffusion limited processes, in the presence of excess supporting electrolyte is described by the Sand

equation, which relates the transition time to the diffusion coefficient of the active species.[1]

$$\tau^{1/2} = \frac{nFAD^{1/2}\pi^{1/2}c}{2i}$$

Equation 2.3.11

Where:

τ = Transition time (s)

n = Number of moles of electrons transferred

F = Faraday constant (96485 C mol^{-1})

A = Area of electrode (cm^2)

D = Diffusion coefficient (cm^2 s^{-1})

i = Applied current (A)

The transition time can be determined provided both the diffusion coefficient and concentration of the electroactive species are known. From the transition time a charge and therefore a capacity can be calculated making this a useful tool in the modelling of battery systems. The equation for a reversible process is given below.

$$E = E_{\tau/4} + \frac{RT}{nF}\, ln \frac{\tau^{1/2} - t^{1/2}}{t^{1/2}}$$

Equation 2.3.12

Where:

E = Potential (V)

$E_{\tau/4}$ = Potential at one-quarter transition time (V)

t = Any time from zero to transition time (s)

The equation for an irreversible process is given as:

$$E = \frac{RT}{\alpha n_a F}\, ln \frac{nFCk_{app}}{i} + \frac{RT}{\alpha n_a F} \ln\left[1 - \left(\frac{t}{\tau}\right)^{1/2}\right]$$

Equation 2.3.13

Where:

n_a = Number of electrons involved in the rate determining step

k_{app} = The rate constant ($mol^{-1}\ cm^2\ s^{-1}$)

C = Concentration of reactant ($mol\ cm^{-2}$)

i = Applied current (A)

α = Transfer coefficient

2.3.3 Ohmic Effects

Forcing a current through a solution will always lead to a drop in voltage in accordance with Ohms law. This means that while current is flowing between two electrodes the potential difference will always be less than the applied potential. The actual potential difference is given by:

$$\Delta E = \Delta V - IR_{solution}$$

Equation 2.3.14

Where:

E = Actual potential difference (V)

V = Applied potential (V)

I = Current (A)

E = Potential (V)

$R_{solution}$ = Solution resistance (Ω)

The magnitude of this IR drop is clearly dependant on both the current measured throughout the experiment, the resistance of the solution between the electrodes and the cell geometry. Therefore, the magnitude of the IR drop will be strongly dependant on the concentration of the active species and the scan rate. If current can be kept low and the electrolyte is a good conductor then it is possible to work using a two-electrode cell, where the counter and reference electrodes are combined. The combined counter/reference electrode must be able to deliver a high current without changing the potential. If this is not possible then a 3-electrode arrangement will be required so there is no current flowing between the working and reference electrodes. This reduces much of the IR drop from the measured potential.

In the case of galvanostatic cycling the IR drop is much easier to interpret as the current is fixed. The IR drop can be seen at the point where the current is first applied. There will be a sharp vertical drop in the potential before the steep curve leading to the plateau. This initial voltage change can be attributed to the IR drop. As the current is known it is also possible to use this to calculate the resistance of the solution.

2.3.4 Differential Electrochemical Mass Spectrometry

Mass spectrometry enables us to analyse the compounds present in, or evolved from a system. This is a highly sensitive technique capable of detection at partial pressures as low as to 5x 10^{-14} Torr. Combining this with electrochemical techniques for *in-operando* measurements is a powerful tool for identifying the reactions taking place within a cell.[37,51,115] The process of mass ion detection can be broken down into three key stages: Ionisation, Mass Filtration and Detection.

Step 1: Ionisation

Gas molecules are typically ionised by electron impact ionisation. The filaments inside the ion source are used to create an electron beam via thermionic emission. These electrons can then remove electrons from the gas particles generating positive ions. The positive ions generated by the filaments are then extracted from the source cage by a focus plate which is held at -90 V. Electrons are repelled by the focus plate preventing them from entering the detector. The figure below illustrates this process.

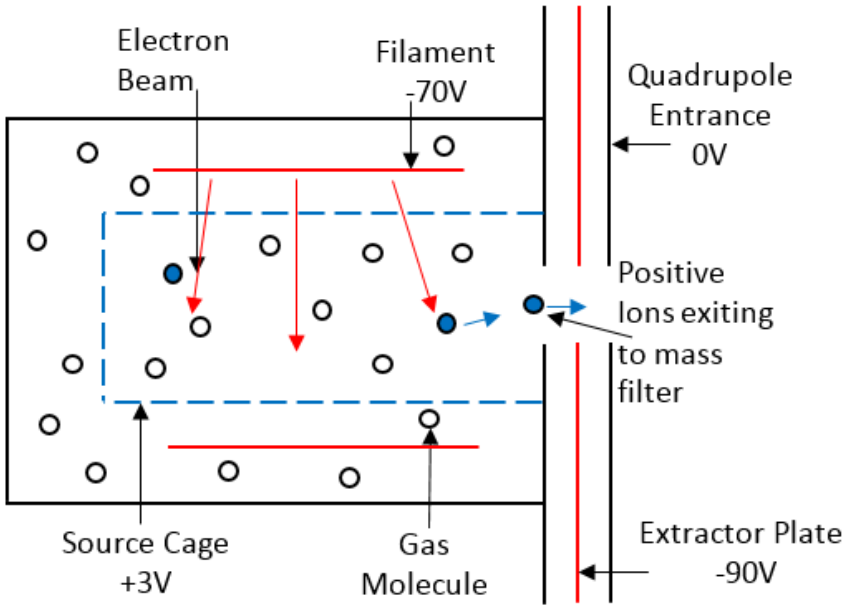

Figure 2.3.5: Electron impact ionisation

Step 2: Mass Filtration. The mass filter differentiates the ions produced selecting a specific mass/charge ratio for detection. A quadrupole detector is used in these experiments which consists of two pairs of parallel equidistant metal rods at equal but opposite potentials. These potentials then alternate at varying radio frequency components. Any ions entering the field experience potential differences deflecting them from their original trajectory. The extent of the deflection is dependent on its mass/charge ratio. At each interval only one mass/charge ratio resonates with the alternating electric field allowing it to pass through to the detector.

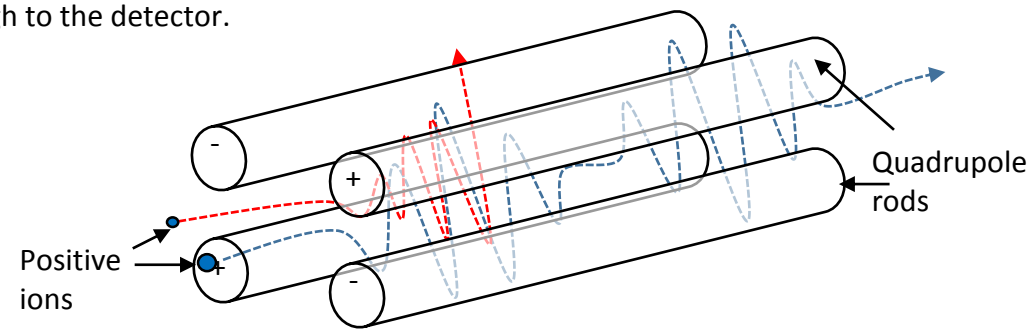

Figure 2.3.6 Quadrupole mass filtration

Step 3: Detection. The filtered ions then strike the detector assembly and the ion current produced is measured by a sensitive amplifier. There are two main types of detector, the Faraday cup and the secondary electron multiplier. The Faraday cup is a conducting surface which when struck by fast moving ions causes a shower of secondary electrons. The cup shape allows these electrons to be collected. While only one electron is required to neutralise the ion, the emission of several provides amplification for the instrument. The secondary electron multiplier uses a surface designed to generate secondary electrons. Once the ion hits the surface two or three electrons are generated, each going on to emit more electrons in a cascade effect leading to greater amplification. This gives a detection limit of up to 10^{-14} Torr compared to 10^{-11} Torr for the Faraday cup.

In order to gain experience working with DEMS systems, some preliminary experiments were carried out at Bonn University, Germany. The cell utilised a teflon membrane which functions to separate the electrolyte from the vacuum while remaining permeable towards volatile compounds formed at the electrode surface. The details of the cell design are shown below in Figure 2.3.7. In order to minimise the contamination of the cell it was continuously purged with oxygen. All experiments were carried out using a gold disc working electrode (A = 0.3 cm^2) a gold wire counter electrode and a Ag/Ag^+ reference electrode (+3 V vs. Li/Li^+). Cyclic voltammograms were then collected while the mass spectrometer monitored the flow of oxygen, carbon dioxide and other possible organic fragments.

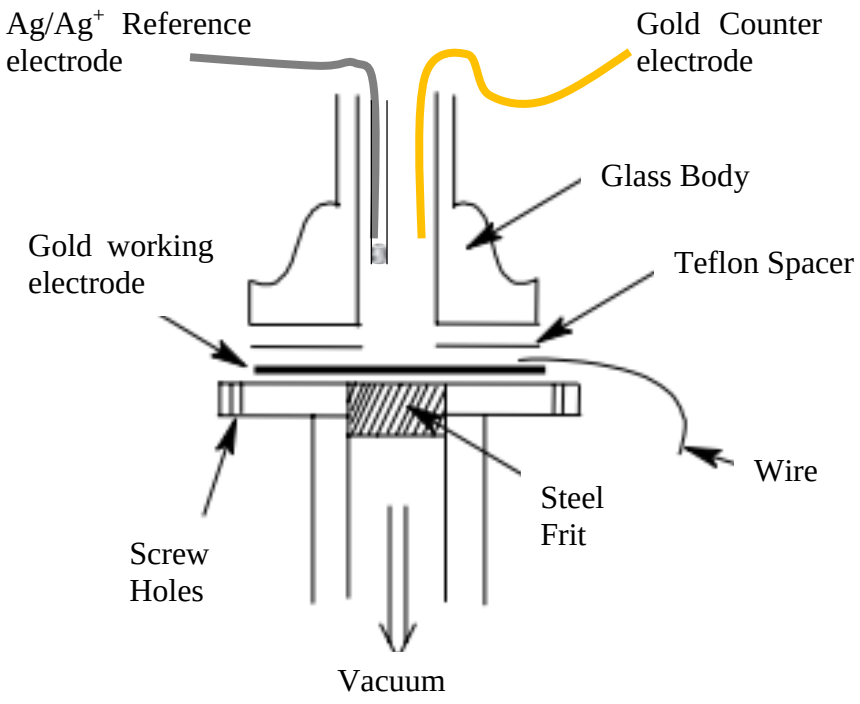

Figure 2.3.7 Design of the teflon membrane electrochemical cell which was coupled to a mass spectrometer for DEMS measurements.

For the subsequent experiments performed in Southampton a carrier gas assembly was employed. This relied upon flowing gas over the cell at a known rate, any changes in the gas composition as a result of the cells behaviour would then be detected by the mass spectrometer. To study the behaviour of lithium-oxygen cells it was necessary to use a mixture of both argon and oxygen. This way, any changes in the partial pressure of oxygen could be detected relative to the argon. Mass flow controllers (Bronkhorst, EL Flow®) were employed to achieve a fixed flow rate of 0.5 mL min^{-1} of argon and 0.5 mL min^{-1} of oxygen, giving a total flow rate of 1 mL min^{-1}. The mass spectrometer itself had a sample rate of 0.8 mL min^{-1} leaving the remaining 0.2 mL min^{-1} to leave the system via the outlet. Each gas line had a dedicated cylinder which was connected to the flow meters using 1/8" stainless steel piping (Swagelok). The same piping was used to connect the electrochemical cell, mass spectrometer and outlet to minimise the possibility for water contamination.

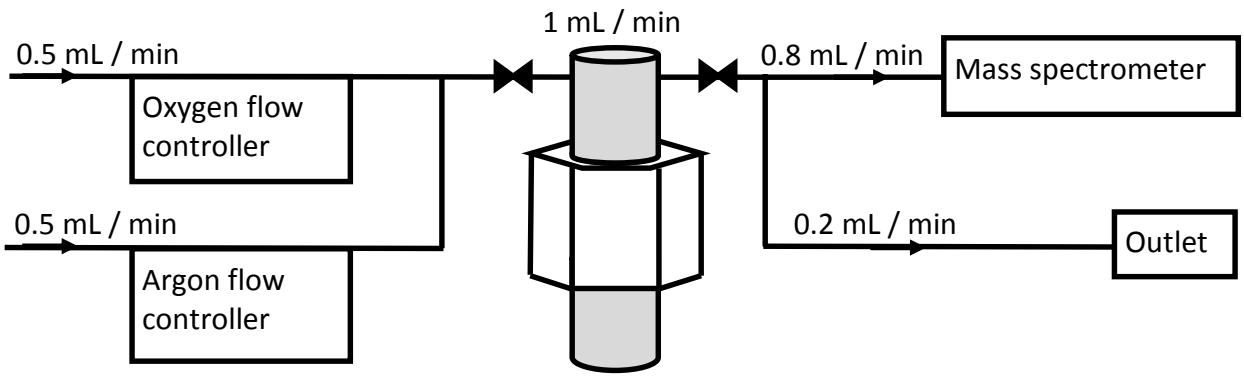

Figure 2.3.8 Schematic of the differential electrochemical mass spectrometry (DEMS) gas flow rig.

2.3.5 Powder X-Ray Diffraction

Powder X-ray diffraction is a technique used to determine the purity and structure of a crystalline material. X-rays of a single frequency are fired at the sample and as the radiation passes through the crystal lattice it undergoes constructive and deconstructive interference according to the Bragg equation shown below in Equation 2.3.15.

$$\lambda = 2d_{hkl}\, sin\theta$$

Equation 2.3.15

Where:

λ = Wavelength (nm)

d_{hkl} = Lattice spacing

θ = Angle of incidence (degrees)

This law relates the wavelength of the X-ray beam, to the diffraction angle and the lattice spacing in the crystalline sample. Constructive interference occurs between the X-rays when the difference in distance travelled is an integer multiple of the wavelength. When there is constructive interference there is a peak in the X-ray intensity observed at the detector. This principle is displayed in Figure 2.3.9.

In powder X-ray diffraction the sample is exposed to a single wavelength of X-rays as the angle of incidence is swept between two limits, typically between 0 and 90 degrees. In a crystalline lattice the spacing between particles is fixed meaning that only at certain angles will the constructive interference be observed. If the crystallites making up a powdered sample are small, the width of the peaks observed are inversely proportional to the crystallite size. The Scherrer equation is related to this theory.[116]

$$\beta = \frac{k\lambda}{\varepsilon \cos\theta}$$

Equation 2.3.16

Where:

β = Peak width at half maximum intensity (rad)

k = Correction factor to account for particle shapes

λ = X-ray wavelength (nm)

ε = Average crystalline size (nm)

θ = Bragg angle (rad)

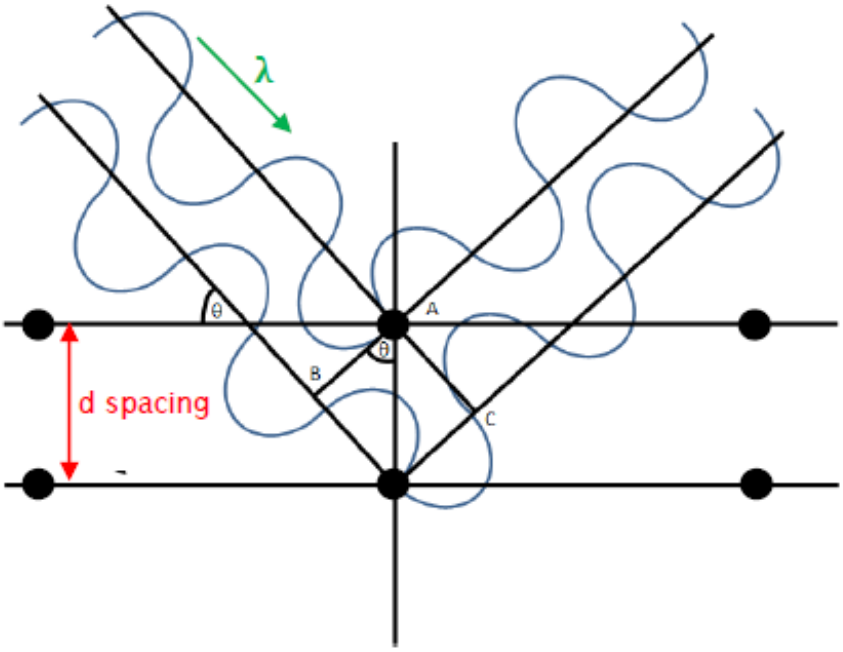

Figure 2.3.9 Schematic describing the principles of the Bragg equation. Where the distance travelled from AB to AC must be an integer number of wavelengths for constructive interference.

In order to carry out X-ray diffraction measurements, a hemispherical air tight sample holder was used (Bruker, A100B33). Discharged electrodes could then be removed from their cell inside the glove box and transferred to this X-ray sample holder to ensure the sample remained in an inert atmosphere. When using Celgard electrodes a silicon wafer was used to position the sample at the correct height. All X-ray diffraction measurements were performed on a Rigaku SmartLab instrument with a copper X-ray source using grazing incidence. The 2-theta angle range was set to scan from 0 to 60 degrees using a 1 second dwell and a 0.2 degree 2-theta increment.

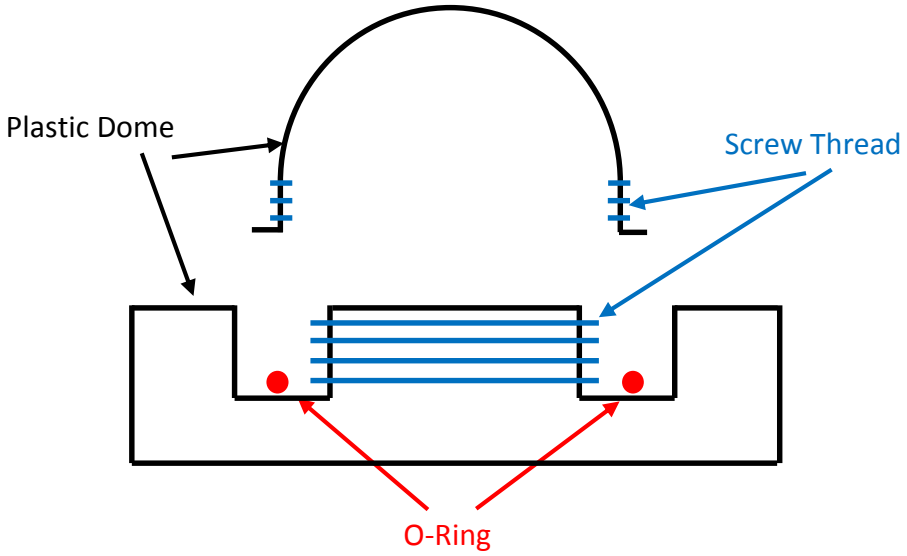

Figure 2.3.10 X-ray diffraction sample holder for air sensitive materials.

Chapter 3: Cyclic Voltammetry of Oxygen Reduction and Evolution

3.1 Introduction

The cyclic voltammetry of oxygen reduction in non-aqueous electrolytes has been shown to be fast and reversible.[28,71] However, the fast kinetics have been shown to be strongly affected by the cations present in the electrolyte. Upon the addition of lithium ions this reversibility decreases rendering the reaction electrochemically irreversible.[28,30] This results in a large overpotential for the reduction and evolution of oxygen when lithium ions are present. In the case of the lithium-oxygen battery, this will dramatically hinder the overall efficiency of an operational cell. The cycle life of lithium-oxygen cells has also been shown to be poor due to the accumulation of the poorly conducting and insoluble lithium peroxide discharge product.[37,58,117]

Using cyclic voltammetry the formal potential of oxygen reduction can be identified in the chosen electrolyte. This electrolyte has been chosen due to the demonstrated stability of glymes towards the superoxide radical and their high oxygen solubility and lower viscosity when compared with ionic liquids, while a non-aqueous electrolyte was chosen due to the instability of lithium metal towards water.[39,70,71] The overpotentials associated with the reduction and evolution can also be determined using cyclic voltammetry. This will facilitate the identification of soluble redox mediators based on the experimentally determined potential range. It is hoped that by using redox mediators both the applied overpotential and the maximum discharge/charge rates of the lithium-oxygen battery can be improved.

3.2 Experimental

3.2.1 Electrochemical Techniques

This chapter is comprised of cyclic voltammetry measurements performed using a Bio-Logic VMP2 (variable multi-channel potentiostat). This technique is discussed in detail in Chapter 2.

3.2.2 Cell Design

All experiments used a glassy carbon working electrode (Ø = 3 mm) which was polished using 0.3 µm aluminium oxide powder between measurements. Cells were assembled under an argon atmosphere (H_2O < 0.5 ppm, O_2 < 0.5 ppm) before purging with oxygen.

3.2.3 Chemical Preparation

Electrolytes were dried and prepared as described in Chapter 2.

3.3 Results and Discussion

3.3.1 Cyclic Voltammetry of Oxygen Reduction and Evolution

In order to understand how mediators might affect the cycling behaviour of the lithium-oxygen system, it is important to first look at the unmediated system. Cyclic voltammograms of oxygen reduction and evolution in a 0.2 M LiTFSI diglyme electrolyte were recorded. The voltammetry in argon was also measured to determine the stability and purity of the electrolyte. Below in Figure 3.3.1, the voltammogram in both argon (black trace) and oxygen (red trace) is shown. The argon trace displays no faradaic currents between 1.5 and 4.5 V vs. Li/Li^+ indicating that the diglyme electrolyte used is stable within these limits as found in previous work.[118,119]

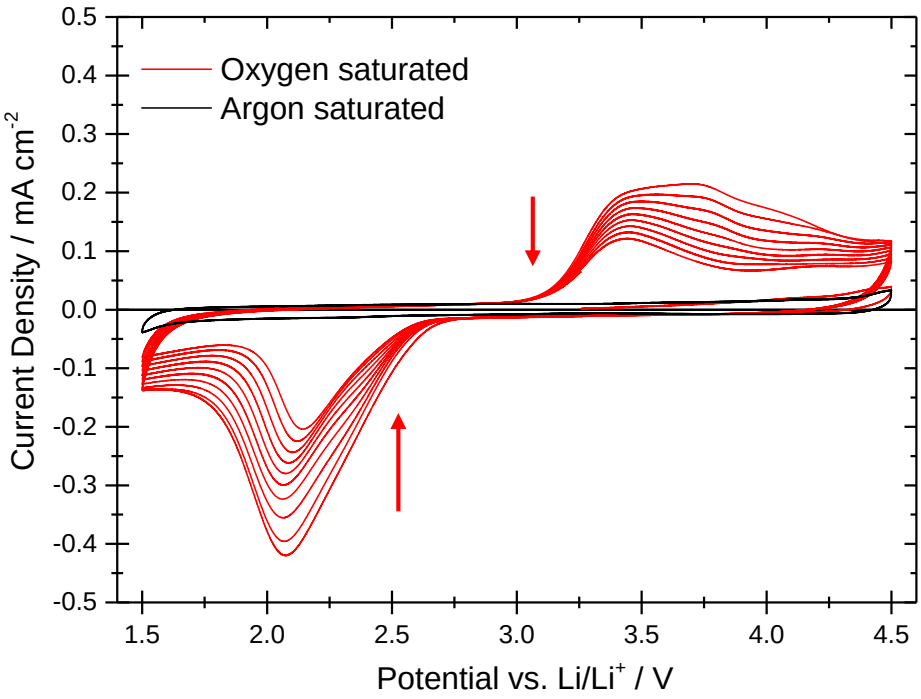

Figure 3.3.1 Cyclic voltammograms of a glassy carbon electrode (Ø = 3 mm) in a 0.2 M LiTFSI diglyme electrolyte under an argon saturated (black) and an oxygen saturated (red) atmosphere. A scan rate of 100 mV s^{-1} was applied using a lithium metal counter/reference electrode.

Once the atmosphere in the cell is exchanged with oxygen two distinctive peaks can be observed. The first starts after the potential is swept negative of 2.6 V vs. Li/Li^+. After this the current steadily rises reaching a peak at 2.1 V vs. Li/Li^+. This peak can be attributed to the reduction of dissolved molecular oxygen present in the electrolyte to produce lithium peroxide.[65,120] As the potential is swept in the reverse direction no current was observed until after the potential passes 3.0 V vs. Li/Li^+. At this point a broad peak was observed representing the decomposition of lithium peroxide back to oxygen.[14,121] Beyond 4.0 V vs. Li/Li^+ it has been shown that the carbon electrode can react with the lithium peroxide forming lithium carbonate. This can subsequently be decomposed electrochemically yielding carbon dioxide.[37]

The total charge passed during reduction is calculated to be 0.20 mC whereas the total charge passed during oxidation is 0.17 mC. This charge imbalance is repeated on each subsequent cycle at consistently 84-85% resulting in the accumulation of the discharge product near the electrode surface. As the electrode continues to be cycled the peak current decreases steadily. This passivation of the electrode surface is a significant obstacle in the development of a commercial lithium-oxygen battery. The use of solution based redox mediators is a promising solution for the high overpotentials currently employed when charging lithium-oxygen cells. Mediators of the discharge reaction could be used to move the site of peroxide formation into solution preventing the surface from being blocked. Whereas an effective charging mediator would facilitate a complete charge on each cycle, clearing the electrode surface therefore eliminating the electrode passivation problem.

In order to ensure these measurements were accurate a second scan was taken using a separate electrode. Electrodes could be exchanged while bubbling O_2 relying on the positive pressure of the cell to prevent contamination. An example of the reproducibility of these measurements is shown below in Figure 3.3.2. These results demonstrate that despite using different electrodes the two current traces are virtually identical. The polishing of electrodes between each measurement was essential to obtain reproducible results due to the formation of solid lithium peroxide at the electrode surface.

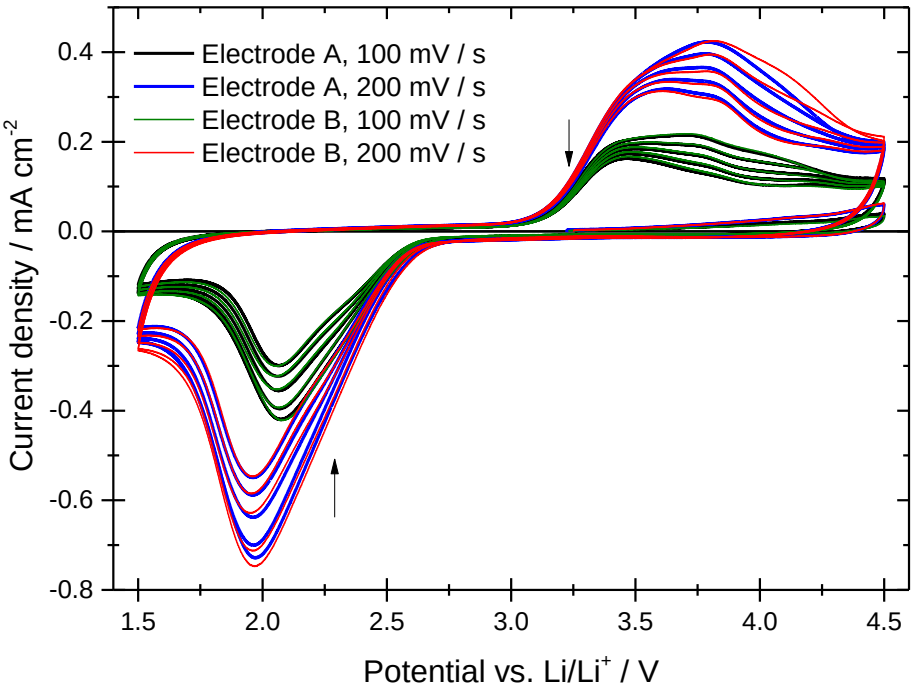

Figure 3.3.2 Cyclic voltammograms of glassy carbon electrodes A and B (Ø = 3 mm) in an oxygen saturated 0.2 M LiTFSI diglyme electrolyte. A lithium metal counter/reference electrode was used.

In Figure 3.3.3 cyclic voltammograms of oxygen reduction and evolution at a glassy carbon electrode using various scans rates are shown. One benefit of using multiple scan rates is that a more accurate estimation of the formal potential can be obtained. At higher scan rates the peak current increases and the peak potential can be seen to shift to more extreme values. This is due to a combination of the IR drop, which can be expected when using a two electrode arrangement, and the kinetics effects resulting from slow electron transfer.

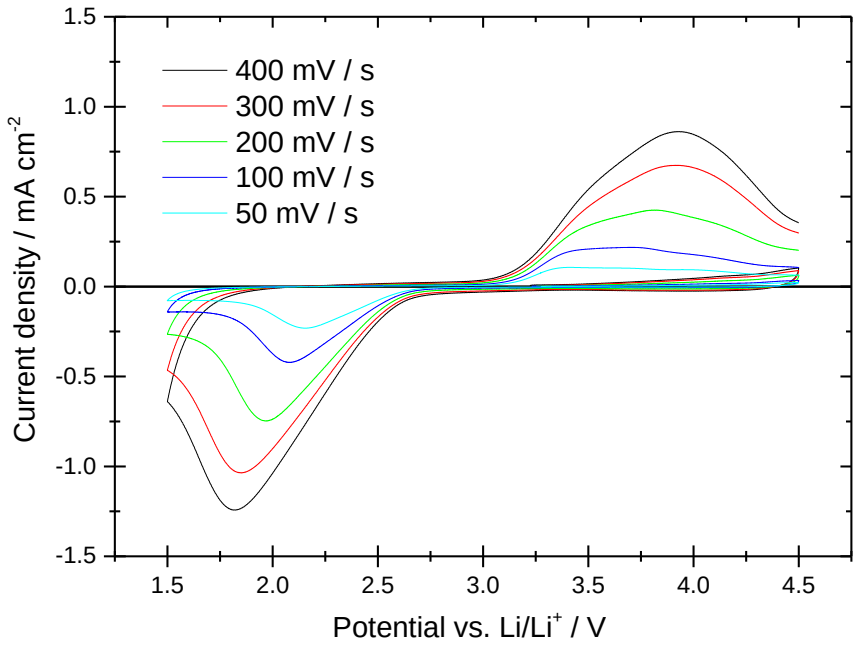

Figure 3.3.3 Cyclic voltammograms of a glassy carbon electrode (Ø = 3 mm) in an oxygen saturated 0.2 M LiTFSI diglyme electrolyte. The scan rate was varied from 50 mV s^{-1} to 400 mV s^{-1} using a lithium metal counter/reference electrode.

By plotting a graph of peak potential vs. peak current it is possible to find the peak position without the effect of IR drop or kinetic effects. The y-axis intercept of the reduction and oxidation process can be used to calculate the formal potential. This graph is shown in Figure 3.3.4. The formal potential is calculated as half way between the anodic and

cathodic peaks. Based on these experiments it is calculated to be 2.97 V which is in line with previous calculations.[14]

$$\frac{3.72\,V\ +\ 2.22\,V}{2} = 2.97\,V$$

Equation 3.3.1

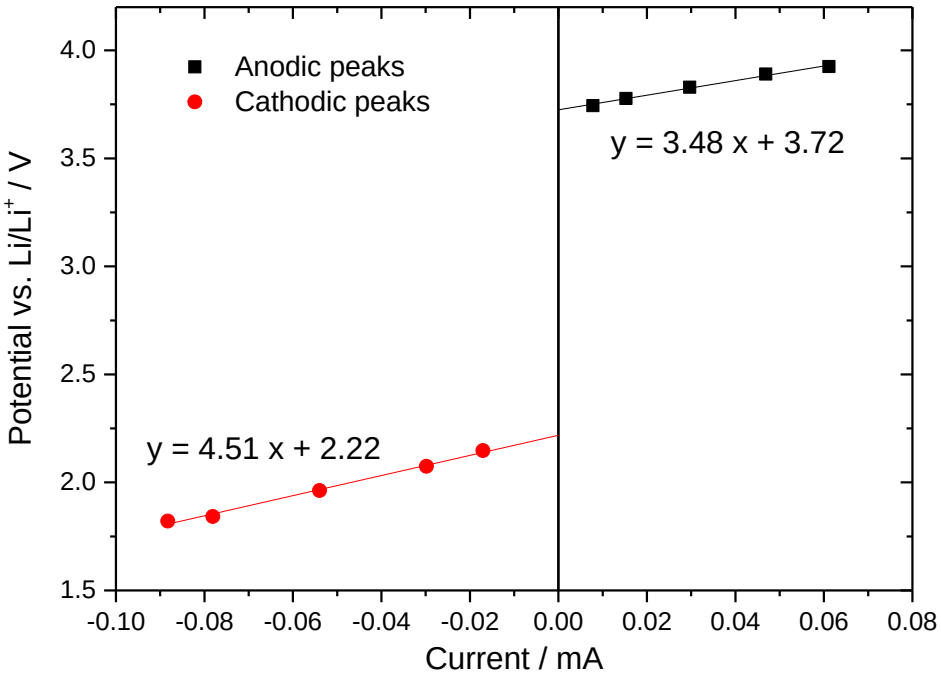

Figure 3.3.4 The peak potentials of the above voltammograms were plotted against the peak current to obtain the formal potential and internal resistance of the system.

AC electrochemical Impedance spectroscopy can be used to determine the internal resistance of a system. Impedance measurements collected using the same experimental set up provide an approximate value of 2300 ± 300 Ω for the internal resistance of the system. These results are included in Appendix A. This is higher than literature based values for the resistivity of this solvent which can be attributed to the glass frit employed to isolate the two electrolyte compartments.[122,123] These calculations are detailed further in Appendix A.

Another interesting comparison that can be drawn using these results is to compare the peak current on reduction and oxidation after normalising to the scan rate. For a solution based process this is expected to be proportional to $v^{1/2}$, shown in Figure 3.3.5 (a). In the case of a surface based reaction the change in peak current will be linear with respect to the scan rate, as shown in Figure 3.3.5 (b). The reduction current of oxygen dissolved in the electrolyte is initially the same for all scan rates when normalised by $v^{1/2}$. After a consistent amount of charge has passed ~100 µC there is a peak and the current begins to decay. This is likely due to the surface coverage of the lithium peroxide product inhibiting further deposition. Given the approximate value of one monolayer equalling 150 µC cm^{-2} and the surface area of the electrodes used (0.071 cm^2), approximately 9 monolayers of lithium peroxide are formed at the peak of oxygen reduction.[1] Beyond this, the rate of oxygen reduction slows with each scan rate forming approximately 16 monolayers in total during the negative sweep on the first cycle.

The oxidation processes normalised by v in Figure 3.3.5 (b) indicate the oxidation of a surface based species. This indicates that the peroxide formed during the negative sweep remains at the electrode surface until it is oxidised in-line with the electrode passivation behaviour described earlier. While the peak current values at all scan rates are very similar in Figure 3.3.5 (b) there is a shift to more extreme potentials with increasing scan rate. This can be attributed to the increasing current resulting in an increased IR drop.

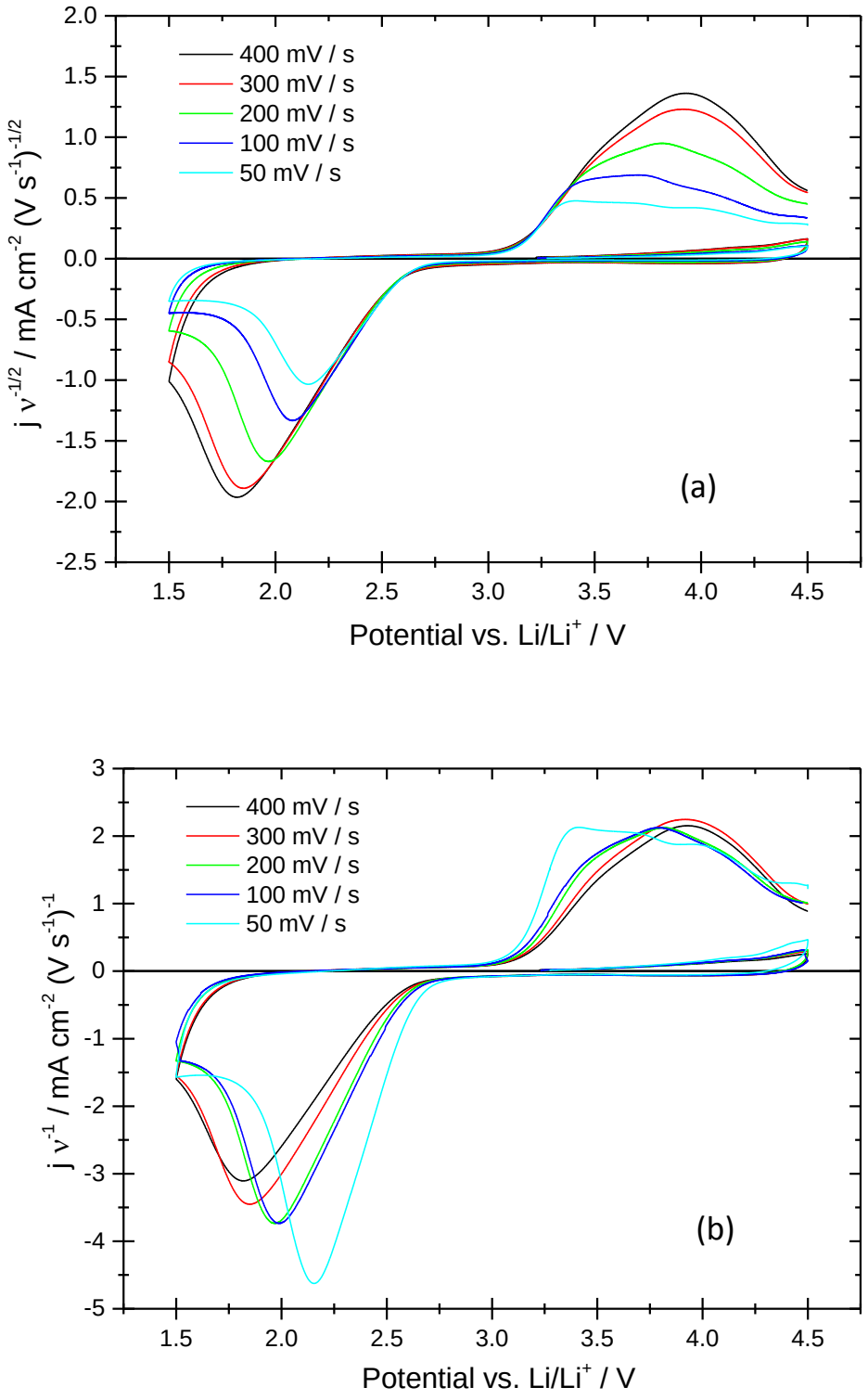

Figure 3.3.5 Cyclic voltammograms of a glassy carbon electrode (Ø = 3 mm) in an oxygen saturated 0.2 M LiTFSI diglyme electrolyte. A lithium metal counter/reference electrode was used with various scan rates. The current density was then normalised by the square root of scan rate (a), and by the scan rate (b).

Given the formal potential of 2.97 V vs. Li/Li^+ that means an overpotential of ~ 0.7 V is required to drive these reactions at a significant rate. A successful mediator will undergo an electron transfer reaction between the formal potential and the peak potential. A final point of interest with these voltammograms is the effect of IR drop on the shape of the curves. With a relatively large solution resistance of 2.3 kΩ a significant distortion of the peak positions especially at high scan rates is to be expected. Correcting the measured voltage can be done using the following equation as discussed in Chapter 2, where 'E' is the applied voltage and 'V' is the voltage measured by the potentiostat.

$$\Delta E = \Delta V - IR_{solution}$$

Equation 3.3.2

The previously calculated value of 2.3 kΩ was used to correct the recorded voltammograms shown previously. The results for the first cycle at different scan rates are shown in Figure 3.3.7. As a result of the correction, the peak potential for oxygen reduction occurs between 2.0 and 2.2 V vs. Li/Li^+ at different scan rates with the remaining offset the result of the slow electron transfer kinetics. Combining this voltage correction with the peak current normalisation yields Figure 3.3.7. Here the overlapping oxidation profiles at different scan rates can clearly be seen. While is a clear trend in the peak shift moving from lower to higher scan rates due to the slow electron transfer this is good evidence that the oxidation peak current is linearly dependant on the scan rate and therefore is a surface based mechanism.

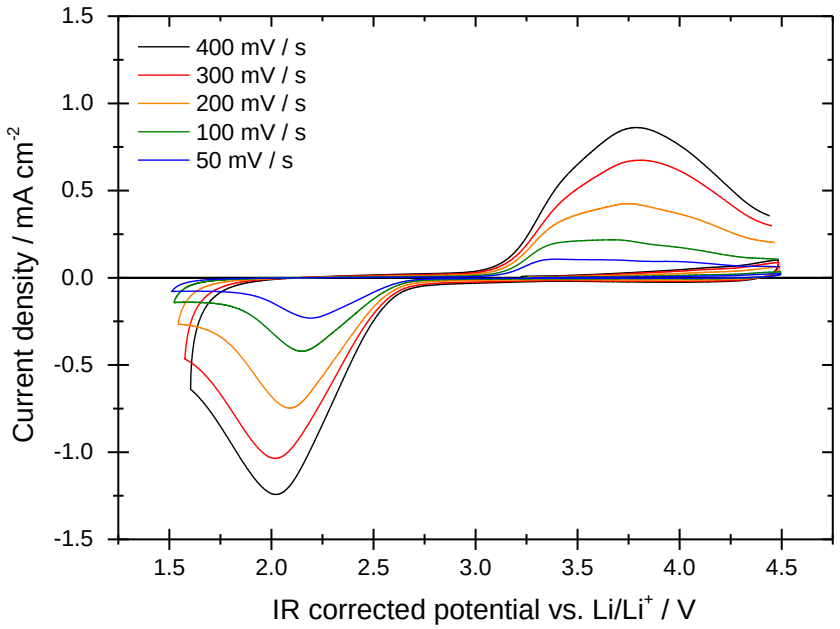

Figure 3.3.6 Cyclic voltammograms of a glassy carbon electrode (Ø = 3 mm) in an oxygen saturated 0.2 M LiTFSI in diglyme electrolyte were recorded at different scan rates. The applied potential has been corrected for IR drop using the previously calculated value of 2.3 kΩ. A lithium metal counter/reference electrode was used.

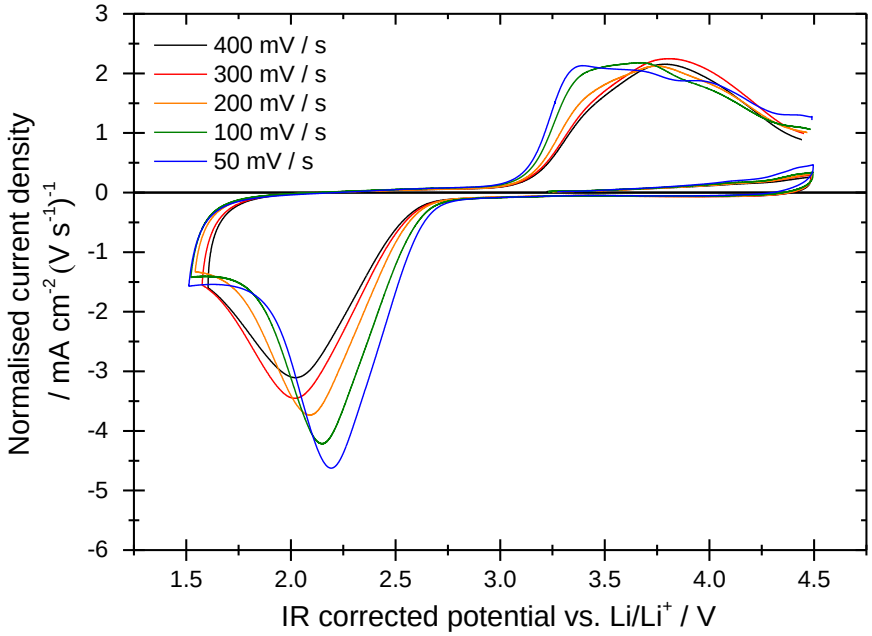

Figure 3.3.7 Cyclic voltammograms of a glassy carbon electrode (Ø = 3 mm) in an oxygen saturated 0.2 M LiTFSI in diglyme electrolyte were recorded at different scan rates. The applied potential has been corrected for IR drop using the previously calculated value of 2.3 kΩ and the recorded current normalised by the scan rate. A lithium metal counter/reference electrode was used.

3.4 Conclusions and Future Work

The electrochemical behaviour of oxygen in a non-aqueous lithium salt containing electrolyte was examined by cyclic voltammetry. The oxygen evolution current was demonstrated vary linearly with the scan rate indicating it is a surface based process. While the reduction reaction was shown to be dependent on the surface coverage, reaching a peak after 9 monolayers of lithium peroxide had formed. There is a consistent charge imbalance where only 85% of the total charge passed during the negative sweep is obtained on the positive sweep. This imbalance leads to the passivation of the electrode surface over subsequent cycles. As a two electrode arrangement was used, the measurements were subject to IR drop. Correcting for this IR drop, the formal potential was determined to be 2.97 V vs. Li/Li^+ with each reaction requiring an overpotential of 750 mV. The voltage efficiency of a lithium-oxygen battery must be greatly improved by lessening this overpotential for it to be a viable energy storage system. To further investigate the oxygen reduction and evolution reactions in a lithium salt containing electrolyte, the reaction products should be determined through the use of XRD and Raman spectroscopy. Due to the small charges passed during cyclic voltammetry it may be more appropriate to utilise a constant current technique such as galvanostatic cycling to pass a greater charge thus improving the chance of detection. Any crystalline products can then be identified by XRD while any amorphous products will be detected by Raman spectroscopy. An additional method that has been proven to be very powerful in quantifying the moles of oxygen consumed and evolved during cell cycling is differential electrochemical mass spectrometry[51,69,115]. To improve upon the high overpotentials required, the use of soluble mediators has been suggested and is looked at in detail in Chapters 4,5 and 6.[52,82]

Chapter 4: Cyclic Voltammetry of Substituted Quinones

4.1 Introduction

Quinones were evaluated using cyclic voltammetry to determine which were most likely to function as effective mediators for the discharge or charge reactions in a lithium-oxygen battery. The most important quinone characteristics to assess were the formal potentials of the 1st and 2nd electron transfers and how electrochemically reversible each of those peaks were. The redox potential for the electron transfer reaction must sit between the formal potential for the reduction of oxygen (2.96 V vs. Li/Li^+) and the observed peak potential. This will ensure that the mediator is sufficiently reducing to reduce oxygen to superoxide while still being able to lessen the required overpotential to drive the reaction.

Quinones were identified as a possible compound for mediating either the oxygen reduction or evolution reaction. The formal potential of oxygen reduction to lithium peroxide is given as 2.96 V vs. Li/Li^+.[14,124] Quinones with a formal potential lower than this could be expected to mediate the oxygen reduction reaction while quinones with a formal potential higher than 2.96 V vs. Li/Li^+ could be expected to mediate the oxygen evolution reaction. Studies have looked at the formal potentials of quinones in various non-aqueous electrolytes such as acetonitrile, DMSO and propylene carbonate.[100,101,103,104] However, there is less information on the use of quinones in a diglyme electrolyte or in the presence of a lithium salt. Initial experiments were performed using 1,4-napthoquinone to provide a benchmark from which to estimate the formal potentials of other quinones based on their relative literature values in other solvents.

4.2 Experimental

4.2.1 Experimental Techniques

This chapter is comprised of cyclic voltammetry measurements performed using a Bio-Logic VMP2 (variable multi-channel potentiostat). This technique is discussed in detail in Chapter 2.

4.2.2 Cell Design

All experiments were carried out using the two compartment U-cell. The cell design was chosen to allow the separation of the organic quinone compounds from the highly reducing lithium metal counter reference electrode. All experiments used a glassy carbon working electrode (Ø = 3 mm) which was polished using 0.3 µm aluminium oxide powder between measurements. In the case of oxygen atmosphere measurements the cell was continuously purged with oxygen while the electrode was polished.

4.2.3 Chemical Preparation

Electrolytes were dried and prepared as described in Chapter 2. All quinones with the exception of 2,3-dichloro-5,6-dicyano-1,4-benzoquinone (DDQ) were dried at room temperature for 12 hours under a vacuum before transferring into an argon filled glove box. DDQ was used as received due to its low stability at room temperature.

4.3 Results and Discussion

4.3.1 Cyclic Voltammetry of Quinones

In order to identify a compound capable of undergoing a reversible electron transfer within the desired potential range, a family of compounds well known for exhibiting fast electron transfer was selected. Quinones have been used previously in electrochemistry to function as mediators in a number of biological and electrochemical processes.[73,125,126] One of the more fundamental quinones is 1,4-napthoquinone (structure shown in Figure 4.3.1). This was used as a starting point to assess the redox potential of quinones in the desired electrolyte.

Figure 4.3.1 displays a cyclic voltammogram recorded at 100 mV s^{-1} between 4.5 V and 1.5 V vs. Li/Li^+ for 5 cycles. The results contain the characteristic two step reduction to form the dianion on the negative sweep, as indicated by the red and blue arrows.[103,104] When the potential is swept positively the oxidation from the dianion back to the semi-quinone (green arrow) has a significant overpotential, while the subsequent oxidation to the neutral quinone (black arrow) appears far more reversible. Where the potential is swept between 2.0 and 1.5 V vs. Li/Li^+ there are no additional faradaic processes indicating the quinone is stable to further reduction. While on the oxidative sweep no further reaction is observed up to 4.5 V vs. Li/Li^+ after the quinone is oxidised. This wide stability window is important if the quinone is to perform at the potentials required to charge and discharge a lithium-oxygen cell. The consistent peak shapes and sizes over multiple cycles also indicate that the reduced forms of the quinone are stable. The experimental results of varying the sweep rate are shown in Figure 4.3.2.

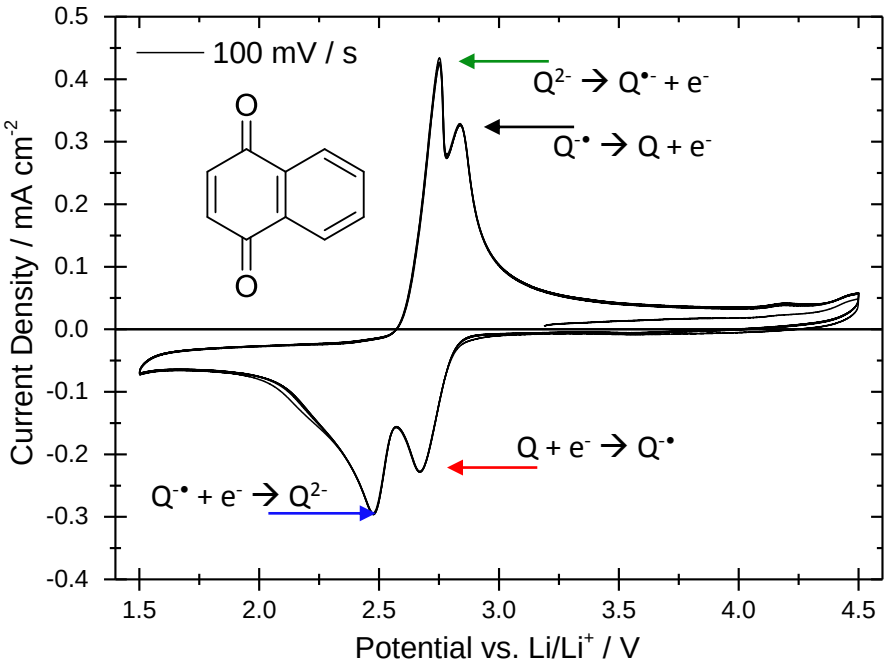

Figure 4.3.1 Cyclic voltammogram of a glassy carbon electrode (Ø = 3 mm) in a 1 mM 1,4-napthoquinone (structure shown) containing 0.2 M LiTFSI diglyme electrolyte recorded at 100 mV s^{-1}. A lithium metal counter/reference electrode was used. The potential began at open circuit, was swept to 4.5 V then returned to 1.5 V for 5 cycles.

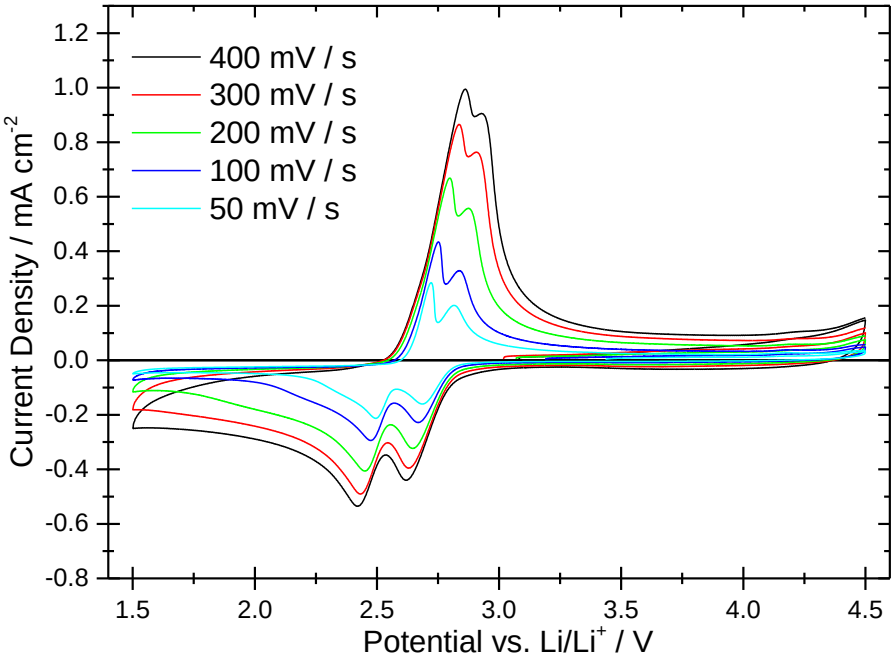

Figure 4.3.2 Cyclic voltammograms of a glassy carbon electrode (Ø = 3 mm) in a 1 mM 1,4-napthoquinone containing 0.2 M LiTFSI diglyme electrolyte recorded at different sweep rates. A lithium metal counter/reference electrode was used. The potential began at open circuit, was swept from open circuit to 4.5 V then down to 1.5 V before finally returning to 4.5 V.

The voltammograms at different scan rates all show the two redox couples which is typical for quinones.[100,104] The first electron reduction again appears much more reversible than the second. Peak to peak separations of 20 mV and 100 mV can be calculated for the first and second redox couples respectively, this was done by extrapolating a plot of peak potential vs. peak current. The value of 20 mV is too low for a reversible solution based mechanism and could be due to the effect of surface processes. This plot for napthoquinone and the other quinones are shown in Figure 4.3.3. The formal potential can then be calculated as half way between the anodic and cathodic peak. The formal potentials and diffusion coefficients for each of these quinones are listed in Table 4.3.1. Based on these values it can be determined that only the first electron transfer is electrochemically reversible in the presence of lithium ions. This is in line with previously reported results conducted in electrolytes not containing lithium.

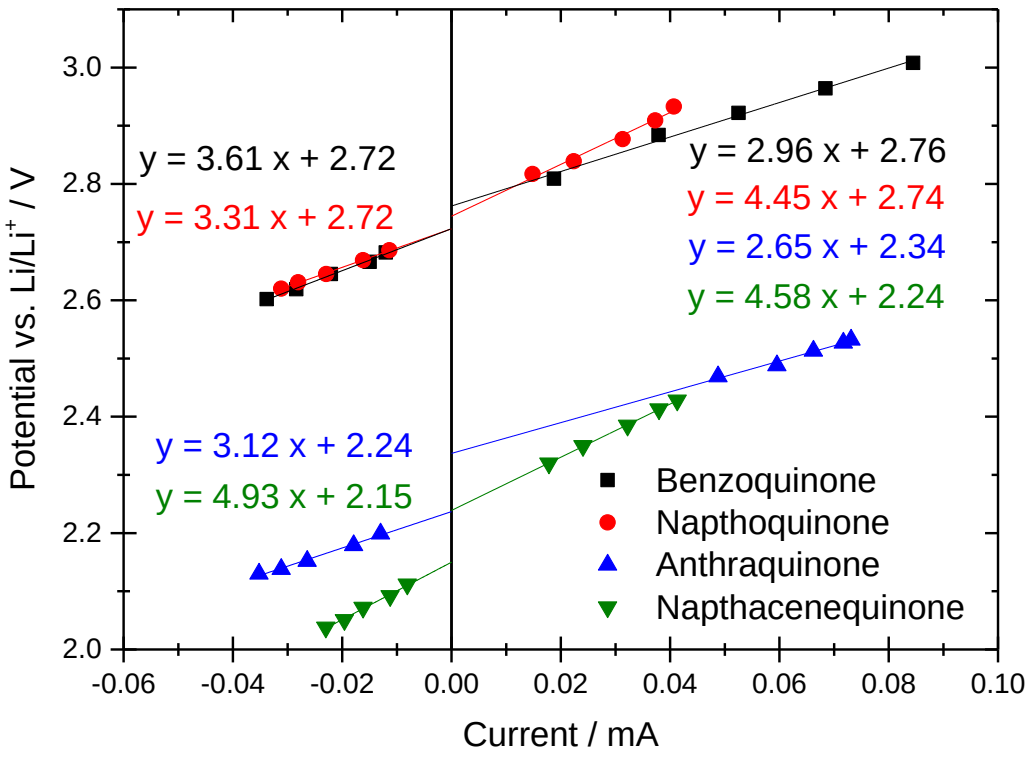

Figure 4.3.3 Plots of peak potential vs. peak current to obtain the formal potential of the first electron transfer for several quinones and the internal resistance of the cell.

The diffusion coefficient was calculated to be 7.1 x 10^{-6} cm^2 s^{-1} and was determined using the Randles-Sevcik equation and Figure 4.3.4 below. Gradients for each of the other quinones tested in this section are also shown. The full calculation can be found in Appendix B and the diffusion coefficients for each quinone is included in Table 4.3.1. As the Randles-Sevcik equation used assumes reversible electrochemistry and the quinone electrochemistry is not reversible and subject to IR drop, these values are likely to contain some error.

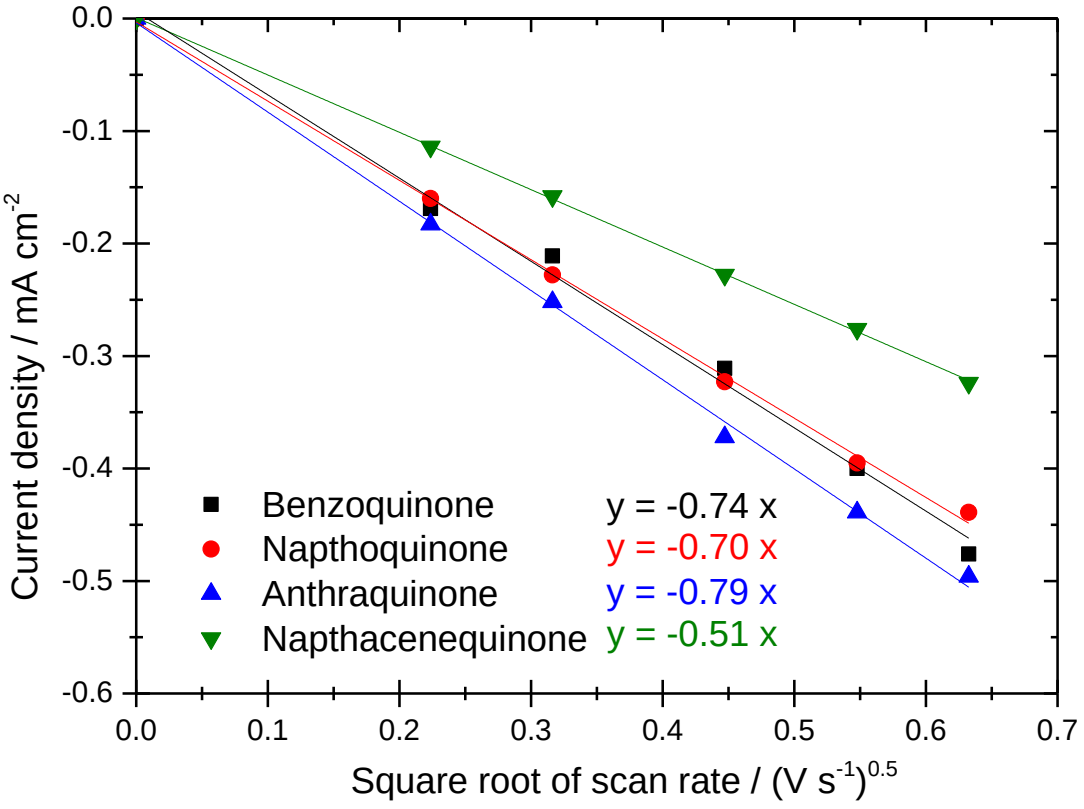

Figure 4.3.4 Determination of the diffusion coefficient for several quinones in a 0.2 M LiTFSI electrolyte.

Building on these initial results, a range of quinones were analysed with increasingly large aromatic groups so as to provide redox couples at a range of different potentials. The structures of these quinones are shown below in Figure 4.3.5. Each of these compounds were tested in the same way as the 1,4-napthoquinone compound discussed previously. A cyclic voltammogram of 1 mM benzoquinone recorded at 100 mV s^{-1} over 5 cycles is shown in Figure 4.3.6 and the voltammograms at various sweep rates are shown in Figure 4.3.7.

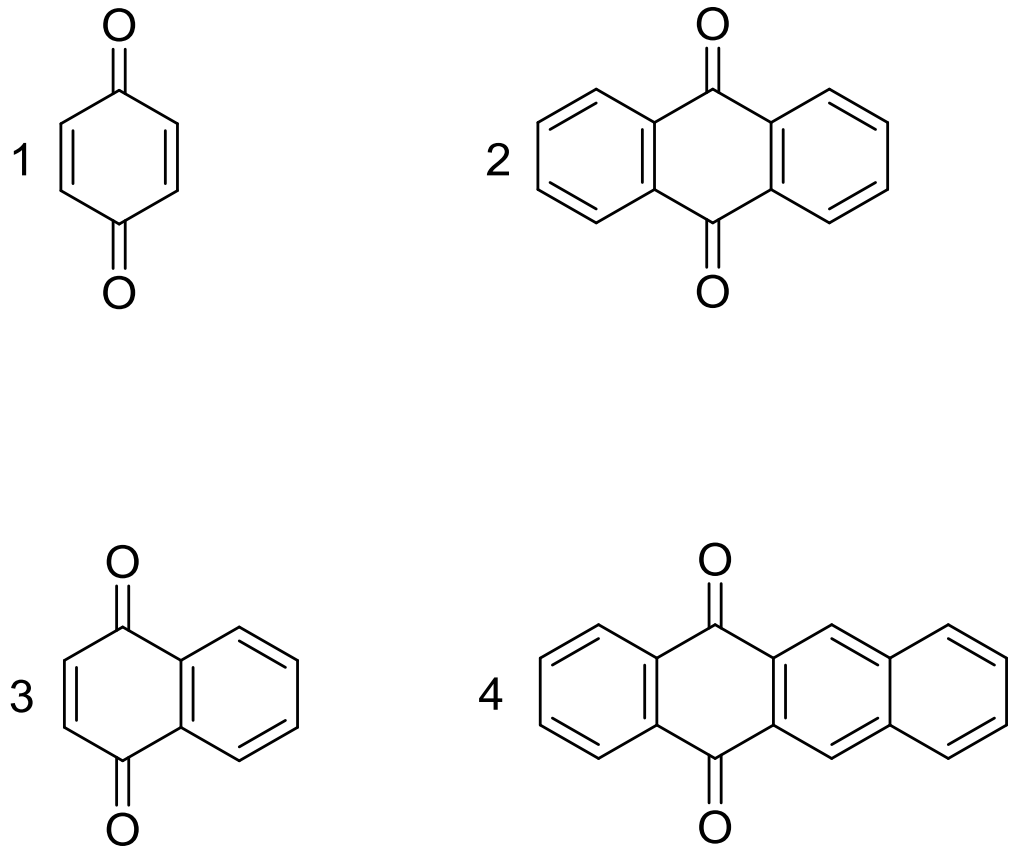

Figure 4.3.5 Chemical structures of quinones examined by cyclic voltammetry. 1) 1,4-Benzoquinone 2) Anthraquinone 3) 1,4-Napthoquinone 4) 5,12-Napthacenequinone

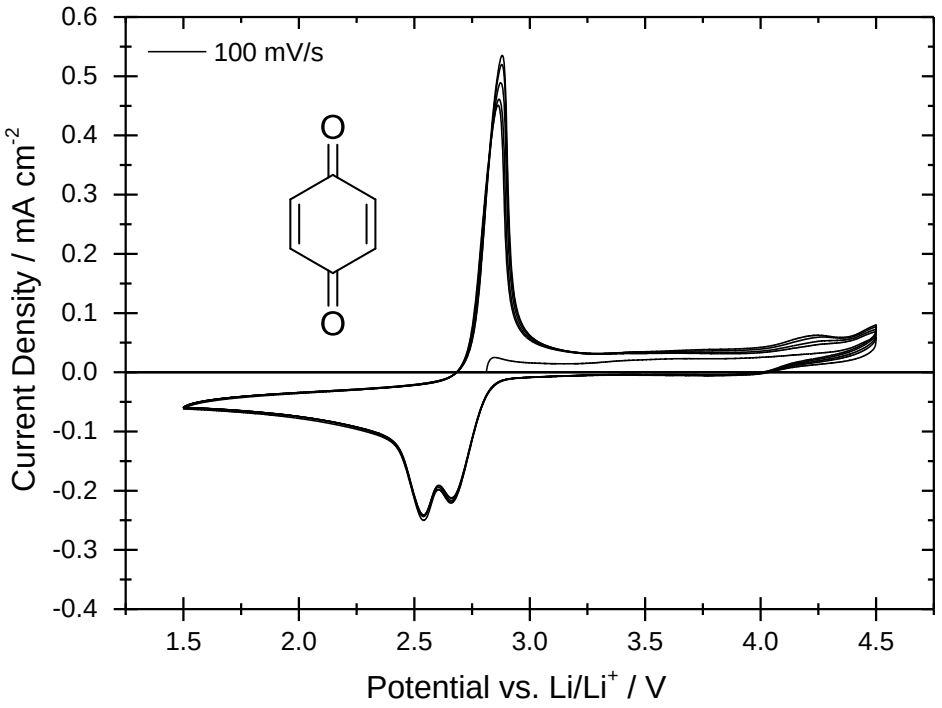

Figure 4.3.6 Cyclic voltammogram of a glassy carbon electrode (Ø = 3 mm) in a 1 mM 1,4-benzoquinone (structure shown) containing 0.2 M LiTFSI diglyme electrolyte recorded at 100 mV s^{-1}. A lithium metal counter/reference electrode was used. The potential began at open circuit, was swept to 4.5 V, then returned to 1.5 V for 5 cycles.

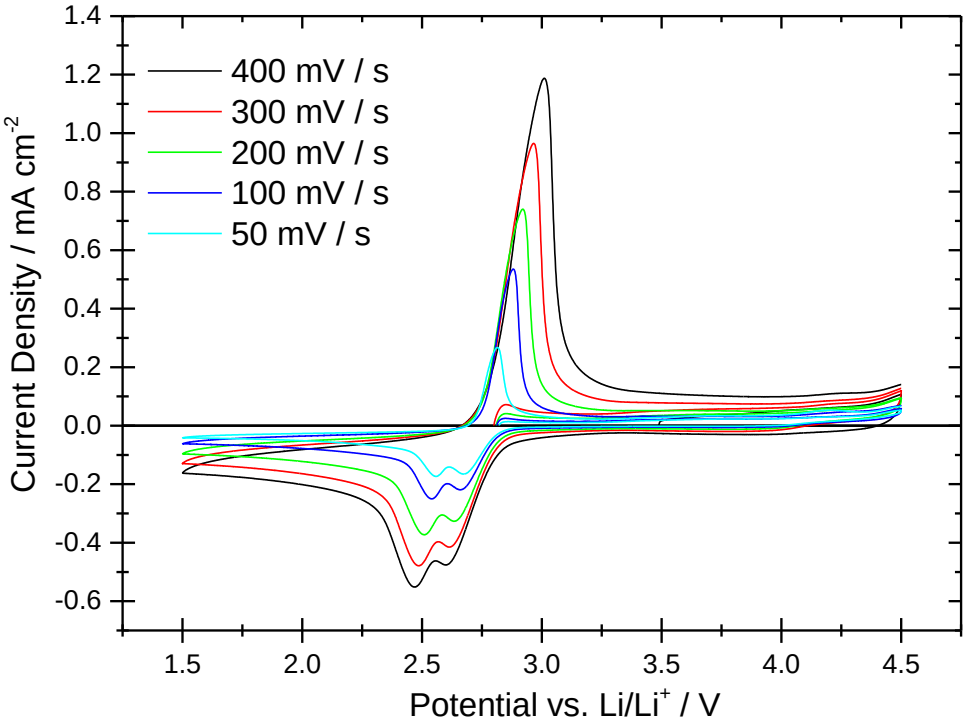

Figure 4.3.7 Cyclic voltammograms of a glassy carbon electrode (Ø = 3 mm) in a 1 mM 1,4-benzoquinone containing 0.2 M LiTFSI diglyme electrolyte recorded at different sweep rates. A lithium metal counter/reference electrode was used. The potential began at open circuit, was swept from open circuit to 4.5 V, then down to 1.5 V before finally returning to 4.5 V.

The initial reduction of benzoquinone in Figure 4.3.6 occurs via the expected two distinct one electron transfers whereas the oxidation process has combined into a singular peak. Over multiple cycles there is a drop in peak current observed for this oxidation from 0.54 mA cm^{-2} on the first cycle down to 0.44 mA cm^{-2} on the fifth. A possible cause of this could be some electrode fouling as a result of the small oxidation peak occurring at 4.1 V. It is most likely the result of an impurity contained within the benzoquinone supplied from Sigma Aldrich (98%) as this was dried on a vacuum line but otherwise used as received. At the lowest voltage of 1.5 V both the electrolyte and the quinone show no signs of further reaction.

Figure 4.3.7 displays the 1 mM benzoquinone containing electrolyte cycled at different sweep rates. Even at the lowest sweep rate of 50 mV s^{-1} the oxidation peak remains as a singular peak indicating the oxidation from the dianion to the neutral quinone occurs in a single step. The 1st reduction occurs at 2.74 V with a peak separation of 40 mV while the 2nd occurs at 2.67 V with a peak separation of 110 mV. This indicates that the first electron transfer is reversible while the second electron transfer is less so. The diffusion coefficient is found to be 7.2 x 10^{-6} cm^2 s^{-1} and was calculated using the same method shown in Figure 4.3.4. This is very slightly larger than the previous value of 7.1 x 10^{-6} cm^2 s^{-1} for napthoquinone but considering the error in these measurements it can be assumed to be equal. The formal potential for the electron transfer in the case of napthoquinone was calculated to be 2.73 V, indicating that the loss of the aromatic group has resulted in a slight positive shift in the potential.

The anthraquinone compound depicted as number 2 in Figure 4.3.5 contains a much larger aromatic group. A cyclic voltammogram recorded at 100 mV s^{-1} over 5 cycles of 1 mM anthraquinone in a 0.2 M LiTFSI diglyme electrolyte is shown in Figure 4.3.8. The larger aromatic group in the compound can be expected to make the reduction less favourable thus driving the redox couples to more negative potentials. There are two peaks present due to reduction and again only one is present for oxidation. The shape of the oxidation peak is characteristic of a surface bound species as the current drops sharply after the peak to almost zero. The anthraquinone shows excellent stability at higher voltages showing only double layer charging current beyond 2.7 V to 4.5 V vs. Li/Li^+.

Looking at the results obtained by varying the sweep rate in Figure 4.3.9, the same sharp decrease in current is observed after the oxidation. The increasing scan rate also appears to affect the cathodic and anodic peak sizes differently. Compared to the previous results, the current at lower scan rates is larger than expected. As the experimental data was collected from faster to slower scan rates it indicates an accumulation of the anthraquinone near the surface over time. The peak to peak separation is recorded at 100 mV and 340 mV for the first and second reduction respectively. The diffusion coefficient for anthraquinone is calculated to be 9×10^{-6} cm^2 s^{-1}. This value is higher than expected and may be due to the accumulation of anthraquinone at the electrode surface over time.

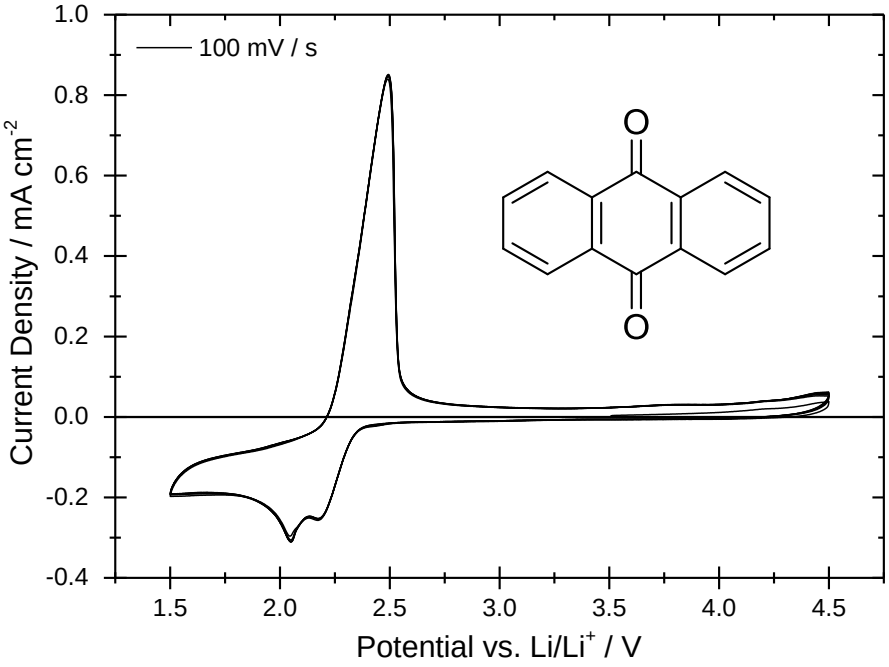

Figure 4.3.8 Cyclic voltammogram of a glassy carbon electrode (Ø = 3 mm) in a 1 mM anthraquinone (structure shown) containing 0.2 M LiTFSI diglyme electrolyte recorded at 100 mV s^{-1}. A lithium metal counter/reference electrode was used. The potential began at open circuit, was swept to 4.5 V, and returned to 1.5 V for 5 cycles.

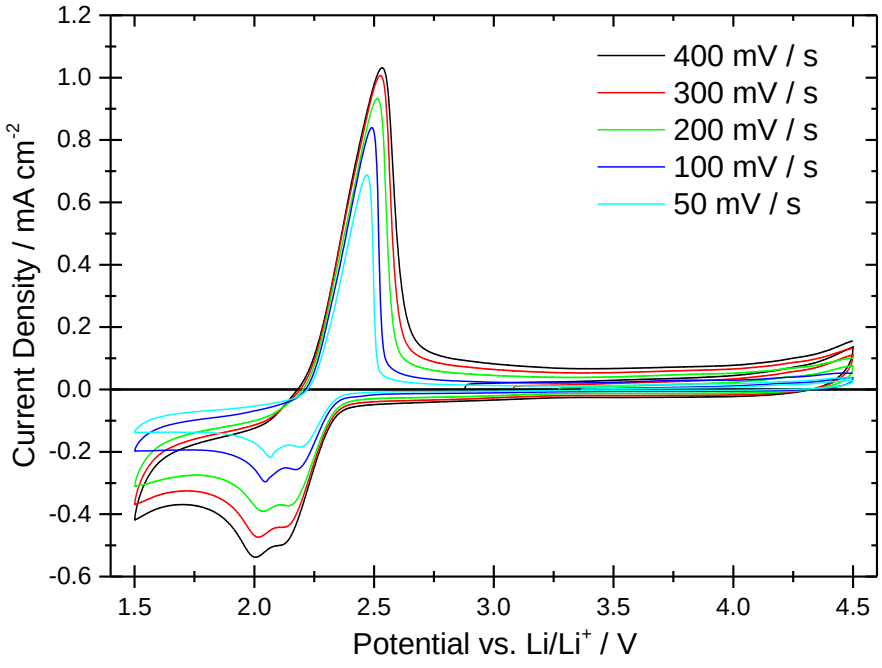

Figure 4.3.9 Cyclic voltammograms of a glassy carbon electrode (Ø = 3 mm) in a 1 mM 1,4-anthraquinone containing 0.2 M LiTFSI diglyme electrolyte recorded at different sweep rates. A lithium metal counter/reference electrode was used. The potential began at open circuit, was swept from open circuit to 4.5 V, then down to 1.5 V, before finally returning to 4.5 V.

The largest quinone tested was 5,12-napthacenequinone which contains one more aromatic carbon ring than the previously tested anthraquinone. The cyclic voltammetry shown in Figure 4.3.10 is similar to the behaviour of the previously observed quinones. Here there are two reduction peaks on the negative sweep and only one oxidation peak on the positive sweep. There is no further oxidation reactions when taking the potential to the electrolyte limit of 4.5 V vs. Li/Li^+ indicating that the neutral quinone is very stable towards further oxidation. Over subsequent cycles there is no discernable change in peak shape or size. At approximately 2.5 V vs. Li/Li^+ there is a small redox couple. Due to its small size this is unlikely to be due to the napthoquinone and instead it can be assumed to be due to the presence of an impurity.

Comparing the voltammograms at different scan rates provides formal potentials of 2.20 V and 2.17 V vs. Li/Li^+ for the first and second electron reductions respectively, while the extrapolated peak separation at zero current is calculated to be 90 mV and 200 mV. This indicates that neither redox couple is electrochemically reversible. This could be attributed to the presence of the lithium ions in the electrolyte as a similar effect is observed in oxygen electrochemistry.[28,29] The diffusion coefficient for 5,12-napthacenequinone was calculated to be 3.5×10^{-6} cm^2 s^{-1}. Given the low formal potential of this quinone it is unlikely that quinones more reducing than this will have a significant effect on the oxygen reduction reaction. This is because the peak of oxygen reduction is measured to be 2.2 V vs. Li/Li^+. Therefore it can be expected that much of the surface would already be coated in lithium peroxide before the proposed mediator is reduced and becomes active.

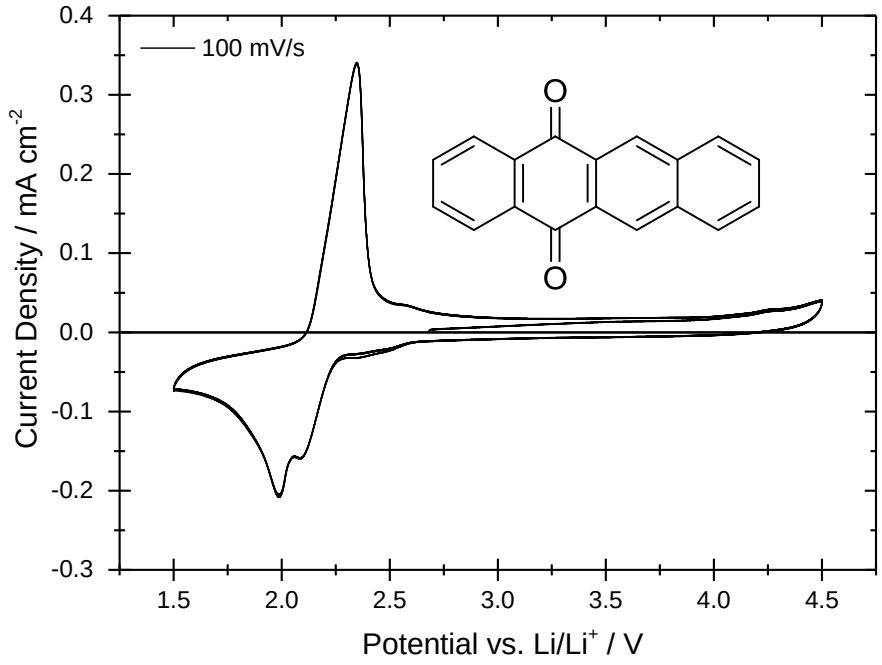

Figure 4.3.10 Cyclic voltammogram of a glassy carbon electrode (Ø = 3 mm) in a 1 mM 5,12-napthacenequinone (structure shown) containing 0.2 M LiTFSI diglyme electrolyte recorded at 100 mV s^{-1}. A lithium metal counter/reference electrode was used. The potential began at open circuit, was swept to 4.5 V, then returned to 1.5 V for 5 cycles.

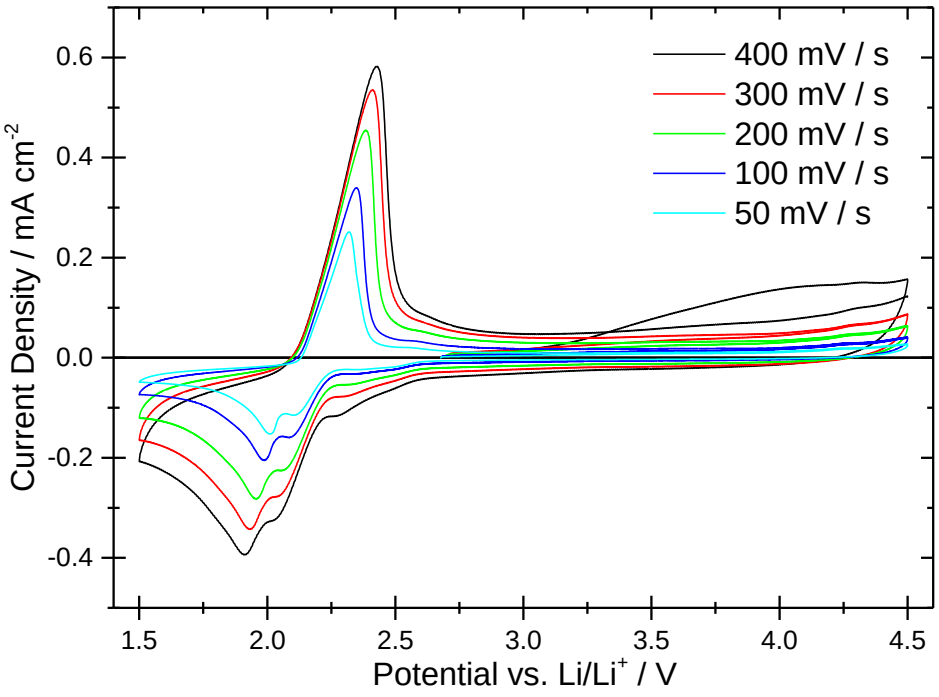

Figure 4.3.11 Cyclic voltammograms of a glassy carbon electrode (Ø = 3 mm) in a 1 mM 5,12-napthacenequinone containing 0.2 M LiTFSI diglyme electrolyte recorded at different sweep rates. A lithium metal counter/reference electrode was used. The potential began at open circuit, was swept from open circuit to 4.5 V, then down to 1.5 V before finally returning to 4.5 V.

The experimentally determined formal potentials, diffusion coefficients and peak to peak separation for each of these quinones are summarised in Table 4.3.1 below. A potential range of ~ 0.5 V was provided solely by the addition of the aromatic groups. In all cases, both quinone reduction reactions happen at more negative potentials than that of the oxygen reduction reaction, with the 2nd reduction reaction occurring within 150 mV of the first. Because of this, these quinones would be suited to mediating the reduction reaction. The benzoquinone and napthoquinone are the most reversible compounds with a 1st electron peak separation close to the 59 mV given by a fast and reversible redox couple. The second electron transfer in all cases has a larger peak separation indicating only quasi-reversibility as found in previous studies.[103,104]

Table 4.3.1 Formal potentials and electrochemical reversibility of quinones in a 0.2 M LiTFSI in diglyme electrolyte.

Quinone	E'^{o}_1 vs. Li/Li^+ / V	Peak Separation / mV	E'^{o}_2 vs. Li/Li^+ / V	Peak Separation / mV	Diffusion Coefficient / $cm^2\ s^{-1}$
1,4-Benzoquinone	2.74	40	2.67	110	7.2×10^{-6}
1,4-Napthoquinone	2.73	20	2.59	100	7.1×10^{-6}
Anthraquinone	2.29	100	2.26	340	9.0×10^{-6}
Napthacenequinone	2.20	90	2.17	200	3.6×10^{-6}

4.3.2 Cyclic Voltammetry of Quinones with Oxygen

Each of these quinones was then examined under an oxygen atmosphere to determine their effectiveness at mediating the oxygen reduction reaction. This was done by comparing the relative peak potentials of the oxygen saturated electrolyte, quinone containing electrolyte under argon and the quinone containing electrolyte under oxygen. Indicators of the mediation of the oxygen reduction reaction would include a smaller oxidation peak for the quinone due to its chemical re-oxidation by the mediation mechanism an earlier onset potential and a larger reduction peak. The cyclic voltammograms for each quinone in an oxygen atmosphere at various scan rates can be found in Appendix B.

The effect of 1 mM benzoquinone on the oxygen reduction reaction can be seen in Figure 4.3.12. Upon comparing oxygen reduction with benzoquinone (red) to without (black) it is observed that the onset potential for the oxygen reduction reaction appears much earlier and closer to the onset of benzoquinone reduction. While the peak current observed is actually significantly smaller (~66%) than in the absence of the quinone. On the positive sweep there is a peak occurring at approximately 3 V vs. Li/Li^+ which could be attributed to one of two things; the oxidation of the benzoquinone with a significantly larger IR drop, due to the insulating peroxide layer formed on reduction, or an earlier onset of peroxide oxidation. The inset demonstrates the effect of varying the sweep rate on the oxidation step. The peak becomes more defined with increasing scan rate suggesting it is due to benzoquinone oxidation. The lessened time for chemical reduction of the benzoquinone by oxygen at higher scan rates results in a larger peak.

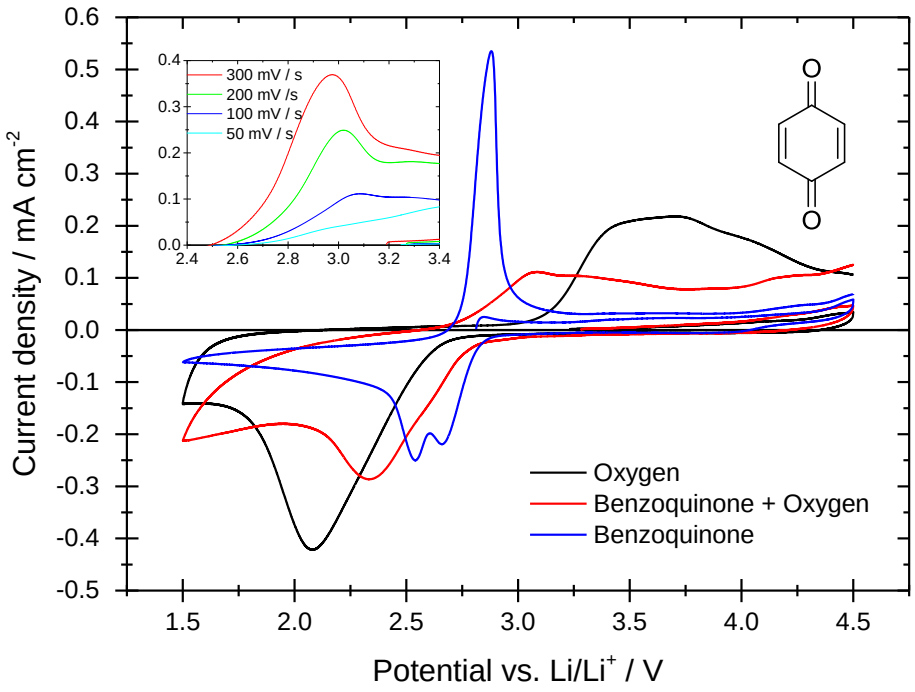

Figure 4.3.12 Cyclic voltammograms using a glassy carbon working electrode (Ø = 3 mm) vs. a lithium metal counter/reference electrode. The electrolyte in each case consisted of 0.2 M LiTFSI in diglyme, but was either oxygen saturated (black), containing 1 mM benzoquinone (blue), or both (red). The potential began at open circuit, was swept positively to 4.5 V, then negatively to 1.5 V before finally returning to 4.5 V. In each case the scan rate was 100 mV s^{-1}. The inset has the same X and Y axis as the main figure and demonstrates the effect of scan rate on the oxidation reaction for the oxygen saturated benzoquinone electrolyte.

Below in Figure 4.3.13 cyclic voltammogram for the larger compound napthoquinone are shown. As before the combination of 1mM napthoquinone and oxygen is compared to their independent scans. Here a peak current for the oxygen reduction reaction of almost double can be seen with the napthoquinone (red) than without (black). The oxygen reduction peaks at 2.3 V vs. Li/Li^+ with the quinone compared to 2.0 V without. As the potential continues to sweep negatively a peak is seen at ~ 1.9 V which is likely due to the unmediated reduction of oxygen. This indicates much of the initial current formed lithium peroxide in solution instead of at the electrode surface. Once the potential is reversed no peaks are observed for napthoquinone oxidation which suggests a chemical reaction is occurring re-oxidising napthoquinone with oxygen. The oxidation of the lithium peroxide appears unaffected which suggests that the quinone plays no part in that process.

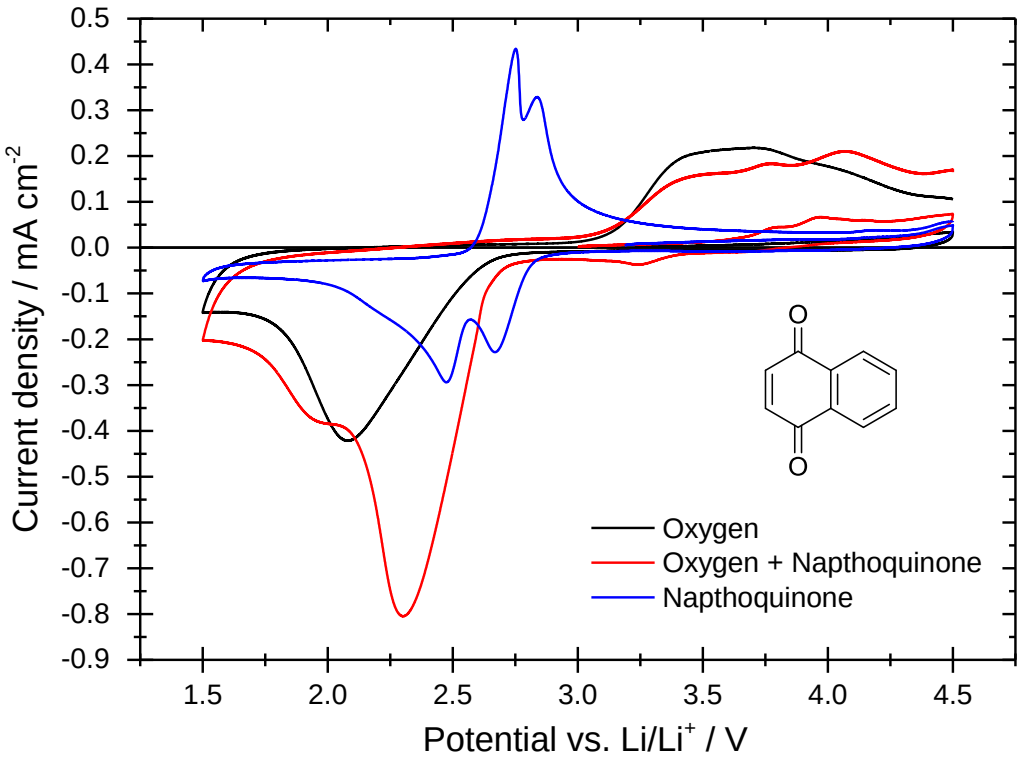

Figure 4.3.13 Cyclic voltammograms using a glassy carbon working electrode (Ø = 3 mm) vs. a lithium metal counter/reference electrode. The electrolyte in each case consisted of 0.2M LiTFSI in diglyme, but was either oxygen saturated (black), containing 1 mM napthoquinone (blue), or both (red). The potential began at open circuit, was swept positively to 4.5 V then negatively to 1.5 V before finally returning to 4.5 V. In each case the scan rate was 100 mV s^{-1}.

The peak current of oxygen reduction when using anthraquinone is once again larger than in the absence of oxygen. The oxygen reduction begins at a similar potential as before and peaks at ~ 2.2 V vs. Li/Li^+. However, on the reverse scan there is no peak for anthraquinone oxidation. This suggests that any anthraquinone reduced during the negative sweep has been chemically re-oxidised. The simplest explanation for this would be re-oxidation by the dissolved oxygen present in solution as given by the mediation mechanism. During the oxidation of lithium peroxide there is noticeably more current beyond 4.0 V vs. Li/Li^+ than in the absence of the quinone. Current at this region is often attributed to the evolution of CO_2 from Li_2CO_3 formed at the electrode surface. It could be the case that the extra current seen on reduction is forming lithium carbonate from the decomposition of the quinone.

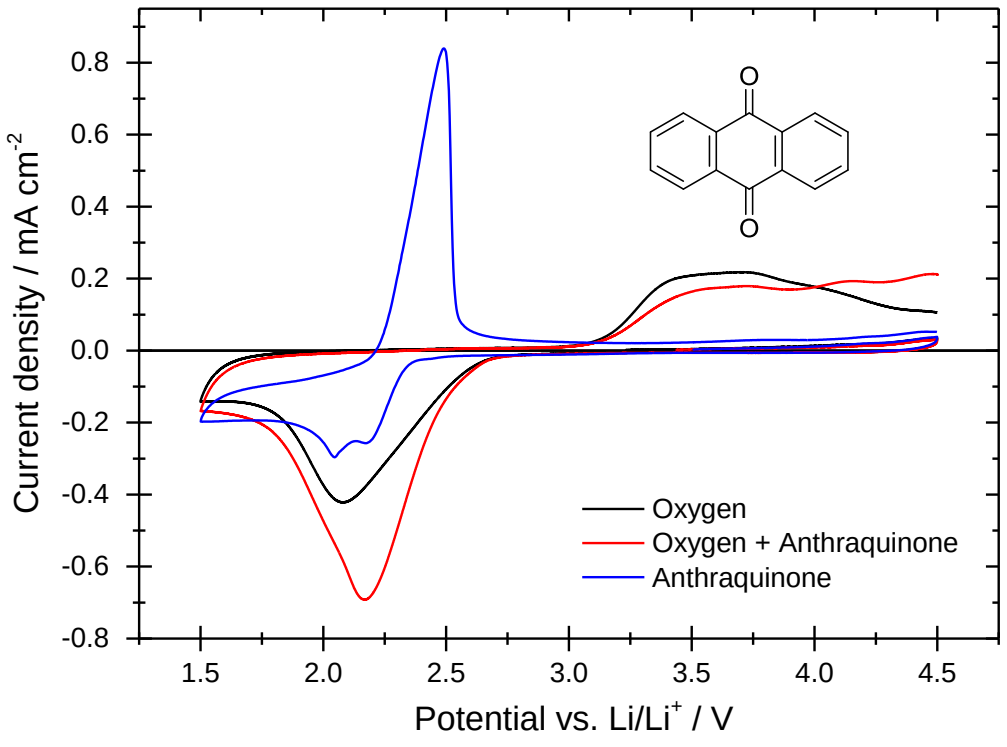

Figure 4.3.14 Cyclic voltammograms using a glassy carbon working electrode (Ø = 3 mm) vs. a lithium metal counter/reference electrode. The electrolyte in each case consisted of 0.2M LiTFSI in diglyme, but was either oxygen saturated (black), containing 1 mM anthraquinone (blue), or both (red). The potential began at open circuit, was swept positively to 4.5 V, then negatively to 1.5 V before finally returning to 4.5 V. In each case the scan rate was 100 mV s^{-1}.

The 5,12-napthacenequinone was the most reducing quinone examined and therefore was the most likely to be able to reduce oxygen to lithium superoxide/ lithium peroxide chemically. However, as is illustrated in Figure 4.3.15 there is actually very little effect on the oxygen electrochemistry. Given that the oxygen reduction reaction starts almost 0.5 V before the napthacenequinone it would seem the surface is already coated in a layer of lithium peroxide before the napthacenequinone can be reduced. What is reduced would be expected to react with the oxygen in a similar manner to the other quinones but it would appear that the formal potential for napthacenequinone is too low to function as an effective mediator to aid the formation of lithium peroxide in solution.

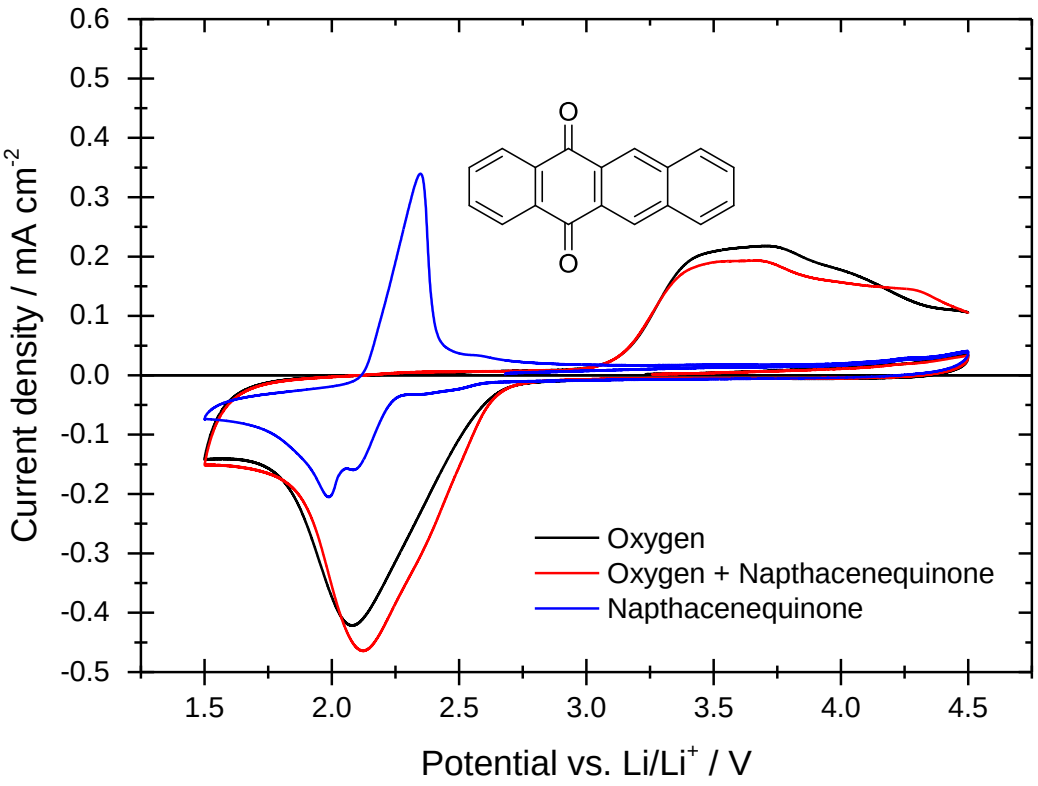

Figure 4.3.15 Cyclic voltammograms using a glassy carbon working electrode (Ø = 3 mm) vs. a lithium metal counter/reference electrode. The electrolyte in each case consisted of 0.2M LiTFSI in diglyme, but was either oxygen saturated (black), containing 1 mM napthacenequinone (blue), or both (red). The potential began at open circuit, was swept positively to 4.5 V, then negatively to 1.5 V before finally returning to 4.5 V. In each case the scan rate was 100 mV s^{-1}.

Combining these results into a table can provide some insight into what potential range is able to provide the greatest enhancement to the current. Finding the right balance between a mediator which is chemically reducing enough to react with the dissolved oxygen but having an appropriately positive potential to electrochemically mediate the oxygen reduction reaction is important in optimising quinones as a potential mediator. The table below includes the formal potential for each quinone in argon, the peak potential and the peak current recorded in oxygen. The results for oxygen in the absence of a quinone are included for reference. The experimentally measured formal potential for oxygen determined in Chapter 3 is 2.97 V vs. Li/Li^+.

The most positive peak potential in the presence of oxygen is observed for the 1,4-benzoquinone compound, whereas the greatest current density was observed when using the 1,4-napthoquinone. By the addition of functional groups to explore the region between the two compounds it may be possible to achieve the best of both.

Table 4.3.2 Peak currents and formal potentials vs. Li/Li^+ for oxygen reduction in 1 mM quinone containing electrolytes. The results for an oxygen saturated electrolyte in the absence of any quinone are included in the top row of the table.

Quinone	E'^o vs. Li/Li^+ in Argon / V	Ep_c vs. Li/Li^+ in Oxygen / V	Jp_c in Oxygen / mA cm^{-2}
N/A	N/A	2.07	-0.42
1,4-Benzoquinone	2.74	2.34	-0.29
1,4-Napthoquinone	2.73	2.30	-0.80
Anthraquinone	2.29	2.17	-0.69
Napthacenequinone	2.20	2.12	-0.47

To monitor the passivation effect over time the peak current of oxygen reduction over several cycles was recorded. In all cases the decline in peak current is seen over subsequent cycling due to the incomplete charge reaction leaving lithium peroxide and lithium carbonate at the surface of the electrode. Where the use of a quinone has facilitated a faster reduction of oxygen the passivation effect is even more pronounced. The results for 5,12-napthoquinone almost perfectly mirror the electrolyte which contains no quinone at all. This backs up the theory that it is having almost no effect on the cycling of the cell due to its low formal potential.

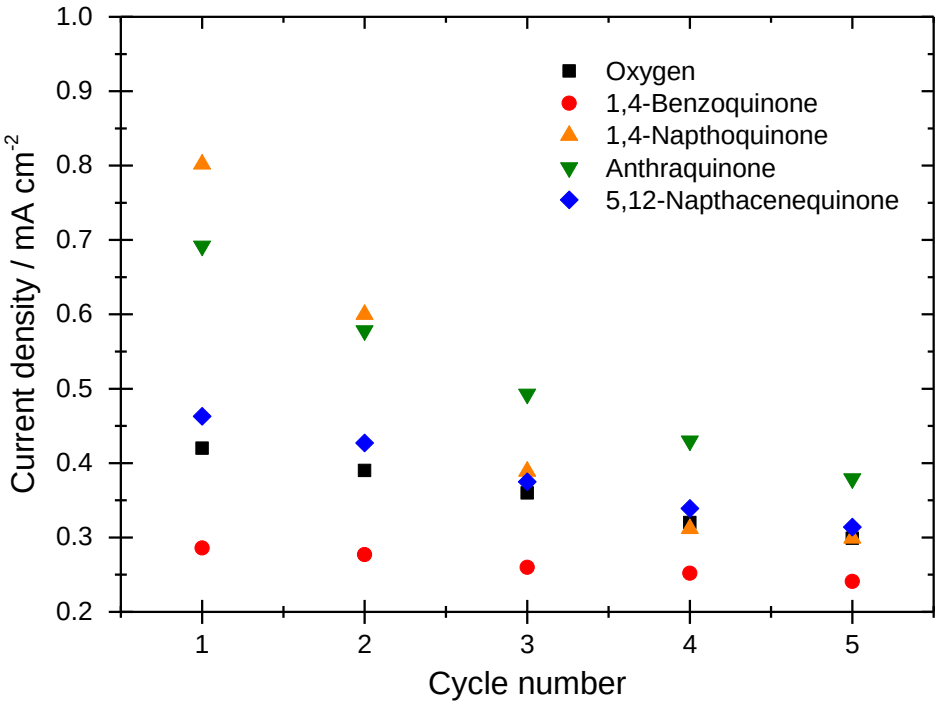

Figure 4.3.16 Oxygen reduction peak current for different 1 mM quinone containing electrolytes made with 0.2 M oxygen saturated diglyme. All scans were conducted at 100 mV s^{-1} using a glassy carbon working electrode (Ø = 3 mm) vs. a lithium metal counter/reference electrode. The potential began at open circuit, was swept to 4.5 V and returned to 1.5 V for 5 cycles.

4.3.3 Functionalised Quinones for the Oxygen Reduction Reaction

Further functionalised quinones were selected based on the previous results. The addition of methyl groups to the benzoquinone compound will donate electron density to the conjugated ring system making the compound harder to reduce. For this reason methyl and dimethyl 1,4-benzoquinone were selected. Using chlorine groups as electron withdrawing substituents will pull electron density away from the aromatic centre resulting in a more electron deficient molecule with a higher formal potential. 2,3-dichloronapthoquinone was tested to try and further reduce the overpotential observed for the oxygen reduction reaction. The structures for these quinones are shown in Figure 4.3.17 below.

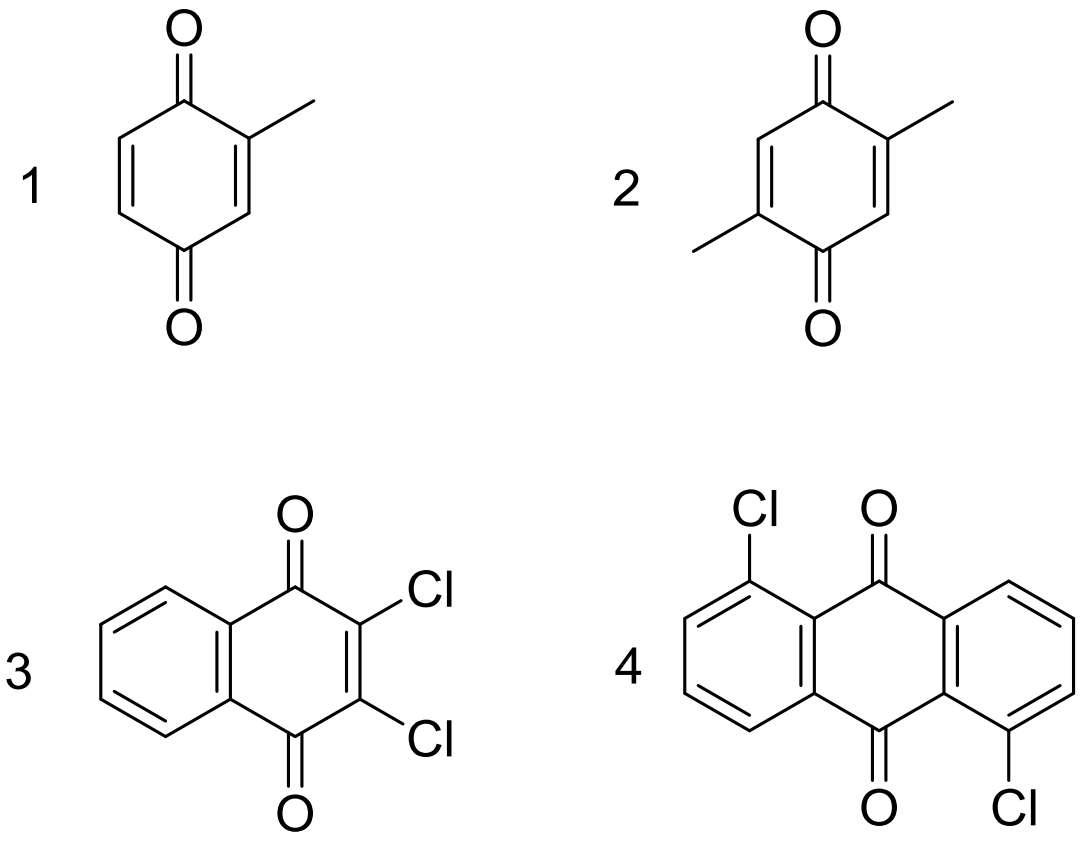

Figure 4.3.17 Chemical structures of functionalised quinones. 1.) Methyl-1.4-benzoquinone, 2.) 2,5-Dimethyl-1,4-benzoquinone 3.) 2,3-Dichloro-1,4-napthoquinone 4.) 2,5-Dichloroanthraquinone

The cyclic voltammograms for the substituted variations of benzoquinone are shown in Figure 4.3.18. The addition of each methyl group shifts the potential of the quinone reduction by approximately 100 mV. Besides the potential shift the voltammograms for the 1,4-benzoquinones display a decreasing peak current size with the addition of each methyl group indicating that the diffusion coefficient decreases. They exhibit no signs of further reduction beyond the dianion and appear very stable towards additional oxidation beyond the neutral quinone. The oxidation for each quinone can only be seen as one peak with the potential shifting much less than that of the reduction peak.

In order to determine the effect of this change in potential on the mediation of the oxygen reduction each electrolyte was saturated with oxygen and the voltammograms repeated. The result for an electrolyte with no quinone present has been included for reference (black trace). The methyl-1,4-benzoquinone shows a greatly enhanced peak current at a reduced overpotential of 500 mV compared to 900 mV in the absence of a quinone. The subsequent addition of a methyl group in the 2,5-dimethyl-1,4-benzoquinone again shows a greatly enhanced current. The peak potential of oxygen reduction has shifted approximately 100 mV more negative when compared with the methyl-1,4-benzoquinone, similar to the reduction potentials seen in argon. When the potential is swept from 1.5 V to 4.5 V vs. Li/Li^+ the oxidation current is significantly lower than what is seen in the absence of the quinones. One possible explanation for this is that the peroxide is not forming at the surface but in clusters in the electrolyte solution. This could also explain the shoulder peak seen at ~ 1.8 V vs. Li/Li^+ relating to the unmediated reduction of oxygen.

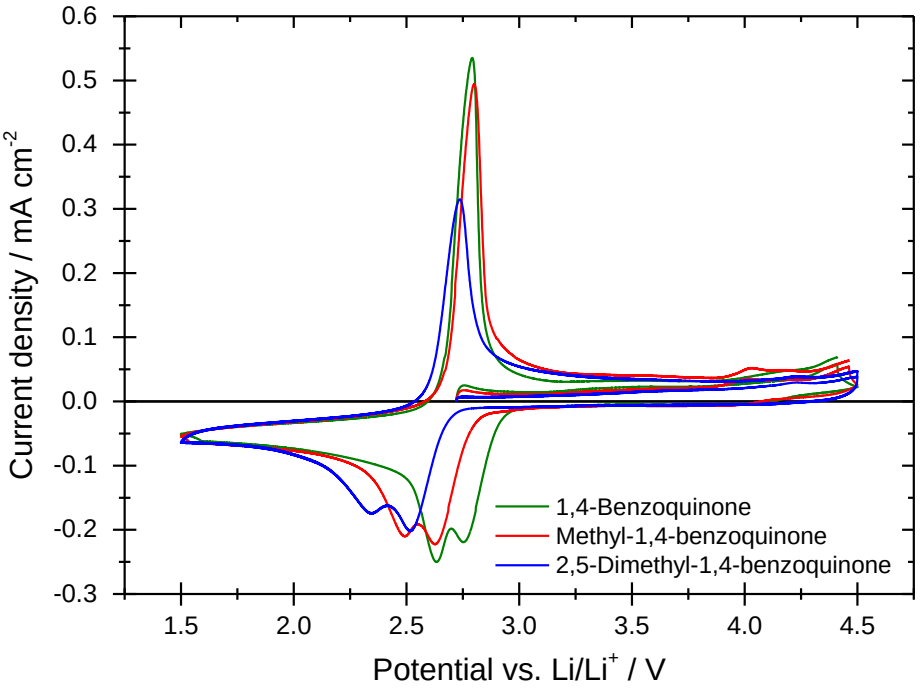

Figure 4.3.18 Cyclic voltammograms of a 0.2 M LiTFSI diglyme electrolyte containing 1 mM of a given quinone. A glassy carbon working electrode (Ø = 3 mm) vs. a lithium metal counter/reference electrode was used. The potential began at open circuit, was swept positively to 4.5 V, then negatively to 1.5 V before finally returning to 4.5 V. In all cases the scan rate was 100 mV s^{-1}.

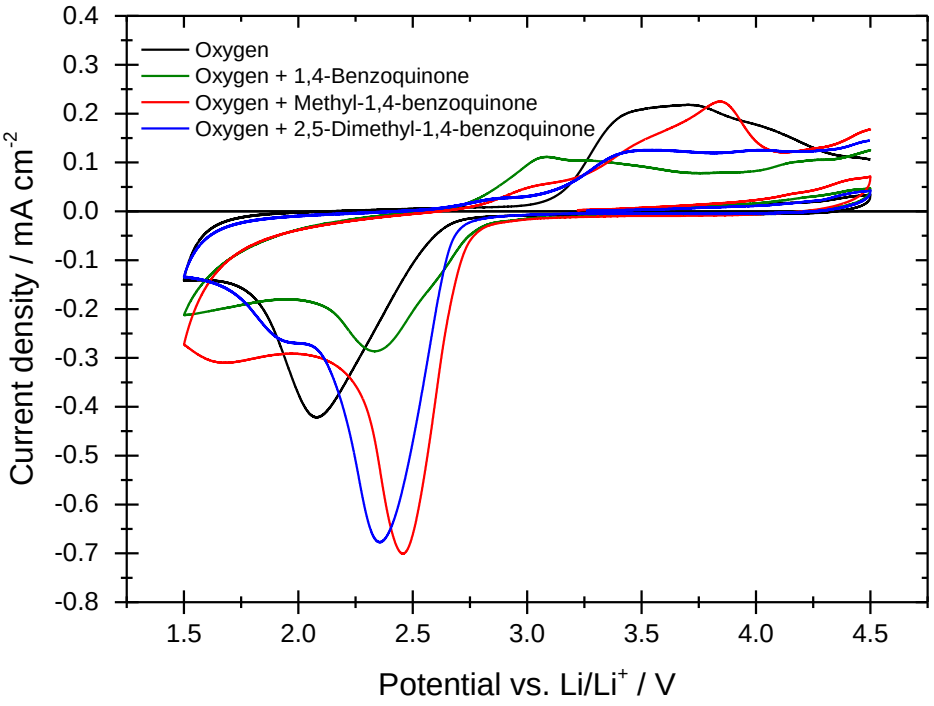

Figure 4.3.19 Cyclic voltammograms using a glassy carbon working electrode (Ø = 3 mm) vs. a lithium metal counter/reference electrode. The electrolyte in each case consisted of oxygen saturated 0.2M LiTFSI in diglyme containing 1 mM of the specified quinone (green, red and blue) or no quinone (black). The potential began at open circuit, was swept positively to 4.5 V, then negatively to 1.5 V before finally returning to 4.5 V. In each case the scan rate was 100 mV s^{-1}.

The 1,4-napthoquinone tested previously showed a large increase in peak current but still showed a significant overpotential compared to the formal potential for oxygen reduction. Anthraquinone showed some improvement on the unmediated reaction but noticeably less than the napthoquinone. Using the dichlorinated versions of each quinone, should raise the formal potential and therefore allow for a large oxygen reduction current at lower overpotentials. Cyclic voltammograms recorded at 100 mV s^{-1} for each of these compounds are shown in Figure 4.3.20. The addition of the chlorine groups to the quinone has caused a positive shift in peak potentials, most noticeably in the oxidation peak. In the case of the 1,5-dichloroanthraquinone the second oxidation process can now be seen as a shoulder after the initial peak.

Each of the new chlorinated quinones exhibit slightly different electrochemistry compared to their unchlorinated counterparts. How this has affected the oxygen reduction reaction can be seen in Figure 4.3.21. Starting with the 1,5-dichloroanthraquinone the peak reduction is very slightly larger and more positive when compared to the unsubstituted anthraquinone. This shows that the addition of the chlorines has had an effect but unfortunately it is only very small. The 2,3-dichloronapthoquinone shows a much smaller reduction peak at 2.6 V followed by a further reduction peak at 2.0 V vs. Li/Li^+. Looking at the argon voltammogram in Figure 4.3.20 for the chlorinated napthoquinone the 1^{st} reduction peak also occurs at 2.6 V vs. Li/Li^+. This is likely to mean that the addition of the chlorines has prevented any mediation of the reduction reaction. Instead the voltammogram displays two separate sets of peaks. One for the quinone reduction followed by another for the reduction of oxygen.

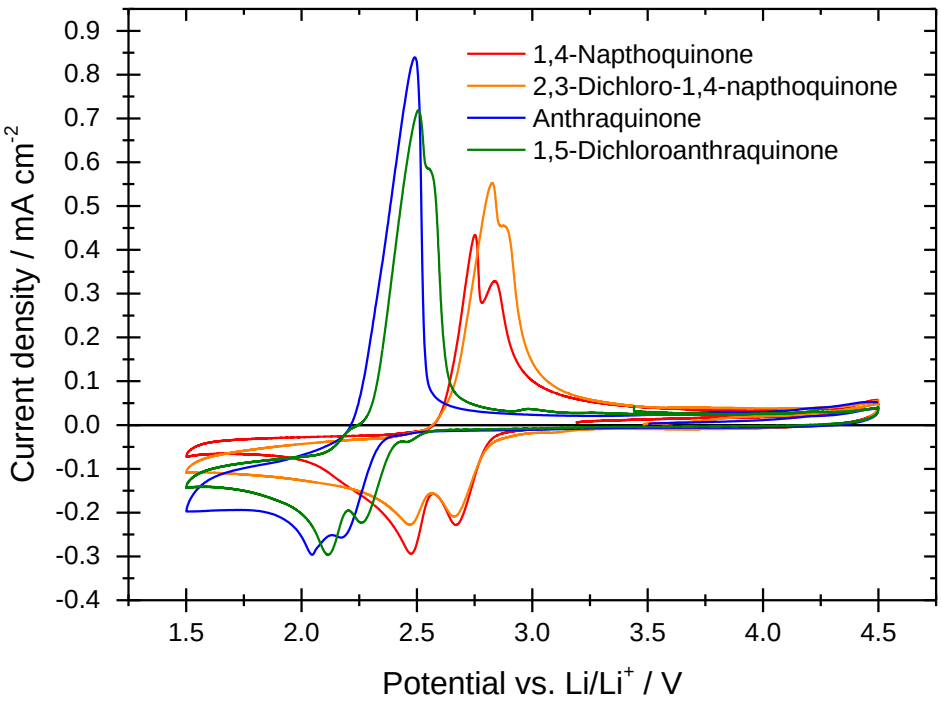

Figure 4.3.20 Cyclic voltammograms of a 0.2 M LiTFSI diglyme electrolyte containing 1 mM of a given quinone. A glassy carbon working electrode (Ø = 3 mm) vs. a lithium metal counter/reference electrode was used. The potential began at open circuit, was swept positively to 4.5 V, then negatively to 1.5 V before finally returning to 4.5 V. In all cases the scan rate was 100 mV s^{-1}.

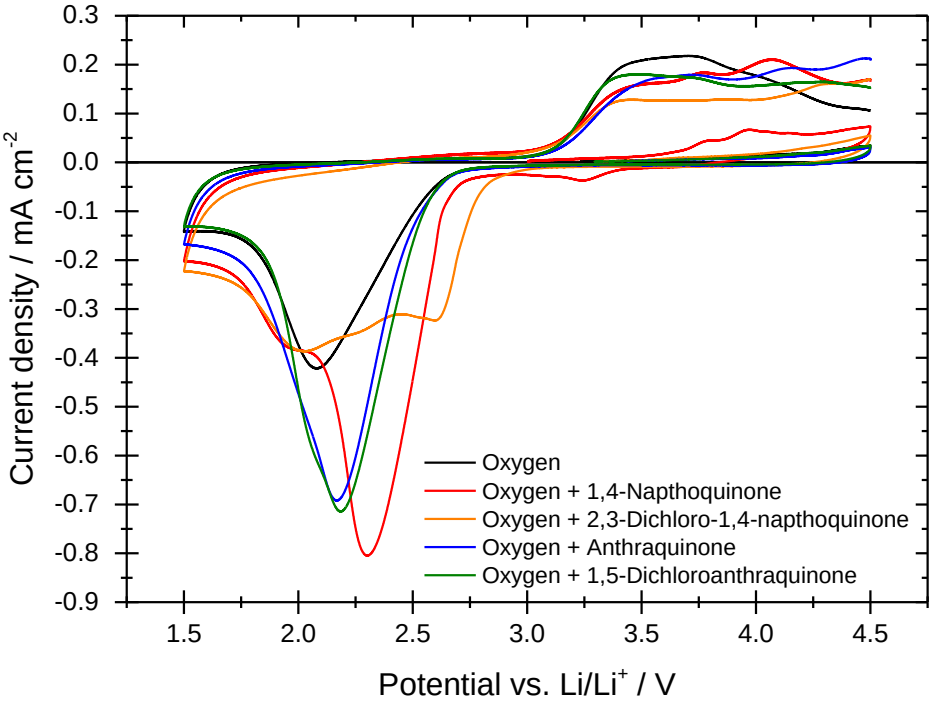

Figure 4.3.21 Cyclic voltammograms using a glassy carbon working electrode (Ø = 3 mm) vs. a lithium metal counter/reference electrode. The electrolyte in each case consisted of oxygen saturated 0.2M LiTFSI in diglyme containing 1 mM of the specified quinone (green, red and blue) or no quinone (black). The potential began at open circuit, was swept positively to 4.5 V, then negatively to 1.5 V before finally returning to 4.5 V. In each case the scan rate was 100 mV s^{-1}.

For comparison the formal potential of each of the substituted quinones, and their respective peak currents and peak potentials in oxygen are shown in Table 4.3.3 below. Plots to determine the diffusion coefficient and the formal potential can be found in Appendix B. Both 2,3-dichloro-1,4-napthoquinone and 1,4-benzoquinone were not sufficiently reducing to produce a significant enhancement of the reduction reaction. The most effective mediation was found using the methylated benzoquinones and 1,4-napthoquinone. The greatest improvement upon the overpotential for the oxygen reduction reaction was using 1 mM methyl-1,4-benzoquinone. The peak oxygen reduction was measured at a potential 400 mV more positive than in the absence of a quinone with a current density 1.7 x larger. As the formal potential for all subsequent quinones decreases similar current density enhancements are seen but with appropriately more negative peak potentials and therefore greater overpotentials.

Table 4.3.3 Peak currents and formal potentials vs. Li/Li^+ for oxygen reduction in 1 mM quinone containing electrolytes. The results for an oxygen saturated electrolyte in the absence of any quinone are included in the top row of the table.

Quinone	E'^o vs. Li/Li^+ / V	Ep_c vs. Li/Li^+ in Oxygen / V	Jp_c in Oxygen / mA cm^{-2}
N/A	2.97	2.07	-0.42
2,3-Dichloro-1,4-napthoquinone	2.76	2.00	-0.39
1,4-Benzoquinone	2.75	2.34	-0.29
1,4-Napthoquinone	2.74	2.30	-0.80
Methyl-1,4-benzoquinone	2.68	2.46	-0.70
2,5-Dimethyl-1,4-benzoquinone	2.63	2.35	-0.68
1,5-Dichloro-1,4-anthraquinone	2.41	2.18	-0.71
Anthraquinone	2.33	2.17	-0.69

The change in the peak current for the oxygen reduction reaction over several cycles is shown in Figure 4.3.22. This is a good indication of the extent of electrode passivation that is occurring when using the quinone containing electrolytes. While high current densities are achieved on the first cycle the accumulation of lithium peroxide and lithium carbonate at the electrode surface quickly reduces the current. After 5 cycles there is almost no benefit to using the quinones. In order to resolve this problem an effective mediator for the charge reaction should be found. If the overpotentials required to oxidise lithium peroxide could be reduced then it may be possible to achieve a complete charge step converting all lithium peroxide formed on discharge back to oxygen.

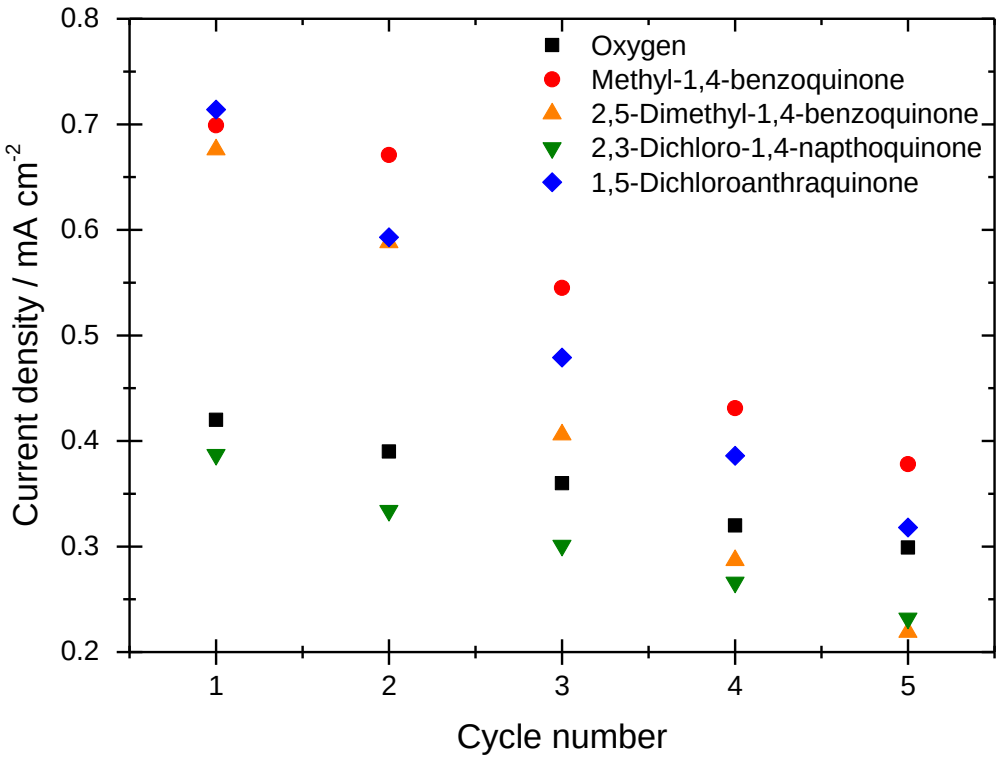

Figure 4.3.22 Oxygen reduction peak current for different 1 mM quinone containing electrolytes made with 0.2 M oxygen saturated diglyme. All scans were conducted at 100 mV s^{-1} using a glassy carbon working electrode (Ø = 3 mm) vs. a lithium metal counter/reference electrode. The potential began at open circuit, was swept to 4.5 V and returned to 1.5 V for 5 cycles.

4.3.4 Functionalised Quinones for the Oxygen Evolution Reaction

Having already demonstrated that quinones could be made more oxidising by the addition of electron withdrawing groups such as chlorine, this idea was extended in an attempt to raise the formal potential to effectively mediate the oxygen evolution reaction. Below in Figure 4.3.23 several halogenated quinones are depicted. Benzoquinone was selected as a base compound as this was found to be the most oxidising of the quinones previously tested. Each of these quinones was tested by cyclic voltammetry first under an argon atmosphere before saturating the electrolyte with oxygen.

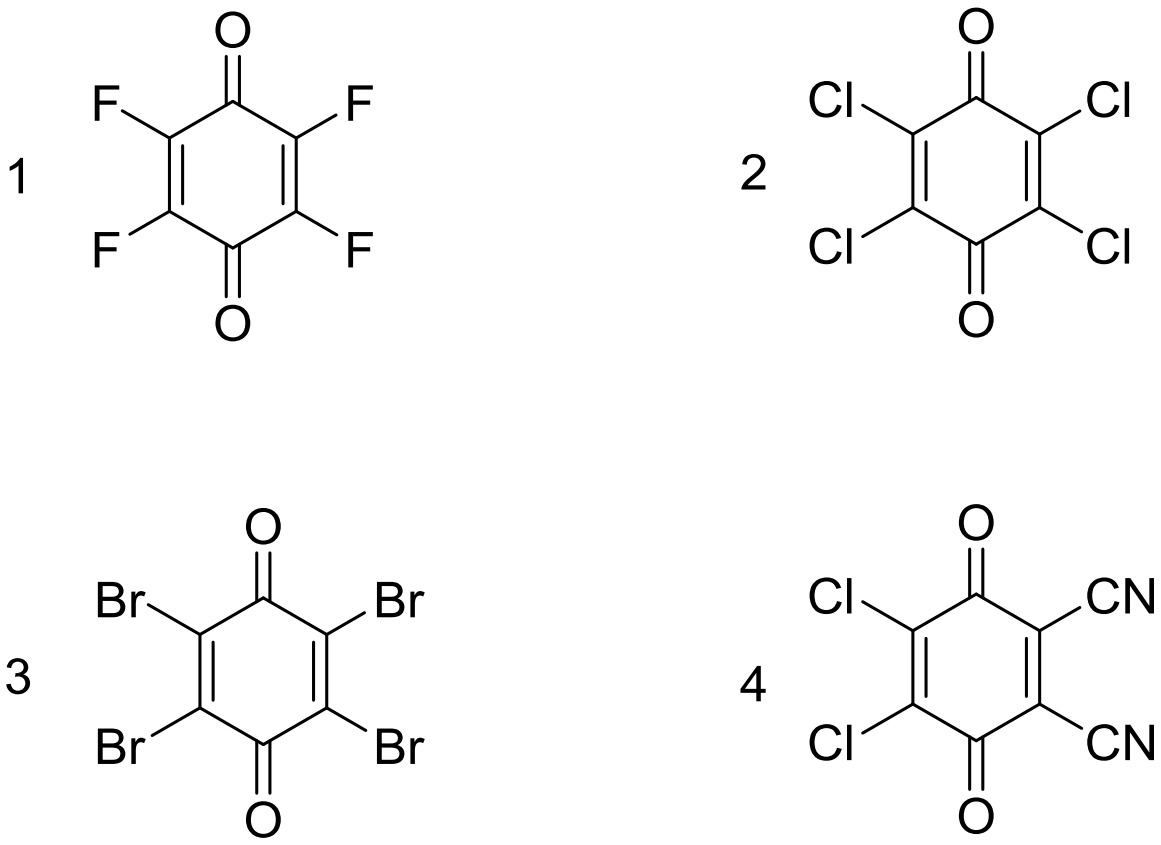

Figure 4.3.23 Structures of halogenated quinones used as possible redox mediators. 1.) Tetrafluoro-1,4-benzoquinone 2.) Tetrachloro-1,4-benzoquinone 3.) Tetrabromo-1,4-benzoquinone 4.) 2,3-Dichloro-5,6-dicyano-1,4-benzoquinone.

Starting with the most electron withdrawing group fluorine, the cyclic voltammograms under an argon atmosphere at various scan rates are shown in Figure 4.3.24. The both sets of peaks are clearly defined at all scan rates with formal potentials and peak separations of 3.11 V vs. Li/Li^+ and 100 mV for the first electron transfer and 2.91 V vs. Li/Li^+ and 290 mV for the second. This represents a positive potential shift of 150 mV in relation to this unfunctionalised benzoquinone. Given the formal potential of the oxygen reduction reaction being placed at 2.97 V vs. Li/Li^+ it can be expected that only the first electron transfer is likely to have an effect on the oxygen evolution reaction. The diffusion coefficient for tetrafluoro-1,4-benzoquinone was calculated to be 1.5×10^{-6} cm^2 s^{-1} using the Randles-Sevcik equation.

The effect of using this quinone on the oxygen reduction and evolution reactions can be seen in Figure 4.3.25. The black trace shows oxygen saturated electrolyte at 100 mV s^{-1} in the absence of a quinone. The blue trace shows the electrolyte containing 1 mM tetrafluoro-1,4-benzoquinone in an argon atmosphere and the red trace shows an oxygen saturated electrolyte which contains 1 mM of the quinone. On the negative sweep both the first and second reductions of the fluorinated quinone appear unchanged while the peak corresponding to oxygen reduction appears at a far more negative potential. On the positive sweep the oxidation of the tetrafluoro-1,4-benzoquinone has merged into the oxygen evolution reaction causing the peak to appear at a slightly earlier potential.

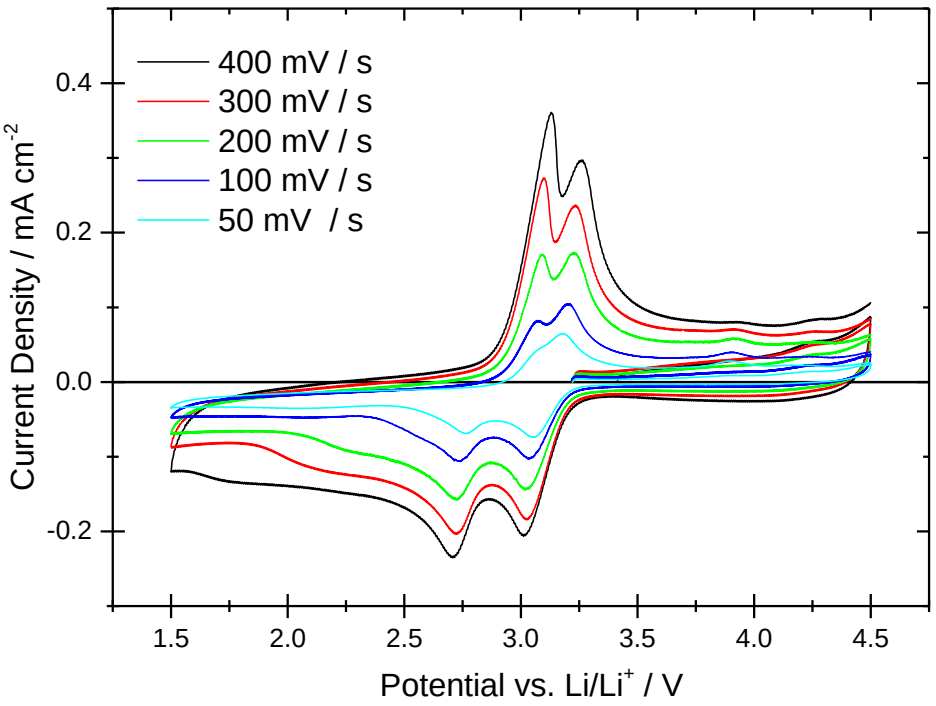

Figure 4.3.24 Cyclic voltammograms of 1 mM tetrafluoro-1,4-benzoquinone in a 0.2 M LiTFSI diglyme electrolyte recorded at different sweep rates. A glassy carbon working electrode (Ø = 3 mm) vs. a lithium metal counter/reference electrode was used. The potential began at open circuit, was swept from open circuit to 4.5 V then down to 1.5 V, before finally returning to 4.5 V.

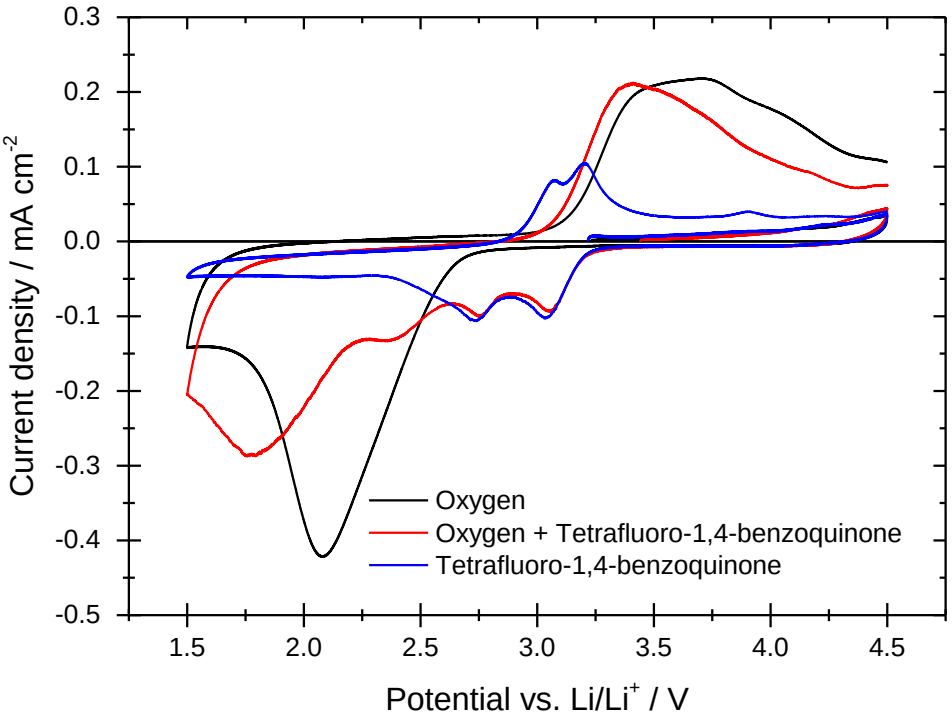

Figure 4.3.25 Cyclic voltammograms using a glassy carbon working electrode (Ø = 3 mm) vs. a lithium metal counter/reference electrode. The electrolyte in each case consisted of 0.2M LiTFSI in diglyme, but was either oxygen saturated (black), containing 1 mM tetrafluoro-1,4-benzoquinone (blue), or both (red). The potential began at open circuit, was swept positively to 4.5 V then negatively to 1.5 V before finally returning to 4.5 V. In each case the scan rate was 100 mV s^{-1}.

The cyclic voltammogram for tetrachloro-1,4-benzoquinone is similar to that of the tetrafluoro-1,4-benzoquinone in that both oxidation steps are distinct. The peaks are not only larger, indicating greater mobility but also appear more reversible than in the case of the fluorinated quinone. Upon calculating the peak potentials at zero current, the peak separations for the first and second redox couple are 61 mV and 60 mV respectively. This indicates good reversibility despite the presence of lithium ions in the electrolyte. The formal potentials are 3.14 V and 2.87 V vs. Li/Li^+ and the diffusion coefficient is calculated to be 3.8 x 10^{-6} cm^2 s^{-1}. The plots used to determine the diffusion coefficient, formal potentials and peak separation are shown in Figure 4.3.26 and Figure 4.3.27. The formal potentials for each of these quinones along with their calculated diffusion coefficients are listed in Table 4.3.4.

Upon saturating the electrolyte with oxygen the red trace in Figure 4.3.29 was obtained. Here the peak reduction for oxygen can be seen to occur at the same potential as in the absence of the quinone. While the peak potential for the evolution occurs 200 mV earlier. Beyond 4.0 V vs. Li/Li^+ there are no further peaks indicating that there is no additional carbon dioxide evolution which could have resulted from the decomposition of the quinone. A surprising feature of this voltammogram is the absence of the 3.0 V oxidation peak of the chlorinated quinone. One possible explanation for this is that the surface passivation occurring on discharge prevents any other electron transfer until the surface film of lithium peroxide is oxidised.

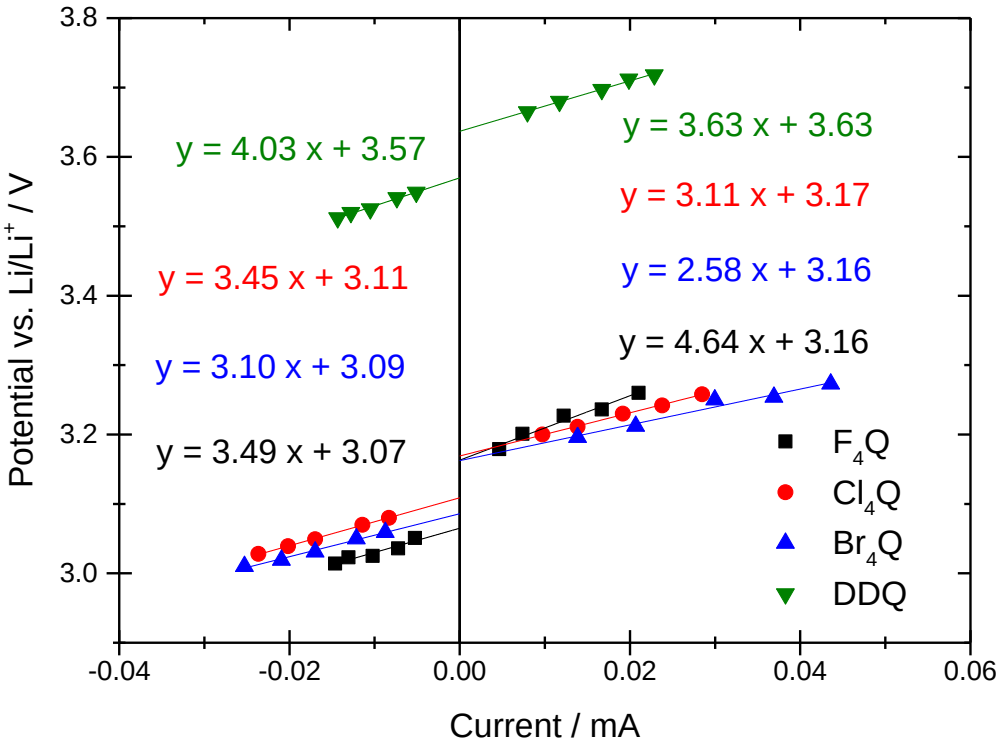

Figure 4.3.26 Peak potential vs. peak current plot for tetrafluoro-1,4-benzoquinone (F_4Q), tetrachloro-1,4-benzoquinone (Cl_4Q), tetrabromo-1,4-benzoquinone (Br_4Q) and 2,3-dichloro-5,6-dicyano-1,4-benzoquinone (DDQ) to determine their formal potential and peak separation in 0.2 M LiTFSI in diglyme.

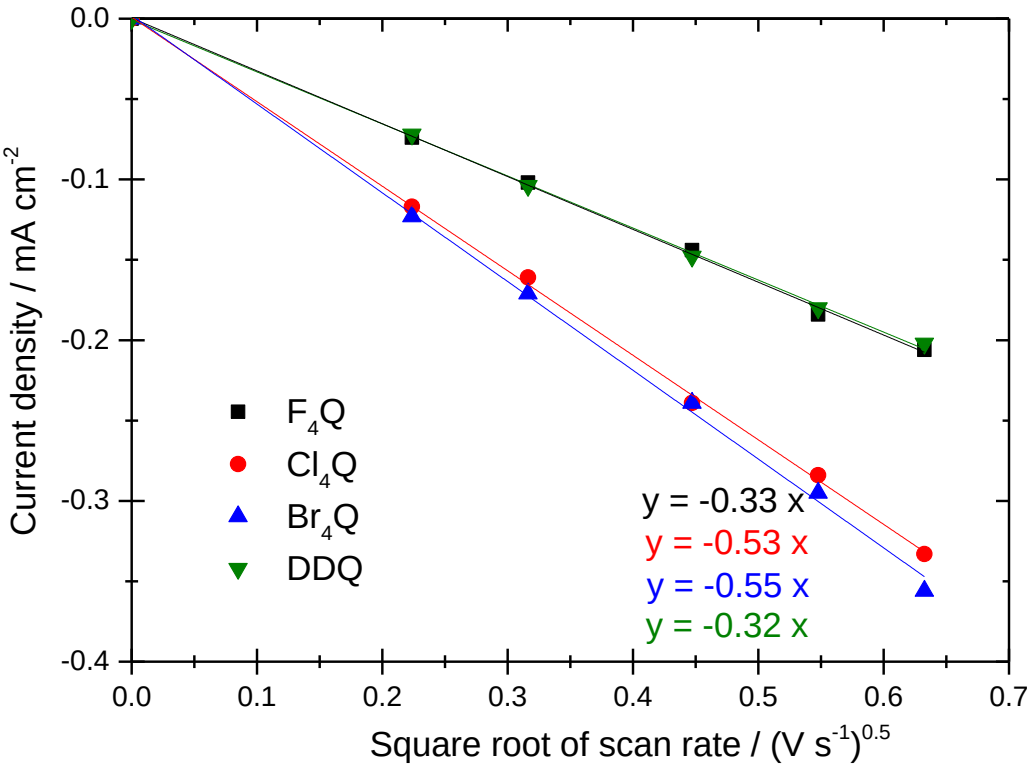

Figure 4.3.27 Determination of the diffusion coefficient for a selection of halogenated quinones.

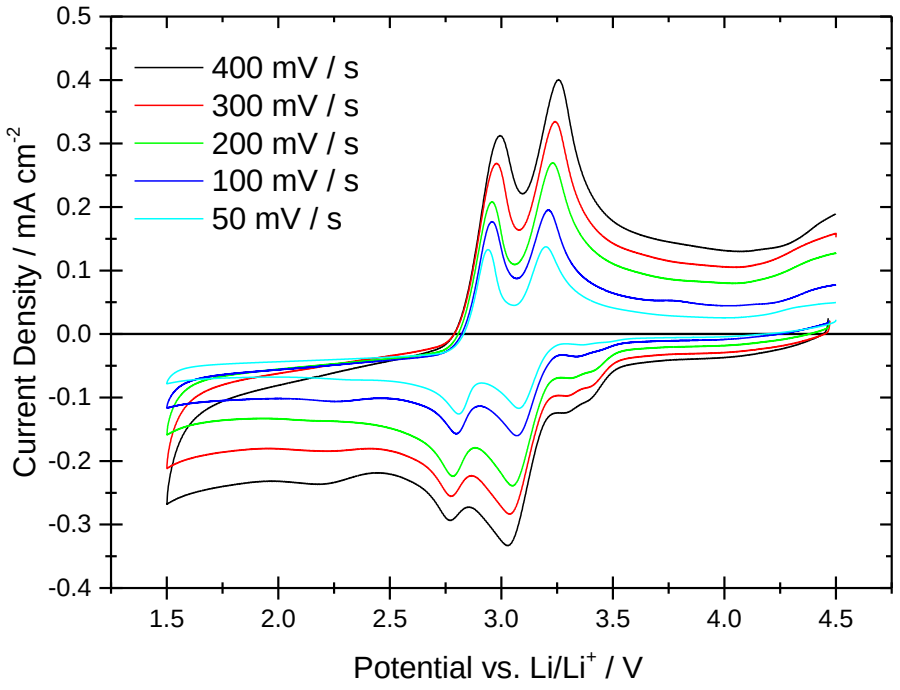

Figure 4.3.28 Cyclic voltammograms of 1 mM tetrachloro-1,4-benzoquinone in a 0.2 M LiTFSI diglyme electrolyte recorded at different sweep rates. A glassy carbon working electrode (Ø = 3 mm) vs. a lithium metal counter/reference electrode was used. The potential began at open circuit, was swept from open circuit to 4.5 V then down to 1.5 V before finally returning to 4.5 V.

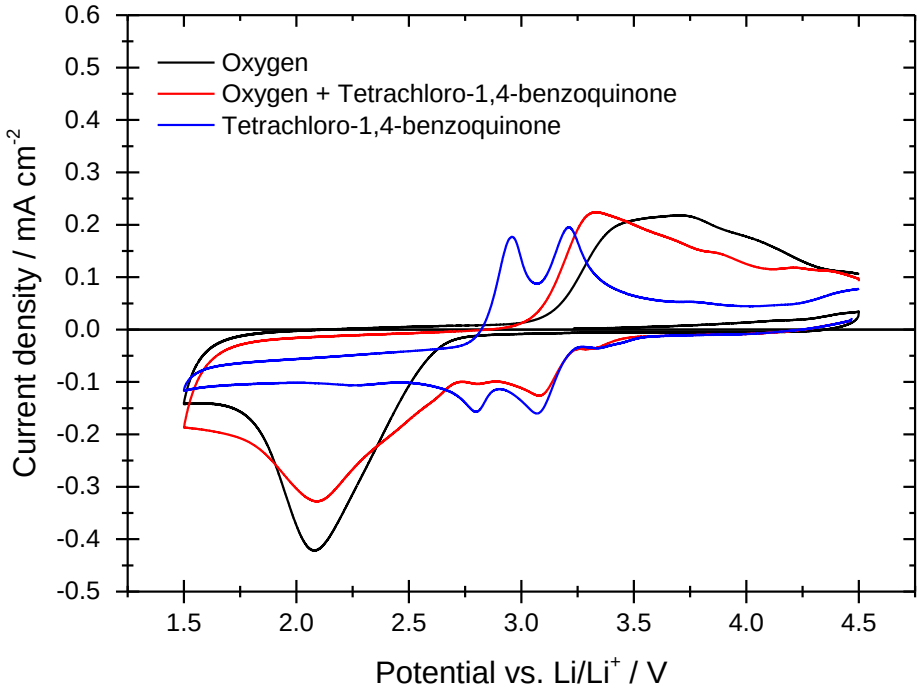

Figure 4.3.29 Cyclic voltammograms using a glassy carbon working electrode (Ø = 3 mm) vs. a lithium metal counter/reference electrode. The electrolyte in each case consisted of 0.2M LiTFSI in diglyme, but was either oxygen saturated (black), containing 1 mM tetrachloro-1,4-benzoquinone (blue), or both (red). The potential began at open circuit, was swept positively to 4.5 V then negatively to 1.5 V before finally returning to 4.5 V. In each case the scan rate was 100 mV s^{-1}.

The tetrabromo-1,4-benzoquinone shows a similar trend to the previously shown halogenated quinones. The two oxidation steps can both be seen, this time with the first oxidation requiring a large overpotential and the second oxidation occurring quickly afterwards. On the negative sweep there is a small broad peak present at 2.0 V vs. Li/Li^+. This is the expected potential for oxygen reduction and suggests a very low concentration may be present in solution. On the positive sweep another small peak is visible at 3.8 V which is likely to be the related oxygen evolution reaction. The formal potential and peak separation is 3.12 V and 77 mV for the first reduction and 2.95 V and 220 mV for the second. The formal potentials for the three tetra-halogenated quinones are very similar suggesting that the type of halogen has had very little effect on the peak position but a significant effect on the reversibility of the electron transfer.

The oxygen saturated electrolyte containing 1 mM tetrabromo-1,4-benzoquinone is shown in Figure 4.3.31. As the potential is swept from 4.5 V to 1.5 V vs. Li/Li^+ the two reduction peaks for the tetrabromo-1,4-benzoquinone appear unchanged in the presence of oxygen. The oxygen reduction peak is much broader than before only beginning to decrease as the potential approaches the 1.5 V limit. The potential sweep direction is then reversed and as before no oxidation is observed until the oxygen evolution process begins. With the 1 mM tetrabromo-1,4-benzoquinone the potential rises much more steeply at the onset of evolution and forms a more defined peak.

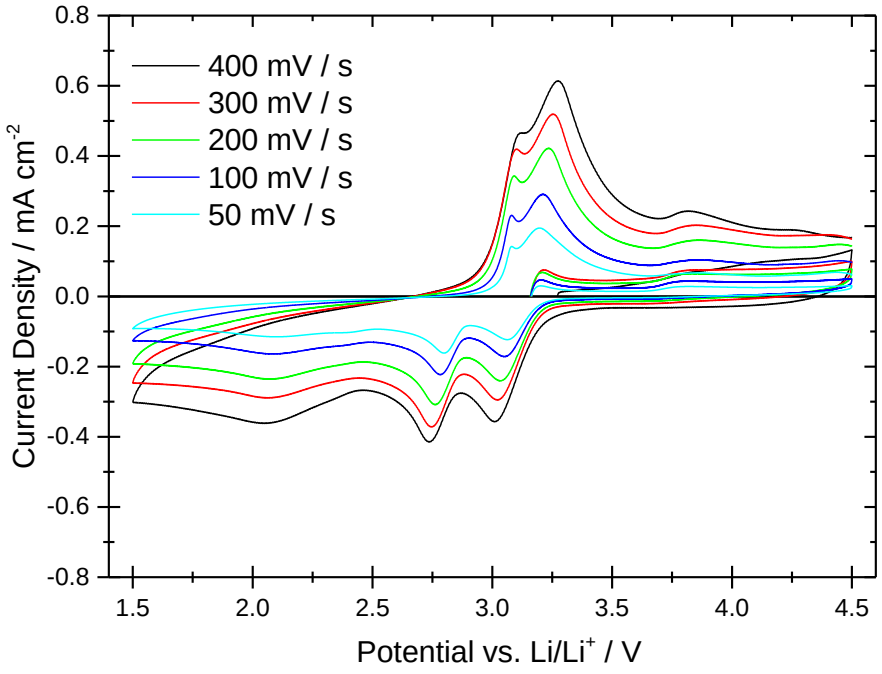

Figure 4.3.30 Cyclic voltammograms of 1 mM tetrabromo-1,4-benzoquinone in a 0.2 M LiTFSI diglyme electrolyte recorded at different sweep rates. A glassy carbon working electrode (Ø = 3 mm) vs. a lithium metal counter/reference electrode was used. The potential began at open circuit, was swept from open circuit to 4.5 V then down to 1.5 V, before finally returning to 4.5 V.

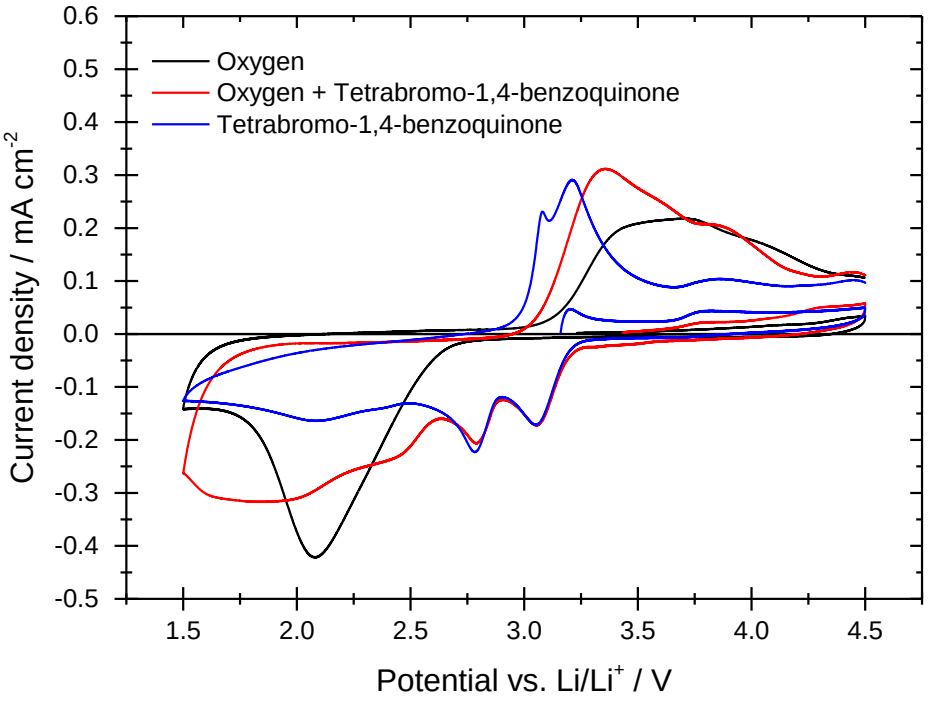

Figure 4.3.31 Cyclic voltammograms using a glassy carbon working electrode (Ø = 3 mm) vs. a lithium metal counter/reference electrode. The electrolyte in each case consisted of 0.2M LiTFSI in diglyme, but was either oxygen saturated (black), containing 1 mM tetrabromo-1,4-benzoquinone (blue), or both (red). The potential began at open circuit, was swept positively to 4.5 V then negatively to 1.5 V, before finally returning to 4.5 V. In each case the scan rate was 100 mV s^{-1}.

The last quinone tested as a possible mediator for the oxygen evolution reaction was 2,3-dichloro-5,6-dicyano-1,4-benzoquinone, hereafter referred to as DDQ. This was by far the most oxidising quinone used with a formal potential of 3.60 V vs. Li/Li^+ for the first electron transfer. This is actually beyond the onset potential for oxygen evolution suggesting it will have little effect on the initial evolution process. The second reduction occurs at 3.15 V vs. Li/Li^+. When the potential is taken below 2.5 V on the negative sweep an additional peak is present which again may be due to a small oxygen contamination. As the potential approaches 1.5 V vs. Li/Li^+ the current begins to drop steeply downwards indicating that DDQ is not stable below this potential. The diffusion coefficient for DDQ was calculated to be 1.5×10^{-6} cm^2 s^{-1}.

After the solution was saturated with oxygen the cyclic voltammogram shown in Figure 4.3.33 was obtained. Unusually there is an increase in the oxygen reduction peak current while the oxygen evolution reaction initially proceeds as in the absence of a quinone. However, after reaching 3.5 V the current increases forming a new peak at 3.7 V. This is in line with the peak potential of the DDQ oxidation suggesting it oxidises after the oxygen evolution reaction and therefore does not mediate the electron transfer. DDQ is a powerful oxidant and its presence in solution may be useful in removing the build-up of lithium carbonate. This would be more apparent over subsequent cycles, as if the surface remains clear of Li_2CO_3 it is able to achieve the same peak current over many cycles.

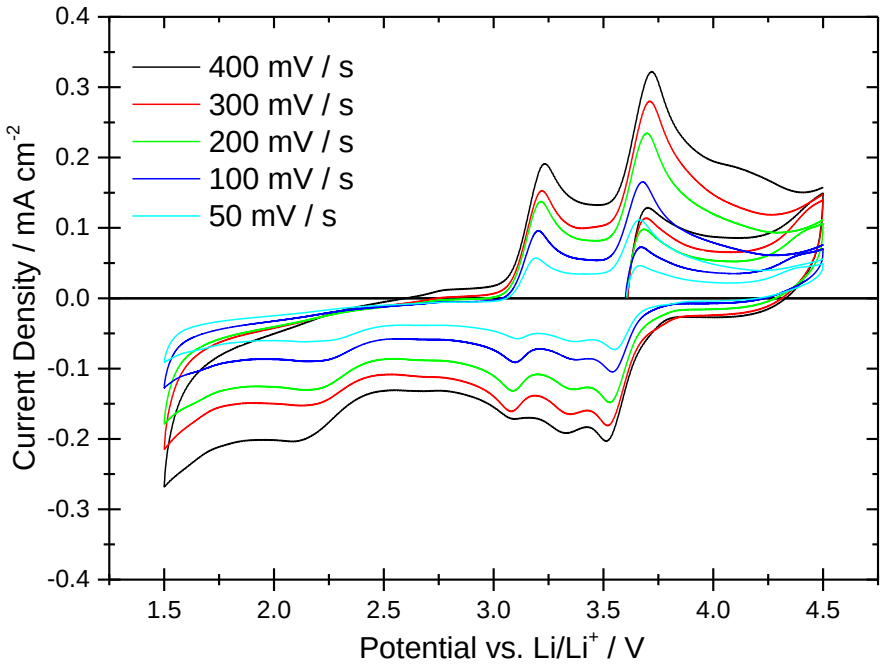

Figure 4.3.32 Cyclic voltammograms of 1 mM tetrabromo-1,4-benzoquinone in a 0.2 M LiTFSI diglyme electrolyte recorded at different sweep rates. A glassy carbon working electrode (Ø = 3 mm) vs. a lithium metal counter/reference electrode was used. The potential began at open circuit, was swept from open circuit to 4.5 V then down to 1.5 V before finally returning to 4.5 V.

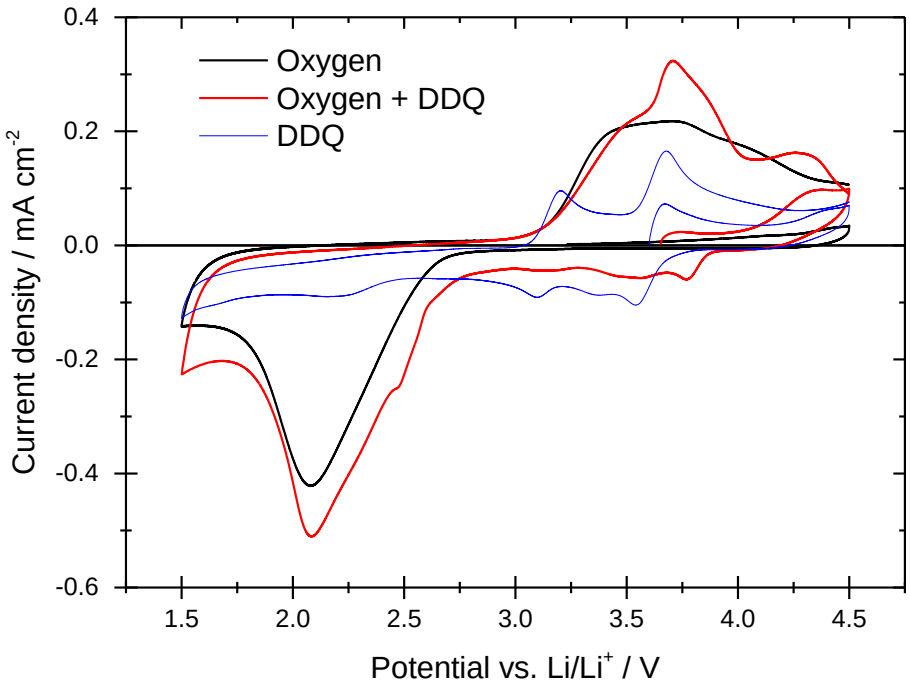

Figure 4.3.33 Cyclic voltammograms using a glassy carbon working electrode (Ø = 3 mm) vs. a lithium metal counter/reference electrode. The electrolyte in each case consisted of 0.2M LiTFSI in diglyme, but was either oxygen saturated (black), containing 1 mM tetrabromo-1,4-benzoquinone (blue), or both (red). The potential began at open circuit, was swept positively to 4.5 V then negatively to 1.5 V, before finally returning to 4.5 V. In each case the scan rate was 100 mV s^{-1}.

The most revealing parameter of how effective these quinones are at mediating the charge reaction can actually be found by looking at the oxygen reduction reaction, as the passivation effect is caused by blocking the surface of the electrode. By monitoring the peak current of oxygen reduction it can provide an insight into whether the quinones are aiding the removal of the poorly conducting lithium peroxide. Figure 4.3.34 shows the peak current over the first 5 cycles. The result of an oxygen saturated electrolyte containing no quinone is included for reference (black). In each case of using 1 mM of a halogenated benzoquinone the peak current remains almost constant. The electronically isolated lithium peroxide that normally inhibits oxygen reduction on subsequent cycles is being oxidised by these small organic compounds enabling a consistent discharge rate to occur.

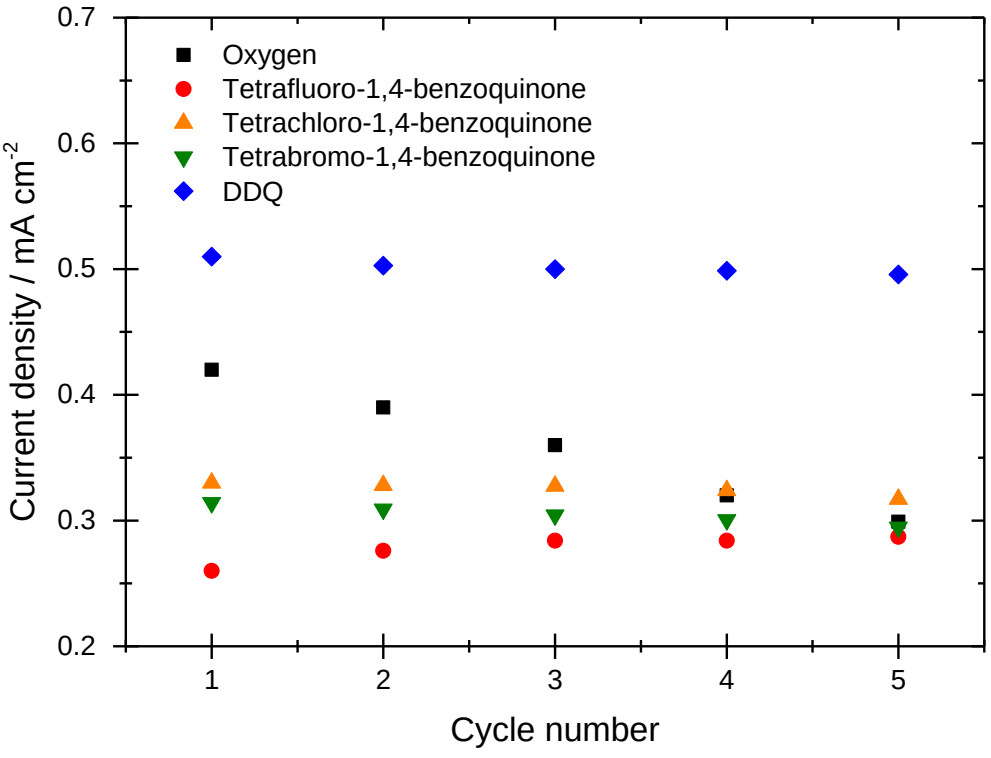

Figure 4.3.34 Oxygen reduction peak current for different 1 mM quinone containing electrolytes made with 0.2 M oxygen saturated diglyme. All scans were conducted at 100 mV s^{-1} using a glassy carbon working electrode (Ø = 3 mm) vs. a lithium metal counter/reference electrode. The potential began at open circuit, was swept to 4.5 V and returned to 1.5 V for 5 cycles.

As a summary of these more oxidising quinones the formal potential and diffusion coefficient under argon is included in the table below. Along with the corresponding peak current and potential of oxygen evolution. The tetra-halogenated quinones have each reduced the overpotential at the peak of oxygen evolution by approximately 300 mV with a concentration of only 1 mM. The most effective quinone for mediating the evolution reaction can be identified as tetrabromo-1,4-benzoquinone.

Table 4.3.4 Formal potentials and diffusion coefficients for 1 mM quinone containing electrolytes. The peak current and potential vs. Li/Li$^+$ for the oxygen evolution reaction in these 1 mM quinone containing electrolytes is also included. The results for an oxygen saturated electrolyte in the absence of any quinone are in the top row of the table.

Quinone	E'^o vs. Li/Li$^+$ / V	Diffusion Coefficient / cm^2 s^{-1}	Ep_c vs. Li/Li$^+$ in Oxygen / V	Jp_c in Oxygen / mA cm^{-2}
N/A	2.97	N/A	3.71	0.22
Tetrafluoro-1,4-benzoquinone	3.11	1.5 x 10^{-6}	3.39	0.21
Tetrachloro-1,4-benzoquinone	3.14	3.8 x 10^{-6}	3.32	0.22
Tetrabromo-1,4-benzoquinone	3.12	4.2 x 10^{-6}	3.35	0.31
DDQ	3.60	1.5 x 10^{-6}	3.70	0.32

4.4 Conclusions and Further Work

The electrochemistry of various quinones was studied and shown to have formal potentials ranging from 3.60 V down to 2.22 V vs. Li/Li^+ by varying the attached functional groups. Several quinones exhibited fast and reversible electron transfer for the first reduction while the second reduction was consistently more irreversible than the first. The literature commonly reports the first electron transfer of quinones to be reversible in non-aqueous media whereas the second is quasi-reversible.[103–105] The greater irreversibility found in some quinones could be attributed to the presence of lithium ions which form a complex with both the semi-quinone and dianion forms. Quinones with formal potentials between 2.33 V and 2.75 V vs. Li/Li^+ were shown to provide a significant enhancement to the oxygen reduction reaction, while those beyond these parameters were found to have little effect. The largest increase in peak current (90%) was achieved using 1,4-napthoquinone while the greatest reduction in the overpotential was 0.4 V when using methyl-1,4-benzoquinone (67% increase in I_p). These results have shown it is possible to discharge a lithium-oxygen battery faster and with greater efficiency using a low concentration of quinone in the electrolyte. The subsequent oxidation of the lithium peroxide formed and therefore the cycle life remains a problem. In the next chapter the use of these quinones in lithium-oxygen cells is studied by galvanostatic cycling and the electrodes are examined by X-ray diffraction to determine the discharge products.

In order to build on these results the concentration of the quinone used in the electrolyte should be varied to determine the highest achievable discharge rate and reduce the applied overpotential as far as possible. The concentration should then be optimised to obtain the maximum mediation effect with the smallest concentration of quinone present.

The identification of the peroxide product and the presence of any products of side reactions should be identified and examined via Raman and X-ray diffraction spectroscopy. This could be done by examining the surface of the electrode at certain points during cycling. Another valuable technique is differential electrochemical mass spectrometry which could be used to measure the moles of oxygen consumed and evolved during cycling.

With the determined active potential range for mediators of the oxygen reduction reaction (2.33 - 2.75 V vs. Li/Li^+) it would also be possible to use density functional theory to compare the potentials observed for quinones in this electrolyte to more commonly used acetonitrile or DMSO electrolytes. Using that shift in potential as a reference other redox active compounds that show reversible electron transfer in the desirable potential range can be identified and tested in the same way.

Chapter 5: Galvanostatic Cycling and X-Ray Diffraction

5.1 Introduction

In order to build on the results obtained in the previous chapter it was desirable to examine the quinones effect on the lithium-oxygen system during galvanostatic cycling. This technique is more representative of actual battery operation as the cell is discharged over several hours and is discussed in detail in Chapter 2. The total volume of electrolyte in a Swagelok cell is much smaller than in a typical electrochemical cell and therefore more representative of an operational battery. This does also make measurements more sensitive towards electrolyte decomposition. The use of quinones can be expected to reduce the overpotentials required to drive the oxygen reduction and evolution reactions allowing the cell to be discharged/ charged at higher rates. If the lithium peroxide is formed away from the electrode surface by a shuttling mechanism an increase in the discharge capacity could also be observed.

In addition to providing a more representative assessment of the quinones as mediators for a lithium-oxygen cell the use of galvanostatic cycling confers another advantage. The total charge passed on a single discharge is far larger than during cyclic voltammetry and can therefore enable the possible detection of the reaction products by X-ray diffraction. After cycling the cell the carbon electrode can be removed and examined *ex situ* to determine what products are forming at the electrode surface. This process can be repeated after the charge step as it has been shown that the carbon electrode can react to form lithium carbonate.[37]

5.2 Experimental

5.2.1 Experimental Techniques

This chapter is comprised of galvanostatic measurements performed using a Bio-Logic VMP2 (variable multi-channel potentiostat). This technique is supported by *ex situ* X-ray diffraction data. These techniques are discussed in detail in Chapter 2.

5.2.2 Cell Design

All galvanostatic measurements were carried out using a Swagelok cell design using a lithium metal counter/reference electrode vs. an ink coated carbon electrode. The Swagelok cell detailed in full in Chapter 2. After assembly the argon atmosphere in each cell was exchanged for oxygen using a dedicated purging line.

X-Ray diffraction experiments were carried out by disassembling the Swagelok cells inside an argon filled glove box to remove the carbon electrode. This was then dipped in diglyme and placed in a specially designed air tight sample holder (Bruker). All XRD measurements were carried out using a Rigaku smart lab instrument.

5.2.3 Electrode Preparation

Carbon electrodes were prepared using an ink containing acetylene black (Chevron) and lithiated nafion (LITHion, Ion power) in a 2:1 ratio in IPA. This was bar coated onto a thin separator (Celgard, C2320) and left to dry. Each electrode was weighed individually before placing into the cell to determine the mass of carbon (typically 700-800 μg).

5.3 Results and Discussion

In order to evaluate the effect of the quinones as potential mediators on the discharge and charge reactions of the lithium-oxygen battery the system must first be looked at in the absence of any mediators. This began by comparing the voltage plateaus and discharge/charge capacities of carbon electrodes in a Swagelok cell. The applied currents were normalised by the mass of carbon deposited during the ink coating process, determined by weighing electrodes individually before and after coating. Therefore all current and charge densities are given per gram of carbon in the electrode. Figure 5.3.1 displays the discharge profiles at 50, 200 and 500 mA g^{-1}. As the current density is increased the voltage plateau lowers from 2.6 V to 2.5 V vs. Li/Li^+ and finally at the highest current density of 500 mA g^{-1} no plateau is observed. At 50 mA g^{-1} the voltage decreases sharply after the plateau indicating the surface is fully covered in the solid lithium peroxide discharge product and no greater overpotential can drive the reaction any further. Whereas at higher discharge rates the voltage drop off after the plateau is more gradual indicating surface sites may still be available.

The charging step appears highly sensitive to the changing current density. At the slowest rate a near complete charge step is observed with 95% of the capacity on discharge seen on charge, whereas at 200 mA g^{-1} only 22% of the capacity is recovered and at 500 mA g^{-1} a similarly poor recovery of 35% is measured. Much of this lost capacity is no doubt due to the high overpotentials required to evolve oxygen from lithium peroxide. A voltage limit of 4.5 V vs. Li/Li^+ must be applied when using the diglyme electrolyte to prevent electrolyte degradation. If it were possible to extend the voltage limit to 5 V vs. Li/Li^+, a plateau at these higher rates may be observed. Some of the charge capacity seen here may be due to

other degradation reactions, with the carbon electrode for example. This is discussed further in Chapter 6. There is a large voltage hysteresis (1.7 V) between the discharge and charging plateaus shown in the 50 mA g^{-1} trace. This is a clear demonstration of the poor kinetics of both the oxygen reduction and evolution reactions. By the incorporation of discharge and charge mediators it can be expected that this hysteresis could be reduced therefore greatly improving the operating efficiency of a lithium-oxygen cell.

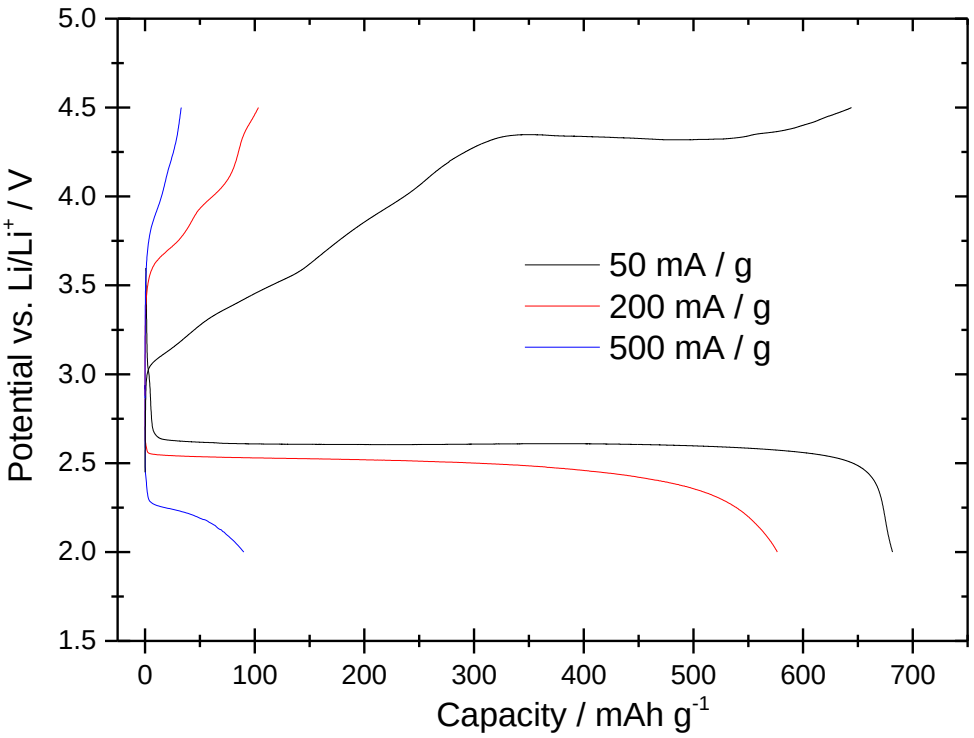

Figure 5.3.1 Discharge profiles of carbon electrodes in an oxygen saturated 0.2 M LiTFSI diglyme electrolyte. Current densities of 50, 200 and 500 mA / g were applied in the black, red and blue traces respectively. In each case the lower voltage limit was 2.0 V vs. Li/Li^+.

Due to the relatively large charges passed during galvanostatic experiments it has been shown to be possible to detect the discharge products using X-ray diffraction (XRD).[31,66,111,127] The carbon electrode discharged at 50 mA g^{-1} was removed from the Swagelok cell inside an argon filled glove box (< 10 ppm H_2O, < 10 ppm O_2) and placed inside

an airtight sample holder for XRD analysis. The diffraction patterns obtained for each cell along with patterns collected from lithium peroxide, lithium oxide, lithium carbonate and a pristine (unused) electrode are shown in Figure 5.3.2. Peaks at 21, 24 and 25 degrees can all be attributed to the carbon electrode. While the peaks at 33 and 35 degrees are characteristic of lithium peroxide. The broadness of these peaks indicate that the peroxide formed is not nearly as crystalline compared to the powdered lithium peroxide sample (blue). There is no evidence of lithium oxide or lithium carbonate present in the sample. This is in line with the literature which has found lithium peroxide to be the main discharge product with lithium carbonate only forming at higher voltages during the charging step.[28,37,128]

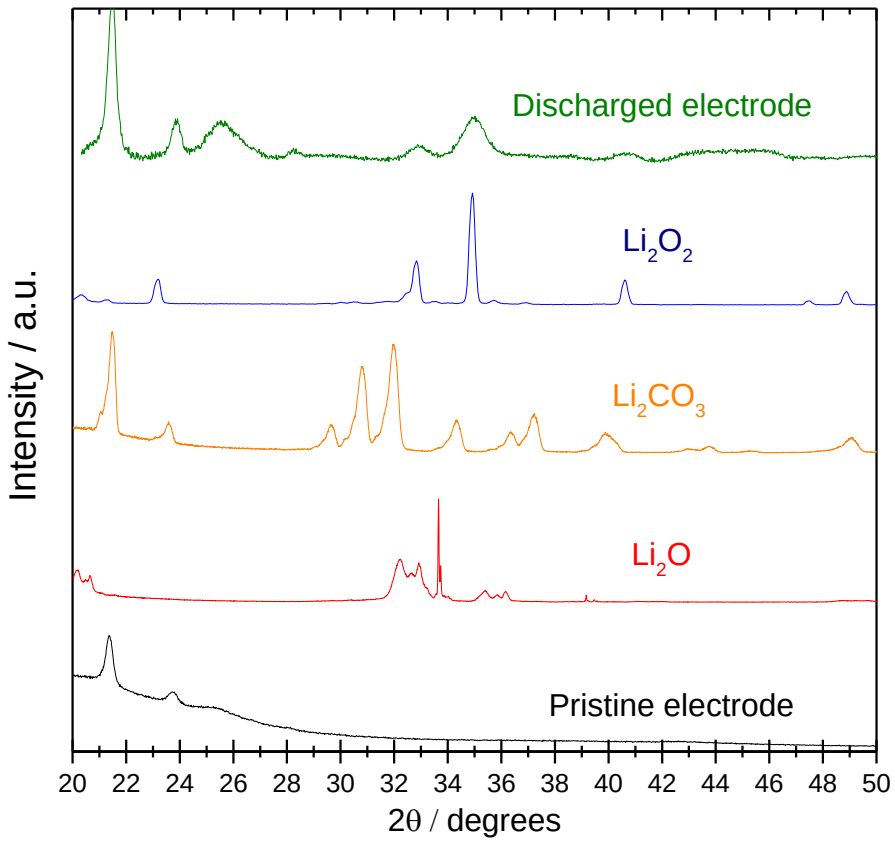

Figure 5.3.2 X-ray diffraction of a carbon electrode discharged at 50 mA g^{-1} with several commonly found products for comparison.

Two more cells were discharged at 500 mA g^{-1} with one containing 1 mM of 1,4-napthoquinone and the other 1 mM of methyl-1,4-benzoquinone. These measurements were then repeated and the resulting discharge curves are shown below in Figure 5.3.3. The addition of 1 mM methly-1,4-benzoquinone increases the discharge capacity by over 100%, while the napthoquinone is able to achieve a 200% increase in discharge capacity. It should be noted that the discharge capacity of the 1 mM quinone containing electrolytes in an argon atmosphere was ~ 10 mAh g^{-1} and therefore any additional capacity beyond this can be attributed to the mediation of the oxygen reduction reaction. The reduced overpotential would enable a lithium-oxygen cell to operate with far greater efficiency.

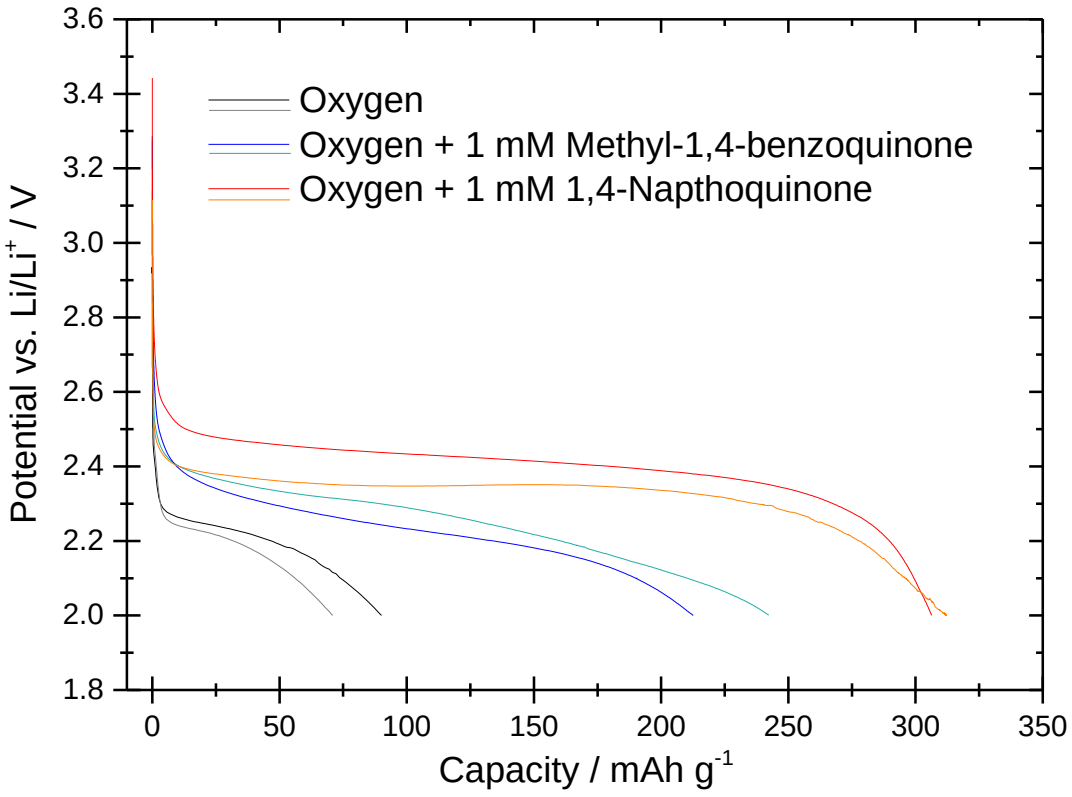

Figure 5.3.3 Galvanostatic discharges of a carbon electrode at 500 mA g^{-1} in an oxygen saturated 0.2 M LiTFSI diglyme electrolyte. The electrolyte also contained either 1 mM methyl-1,4-benzoquinone (dark and light blue traces), 1mM 1,4-Napthoquinone (red and orange traces) or neither (black and grey traces).

In order to determine if the product of the reaction was still lithium peroxide the electrodes from each of these measurements were removed from the Swagelok cells and examined by X-ray diffraction. However, no crystalline products were detected which could be attributed to the lower discharge capacity than the 50 mA g^{-1} cell. In order to resolve this further discharges were carried out at the lower rate of 50 mA g^{-1}. The electrochemical results of these 50 mA g^{-1} discharges are shown in Figure 5.3.4 along with the 500 mA g^{-1} discharges (dotted lines) for comparison. Here the overpotential required to drive the reaction at 50 mA g^{-1} is far less than at 500 mA g^{-1}. However, there is still an improvement when using the quinones as can be seen by the change in plateau potential when using the quinones. The discharge capacities at 50 mA g^{-1} are all significantly larger with the quinones providing significant improvements in the discharge capacity. This can be explained by the formation of lithium peroxide in the electrolyte allowing more charge to pass before the electrode becomes passivated.

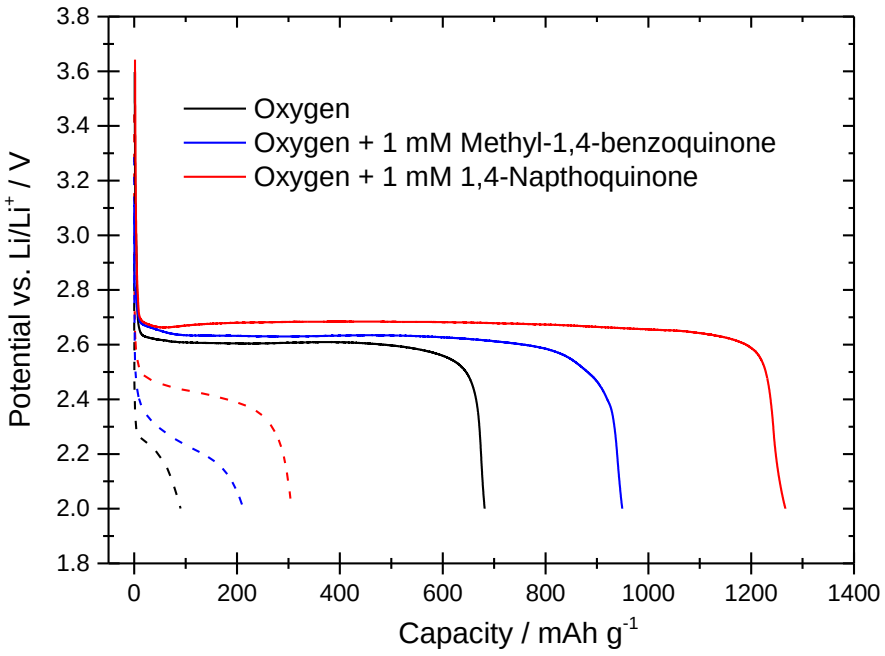

Figure 5.3.4 Galvanostatic discharges of a carbon electrode at 50 mA g^{-1} (solid lines) and 500 mA g^{-1} (dotted lines) in an oxygen saturated 0.2 M LiTFSI diglyme electrolytes. The electrolyte also contained either 1 mM methyl-1,4-benzoquinone (blue traces), 1mM 1,4-Napthoquinone (red traces) or neither (black traces).

After discharge these cells were taken into an argon filled glove box so the carbon electrodes could be removed and examined by X-ray diffraction. The patterns obtained are shown below in Figure 5.3.5 with the powder diffraction pattern for lithium peroxide included for reference. Each of the electrodes discharged show peaks at 33, 35 and 41 degrees representing the lithium peroxide discharge product. In all cases the peaks are broad indicating low crystallinity. As before there is no evidence of any lithium oxide or lithium carbonate present on the electrode surface.

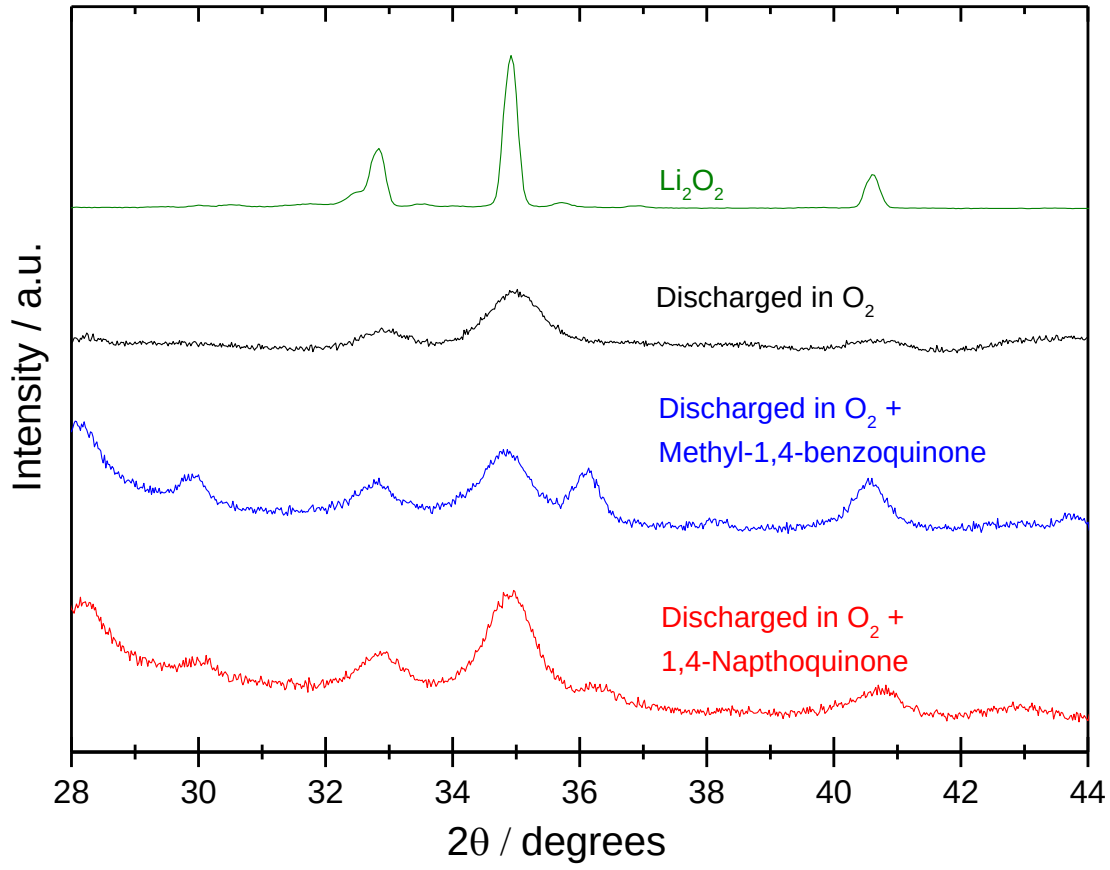

Figure 5.3.5 X-ray diffraction patterns of carbon electrodes discharged at 50 mA g^{-1}. The electrolyte was 0.2 M LiTFSI in diglyme containing either 1 mM methyl-1,4-benzoquinone (blue), 1 mM 1,4-napthoquinone (red) or neither (black)

In order to improve upon the charge reaction the halogenated quinones looked at in Chapter 4 were cycled using galvanostatic cycling at 50 mA g^{-1}. The voltage profiles are compared in Figure 5.3.6 against the unmediated result. In each case the discharge capacity was found to be slightly larger (10%) due to the additional current from the quinone reduction, while the discharge voltage was almost identical. During the charge step the overpotential required decreases moving from the fluorinated to the chlorinated and finally the brominated quinone. The charge capacity when using the quinones is increased from 95% to 96, 99 and 99% for the tetrafluoro, tetrachloro and tetrabromoquinone respectively. Improving the charging reaction is likely to prevent electrode passivation on subsequent cycles.

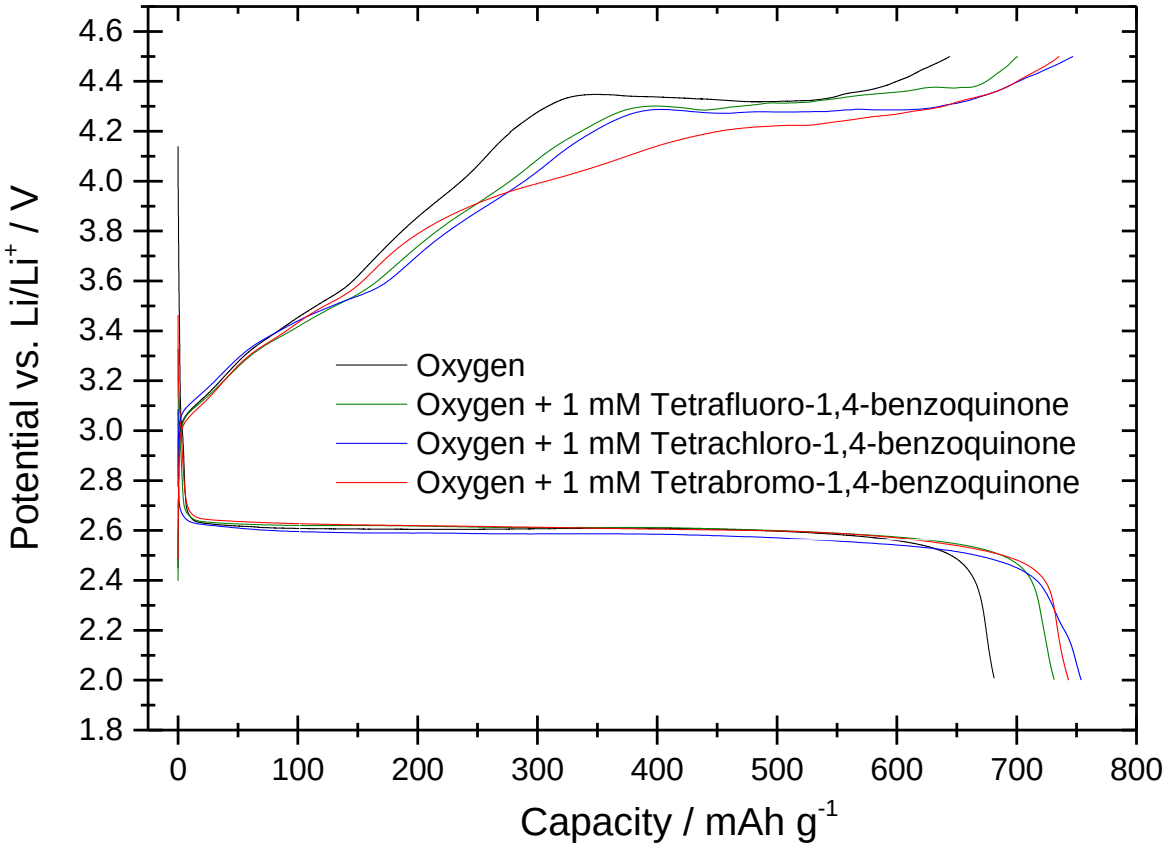

Figure 5.3.6 Galvanostatic cycle at 50 mA g^{-1} of a carbon electrode in an oxygen saturated 0.2 M LITFSI electrolyte (black). 1 mM of a specified quinone (green, blue and red traces) was added to determine their effect on the charging process.

To determine whether the charge reaction was evolving oxygen or if the carbon electrode was instead being oxidised to form lithium carbonate further X-ray diffraction measurements were performed. This time carbon electrodes were removed after a 50 mA g^{-1} discharge (red and blue traces) and after a 50 mA g^{-1} charge. The results shown in Figure 5.3.7 confirm that lithium peroxide is still the main product on discharge. While after the charging step the lithium peroxide peaks are no longer visible and there are no signs of crystalline lithium carbonate present on the electrode. However, due to the limitations of x-ray diffraction it should be mentioned that any amorphous products would not be detected. This could instead be confirmed by the use of Raman spectroscopy.

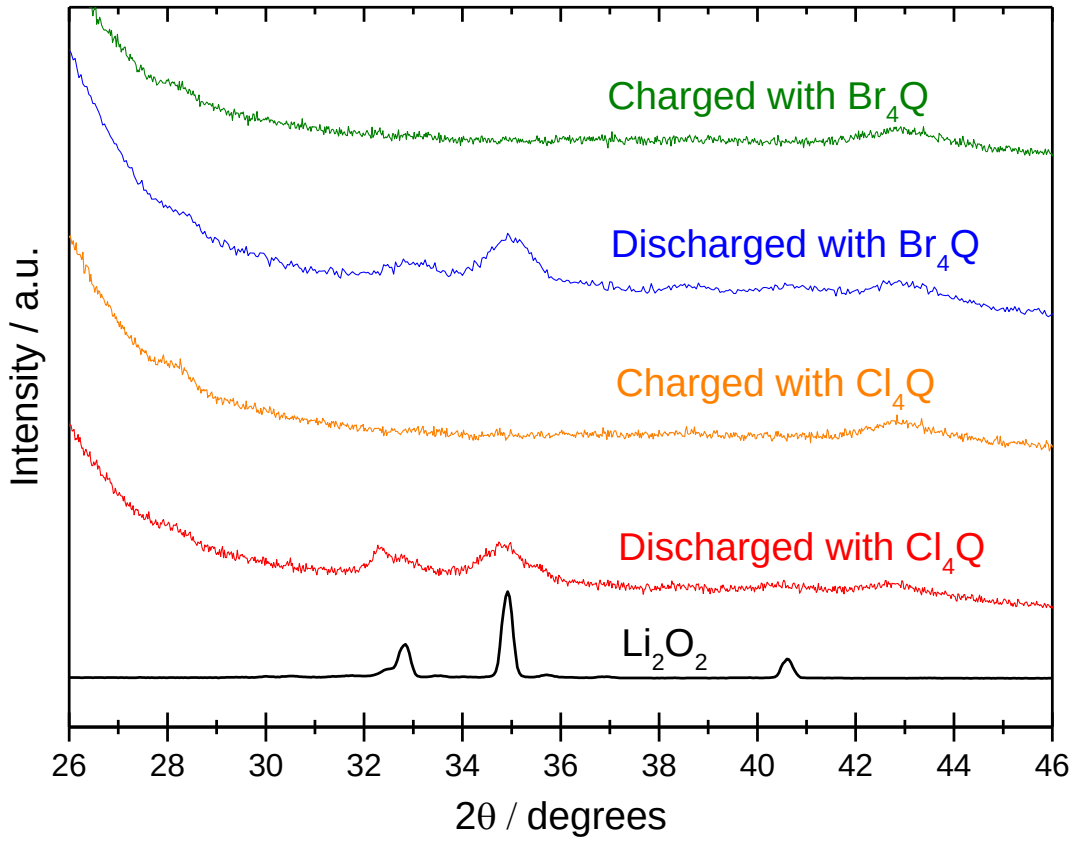

Figure 5.3.7 X-ray diffraction patterns of carbon electrodes after discharge (red and blue) and after charge (orange and green) in a 1 mM quinone, 0.2 M LITFSI, oxygen saturated diglyme electrolyte.

5.4 Conclusions and Further Work

Through the use of galvanostatic cycling the behaviour of the lithium-oxygen battery system at high rates has been examined. Both the discharge and charge capacities are found to be significantly decreased at high cycling rates (>200 mA g^{-1}). The charge step must be performed at low rates to ensure that the oxidation of the discharge product can occur. The use of low concentrations of quinones has been shown to reduce the overpotential required when both discharging and charging the cell. The use of quinones therefore could facilitate the operation of lithium-oxygen batteries at higher rates. Through the use of the mediation mechanism it has also been shown that the discharge capacity can be improved by forming lithium peroxide in the electrolyte away from the electrode surface. The presence of quinones has been shown to have no effect on the products formed during the discharge as lithium peroxide was demonstrated to be the dominant product both with and without quinones. While during the charge reaction no decomposition products have been detected, the mediation of the charge reaction is not very evident, possibly due to the low concentrations of the quinones used.

The use of higher concentrations of the quinones mediators > 10 mM could enable the cells to cycle at far higher rates than what is currently observed. In order to build on this work *ex situ* Raman spectroscopy should be performed to determine if any amorphous products are present after the discharge and charge steps. In Chapter 6 in-operando measurements such as using differential electrochemical mass spectrometry (DEMS) are performed to provide important information about the columbic efficiency of the discharge and charge reactions by enabling a quantitative measurement of the oxygen consumed and evolved during the cycling process.

Chapter 6: Differential Electrochemical Mass Spectrometry

6.1 Introduction

Differential electrochemical mass spectrometry (DEMS) has been used increasingly in lithium-oxygen research.[37,38,52,69,129] The technique enables the quantitative analysis of volatile products during the cycling of a cell. For this reason the technique is especially relevant to lithium-oxygen research as oxygen is exchanged between the head space in the cell and the electrolyte during cycling. In this chapter early DEMS measurements were carried out at the Institute for Physical and Theoretical Chemistry, University of Bonn, Germany, before installing a DEMS system in Southampton to allow for similar in-operando measurements to be carried out.

In Bonn experiments were carried out with the help of Christoph Bondue and Helmut Baltruschat. A teflon membrane assembly was used which relies upon an applied vacuum behind the electrode surface which functions to remove any volatile products formed at the electrode and draws them into the mass spectrometer. This method provides a fast response time where products are swiftly purged from the system and detected making it ideal for fast techniques such as cyclic voltammetry. However, in order to prevent the electrolyte from being drawn into the vacuum the electrolyte must be sufficiently polar to be repelled by the hydrophobic membrane. The carrier gas assembly implemented in Southampton has a slower response time as the products must be purged from the electrolyte by diffusion but has the benefit of greater flexibility in solvent choice. Galvanostatic cycling was used in Southampton as it is a slower technique and more commonly used throughout battery research.

6.2 Experimental

6.2.1 Experimental Techniques

Throughout this chapter both cyclic voltammetry and galvanostatic cycling have been used in combination with mass spectrometry. These techniques are discussed in detail in Chapter 2. For the experiments performed in Southampton all galvanostatic cycling was performed on a Bio-Logic VMP2 (variable multi-channel potentiostat) while all mass spectrometry was measured using a Hiden quantitive gas analyser with a quadrupole detector. The cyclic voltammetry measurements were taken using a custom made potentiostat in Bonn, Germany. The mass spectrometer was also assembled on site and utilised a quadrupole detector.[115]

6.2.2 Cell Design

The Swagelok cell design used in Southampton and the teflon membrane cell used in Bonn are described in detail in Chapter 2. For chemical measurements such as the H_2O_2 calibrations an adapted media bottle was used with Swagelok connectors to allow the bottle to be continuously purged. The outlet was then connected to the mass spectrometer for analysis.

6.2.3 Electrode Preparation

Carbon electrodes of larger diameter (Ø = 20 mm) and greater carbon content were cast in order to allow measurements to be performed at higher absolute currents. This was done to improve the signal when taking measurements using the carrier gas assembly. In Bonn a gold sputtered teflon membrane (Ø = 6 mm) was used for the working electrode. A gold wire was used as the counter electrode and a silver wire immersed in 0.1 M $AgNO_3$ in DMSO was used as the reference electrode.

6.3 Results and Discussion

The first mass spectrometry experiments were carried out in Germany using the teflon membrane assembly described in Chapter 2. The teflon membrane prevented solvent being drawn into the vacuum by a combination of the hydrophobicity of the teflon, the surface tension of the solvent and the contact angle between the teflon and the solvent. Therefore, the set up only allowed for the use of certain solvents, meaning DMSO was used instead of diglyme. To demonstrate the system oxygen reduction and evolution was performed in the absence of any mediators. The electrolyte was 0.1 M lithium perchlorate in DMSO and was purged with oxygen throughout the experiment to maintain a positive pressure within the cell. The potential limits applied were -1.5 V to 1.0 V vs. Ag/Ag^+ for 3 cycles. The mass charge ratios 32, 29 and 44 were recorded to detect signs of oxygen, CHO and carbon dioxide respectively.

Figure 6.3.1 displays the voltage, current and ion currents vs. time. On the negative sweep to -1.5 V vs. Ag/Ag^+ the reduction of oxygen is confirmed by the decrease in m/z 32 (highlighted by the black dotted line) while there is no apparent change in CO_2. When the potential is swept positively to 1.5 V vs. Ag/Ag^+ there are two distinct peaks in the current. One at -0.5 V (blue dotted line) and another which is cut off by the potential limit at +1.0 V (red dotted line). At -0.5 V vs. Ag/Ag^+ all the current is shown to be due to the evolution of oxygen. The evolution of oxygen stopped by 0.5 V, marking a temporary dip in current. Beyond this point CO_2 evolution takes over as is evidenced from the peaks in the m/z ratio 44. The peak in CO_2 evolution occurs at the voltage limit of 1.0 V vs. Ag/Ag^+ indicating that more CO_2 would have been evolved had the potential continued to increase.

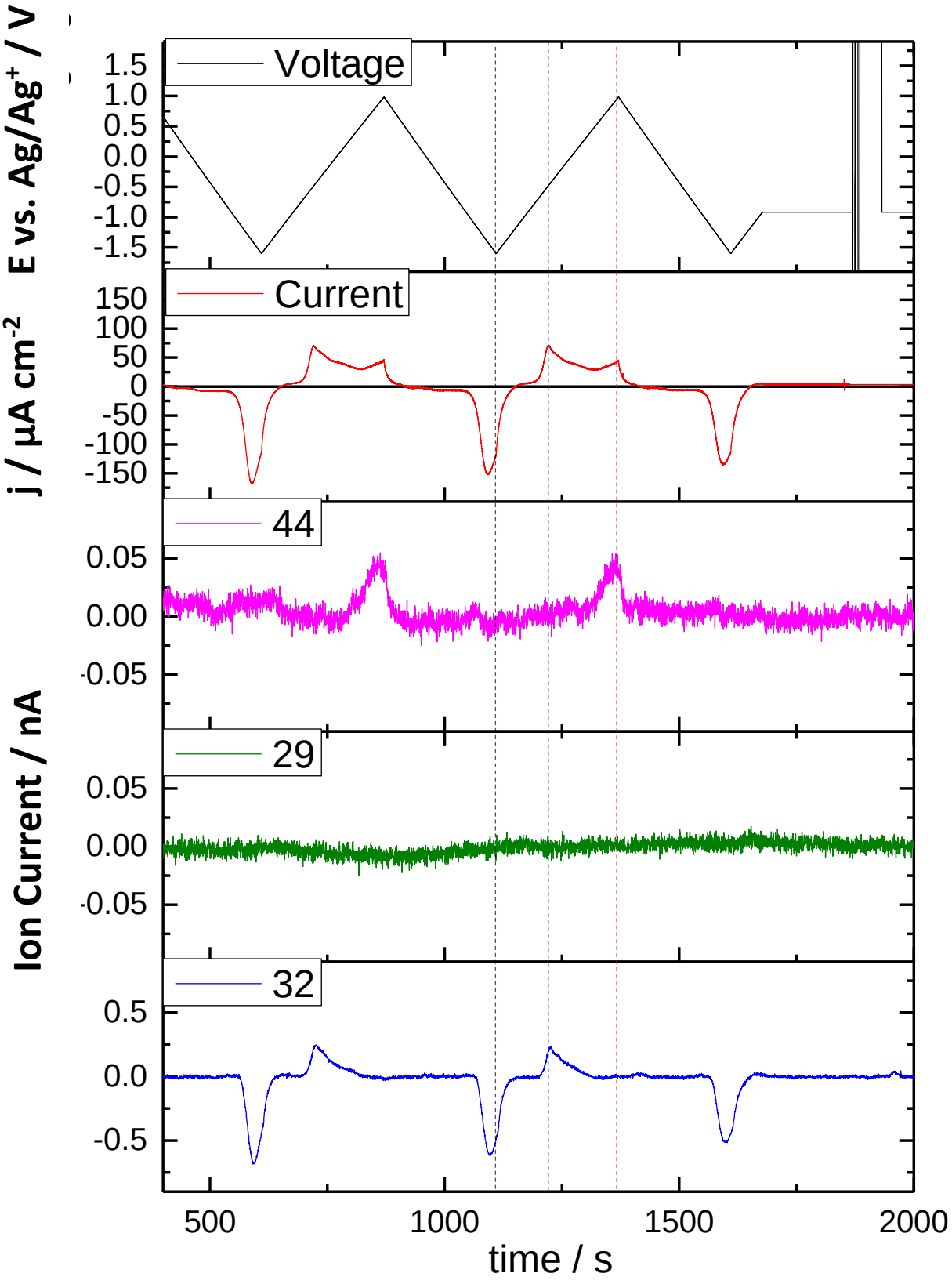

Figure 6.3.1 DEMS results of a gold working electrode (Ø = 6 mm) in an oxygen saturated 0.1 M $LiClO_4$ DMSO electrolyte. The potential was the cycled between -1.5 and 1.0 V vs. Ag/Ag^+. The mass spectrometer recorded m/z ratios 44, 29 and 32 relating to CO_2, CHO, and O_2 respectively.

These initial results highlighted how useful DEMS could be in analysing lithium-oxygen systems. The setting up of the carrier gas assembly in Southampton began with measurements of oxygen evolution from the catalysed decomposition of hydrogen peroxide by manganese dioxide. These results illustrate the effect of different carrier gas flow rates on the measured peak size. In each case enough hydrogen peroxide was added to evolve 50 mL of oxygen. An argon carrier gas was passed through the reaction vessel (100 mL flask) to purge the system at various flow rates. This gas was then sampled by the mass spectrometer providing the results shown below in Figure 6.3.2. In each case the expected oxygen volume of 50 mL, based on the volume of hydrogen peroxide added, was detected. Initial peak size increases with increasing flow rate as the cell volume is exchanged much more rapidly. This allows the cell atmosphere to be purged of oxygen in minutes. However, at high flow rates the percentage of oxygen in the total gas flow is lower resulting in a smaller signal and less well defined peaks as obtained at the slower flow rates.

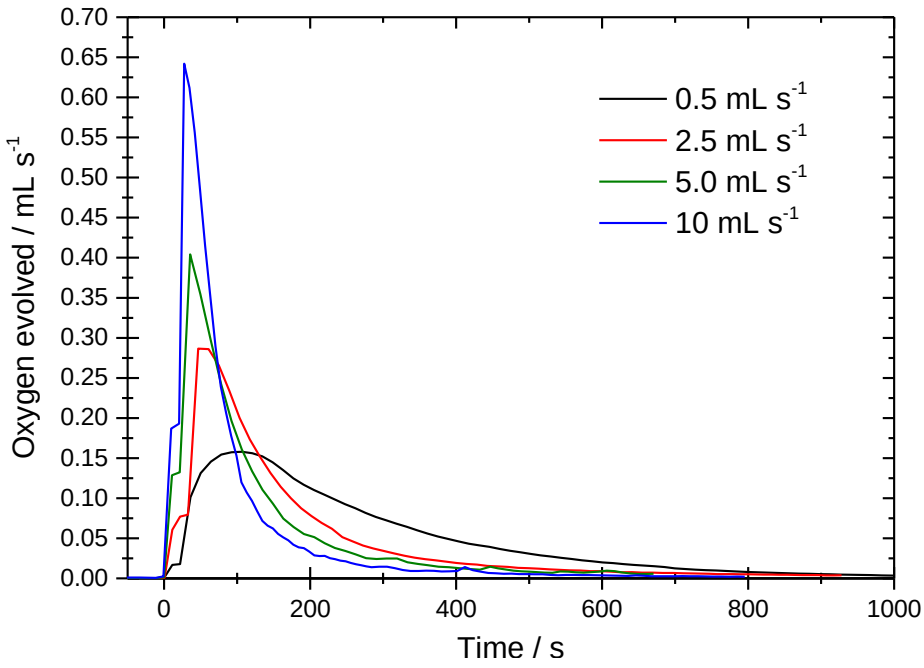

Figure 6.3.2 Oxygen evolution from the decomposition of hydrogen peroxide by manganese dioxide. In each case 50 mL of oxygen was evolved. An argon carrier gas was used to purge the system at different rates providing the different curves shown above.

In order to measure the oxygen reduction reaction in diglyme a carrier gas assembly was used as described in chapter 2. This way the same electrolyte used for the work in chapters 3, 4 and 5 could again be used. Due to the slower response time of a carrier gas system galvanostatic cycling instead of cyclic voltammetry was employed. This allowed for a significant rest period (30 minutes) between charge and discharge steps to fully purge the cell and re-establish a baseline for the oxygen flow. The second challenge was finding an appropriate flow rate for the carrier gas. Based on the experiments in Figure 6.3.2 in order to enhance the signal for any changes in oxygen flow, a low total flow rate of 1 mL min^{-1} was used. Two flow meters, each set to a flow rate of 0.5 mL min^{-1}, supplied argon and oxygen to the cell. It was necessary to include argon to serve as a reference point from which any changes in the oxygen partial pressure could be measured. The mass spectrometer was calibrated using a gas mixture of 2000 ppm oxygen and 2000 ppm CO_2 in argon (BOC). In addition to this, at the end of each measurement an additional 0.5 mL and 1 mL pulse of oxygen was passed through the system using the flow meters. This provided a peak of known oxygen volume within each measurement to serve as an additional means of calibration.

An applied current of approximately 400 µA was found to be required in order to produce a clear signal which equated to approximately 500 mA g^{-1} depending on the electrode. The results for a Swagelok cell containing an oxygen saturated 0.2M LiTFSI in diglyme electrolyte are shown in Figure 6.3.3. The mass spectrometer was set to record mass charge ratios of 32 (oxygen), 18 (water), 44 (carbon dioxide) and 28 (carbon monoxide).

The discharge begins at t = 0 and continues for 3.5 hours giving a total discharge capacity of ~ 1750 mAh g^{-1}. This is significantly larger than what was seen in Chapter 5 and may be

due to the introduction of water into the system. This is more likely than in a sealed cell as the electrolyte is now exposed to a continuous gas flow. Low water concentrations have been shown to increase the discharge capacity of lithium-oxygen cells by encouraging the formation of lithium peroxide clusters instead of a thin film.[32,92] At the onset of discharge, shown in the red trace, the oxygen flux decreases sharply before holding at -2 nmoles s^{-1}. These results confirm that the discharge reaction is consuming oxygen from the atmosphere. When the discharge reaction stops the cell is left to rest for 30 minutes. At this point the oxygen flux returns to its original level. At the onset of charge an increase in oxygen flux is observed holding at 2 nmoles s^{-1}. This indicates that oxygen is now being evolved by the charging reaction at the same rate as it was previously being consumed. Unfortunately due to the high charging rate only a small portion of the lithium peroxide is oxidised before reaching the voltage cut off.

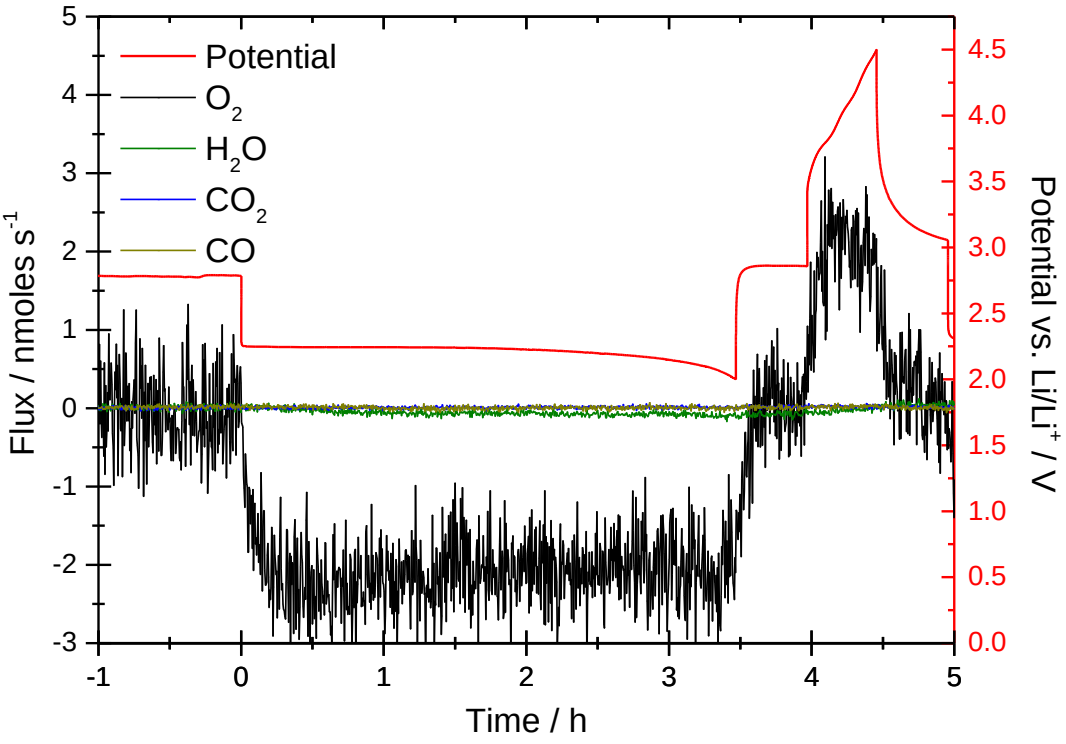

Figure 6.3.3 Galvanostatic cycle of a carbon electrode in an oxygen saturated 0.2 M LiTFSI diglyme electrolyte at 500 mA g^{-1}. The cell contents were monitored by DEMS using an argon/ oxygen 50:50 carrier gas flow at 1 mL min^{-1}.

No changes are observed in CO_2 or CO peaks however there is a slight decrease in the flux of water as the discharge progresses. This could suggest a reaction between lithium peroxide and water forming lithium hydroxide.

In order to determine the coulombic efficiency of these reactions the applied current was converted to an electron flux in nmoles of electrons per second. This electron flux was then divided by two to represent the two electron reduction of oxygen to lithium peroxide and the subsequent two electron oxidation to form oxygen. The change in oxygen flux matches the electron flux, as shown in Figure 6.3.4, demonstrating that for every two moles of electrons one mole of oxygen is consumed with the same result seen on charge. It should be mentioned that the oxygen signal has been smoothed to more easily see the comparison of the two lines. The high oxygen noise comes from the large background signal resulting from the 50 % oxygen gas mixture.

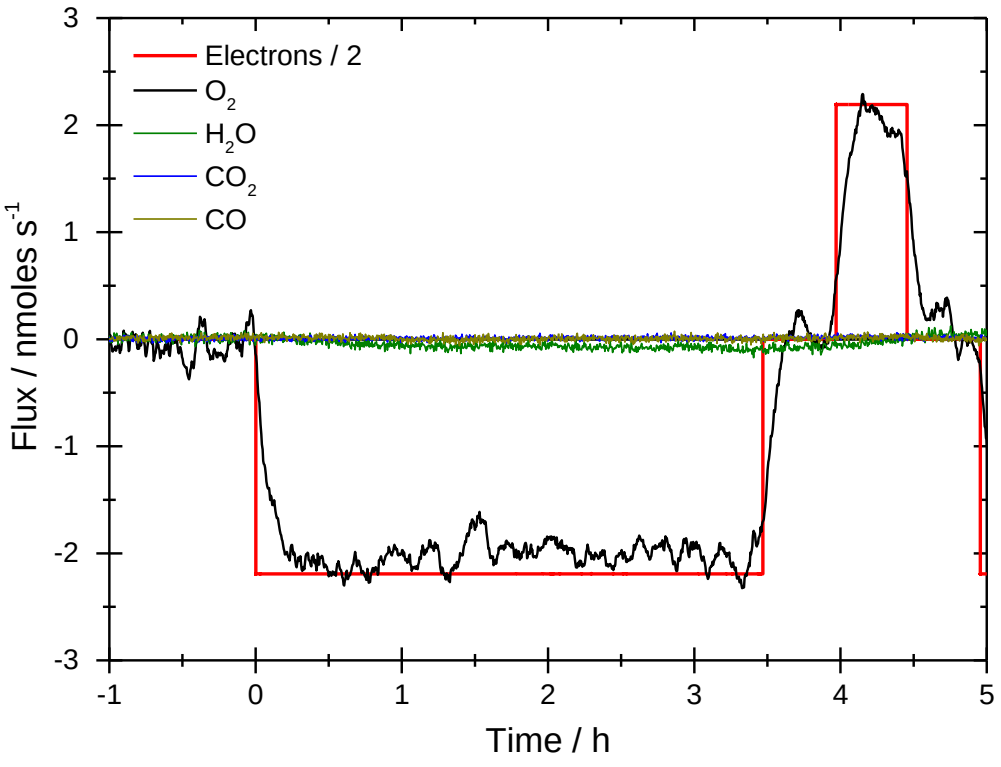

Figure 6.3.4 Galvanostatic cycle of a carbon electrode in an oxygen saturated 0.2 M LiTFSI diglyme electrolyte at 500 mA g^{-1}. The applied current has been converted to an electron flux and divided by two. The cell contents were monitored by DEMS using an argon/ oxygen 50:50 carrier gas flow at 1 mL min^{-1}.

In previous chapters it has been shown that quinones are able to increase the discharge capacity of lithium-oxygen cells. By discharging a cell containing 1 mM of a given quinone the quantity of oxygen consumed during the discharge can be determined. This will show if the additional capacity observed is due to the presence of any side reactions. The results obtained using 1 mM methyl-1,4-benzoquinone are shown below in Figure 6.3.5. As before the cell was rested while monitoring the oxygen flow to establish a baseline. At t = 0 the discharge was started resulting in the immediate consumption of oxygen. Comparing the total discharge capacity to the moles of oxygen consumed provides an average value of 2.14 electrons per mole of oxygen over the first 2 cycles. Between the charge and discharge steps the cell was rested for 0.5 hours to ensure the oxygen flux had returned to its original level, the charge step of the reaction has a poor capacity due to the high rate. The electrons required per mole of oxygen evolved are calculated from the flux to be 2.26.

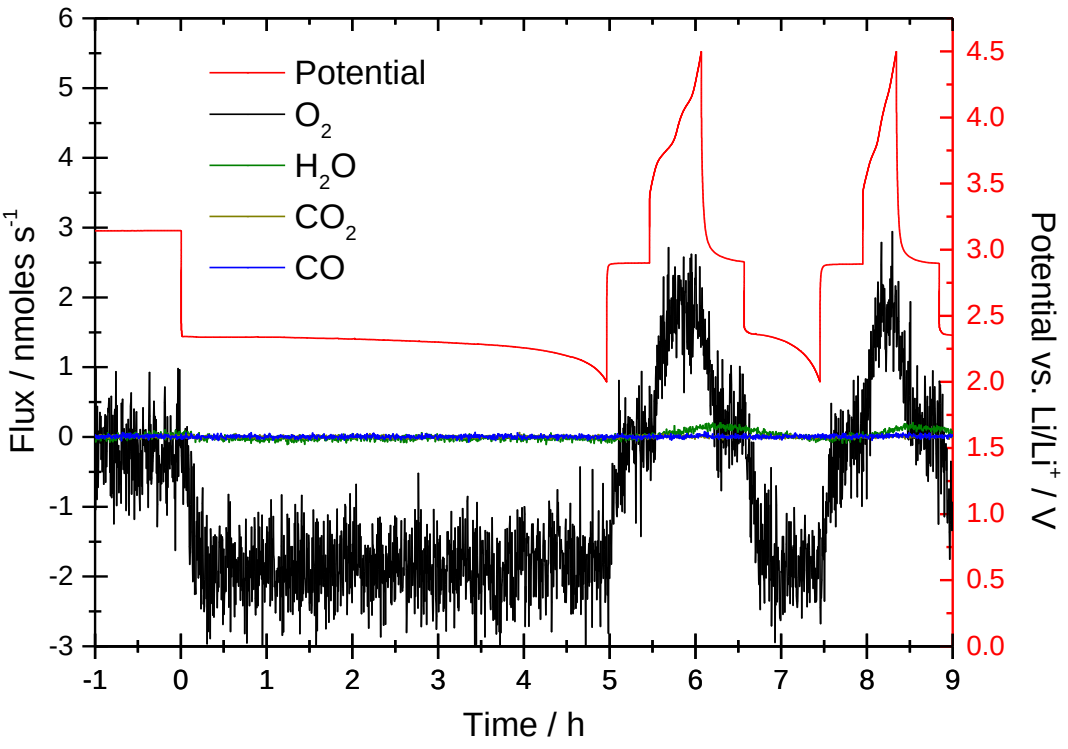

Figure 6.3.5 Galvanostatic cycles of a carbon electrode in an oxygen saturated 0.2 M LiTFSI diglyme electrolyte containing 1 mM methyl-1,4-benzoquinone at 500 mA g^{-1}. The cell contents were monitored by DEMS using an argon/ oxygen 50:50 carrier gas flow at 1 mL min^{-1}.

This experiment was repeated for 1 mM napthoquinone as this quinone has also shown promise at mediating the discharge reaction. In the DEMS cell however a noticeably lower capacity of 875 mAh g^{-1} was recorded using the napthoquinone when compared to the 2500 mAh g^{-1} recorded when using methyl-1,4-benzoquinone or even the 1750 mAh g^{-1} when using the plain electrolyte. As seen with the previous measurements there is no noticeable change in the carbon dioxide or carbon monoxide signals throughout the charge or discharge processes while the oxygen flux changes by ~ 2 nmoles s^{-1}. Again the charge is short and does not reach a plateau due to the high currents applied to generate sufficient signal. The electrons required per mole of oxygen consumed and evolved were calculated to be 2.02 and 2.15 respectively.

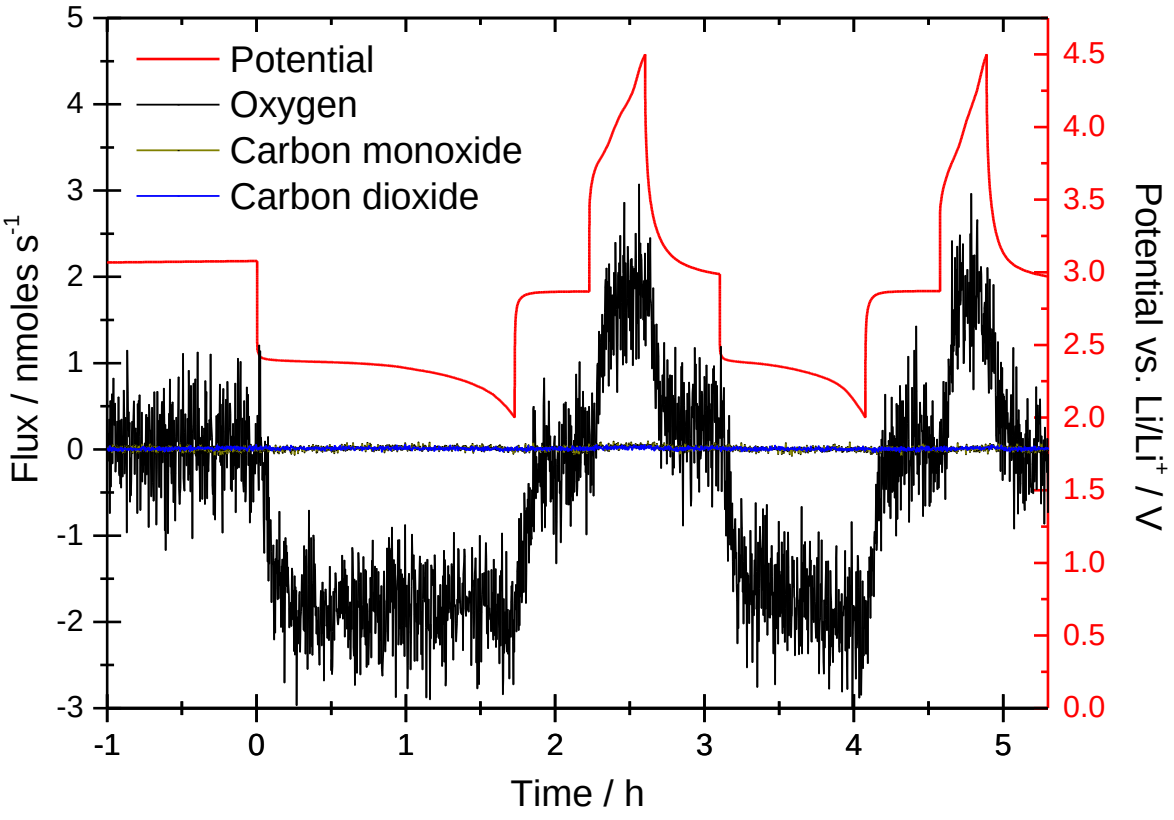

Figure 6.3.6 Galvanostatic cycles of a carbon electrode in an oxygen saturated 0.2 M LiTFSI diglyme electrolyte containing 1 mM naptho-1,4-benzoquinone at 500 mA g^{-1}. The cell contents were monitored by DEMS using an argon/ oxygen 50:50 carrier gas flow at 1 mL min^{-1}.

The charge reaction, evolving oxygen from lithium peroxide, has also been examined using halogenated quinones. This technique can show if the improved charging plateau is due to the evolution of oxygen or if it is instead due to a side reaction. The most effective mediators for the charge reaction determined in Chapters 4 and 5 were tetrabromo-1,4-benzoquinone and tetrachloro-1,4-benzoquinone. The results of adding 1 mM of the brominated quinone are shown in Figure 6.3.7. The results are almost identical to what is observed in the absence of the quinone. Despite the addition of the brominated quinone the charge reaction is largely incomplete due to the high currents. No CO_2, CO or H_2O evolution is observed during the charge or discharge steps. This is in conflict with previously reported measurements and is likely due to the incomplete charging step.[37,38,67]

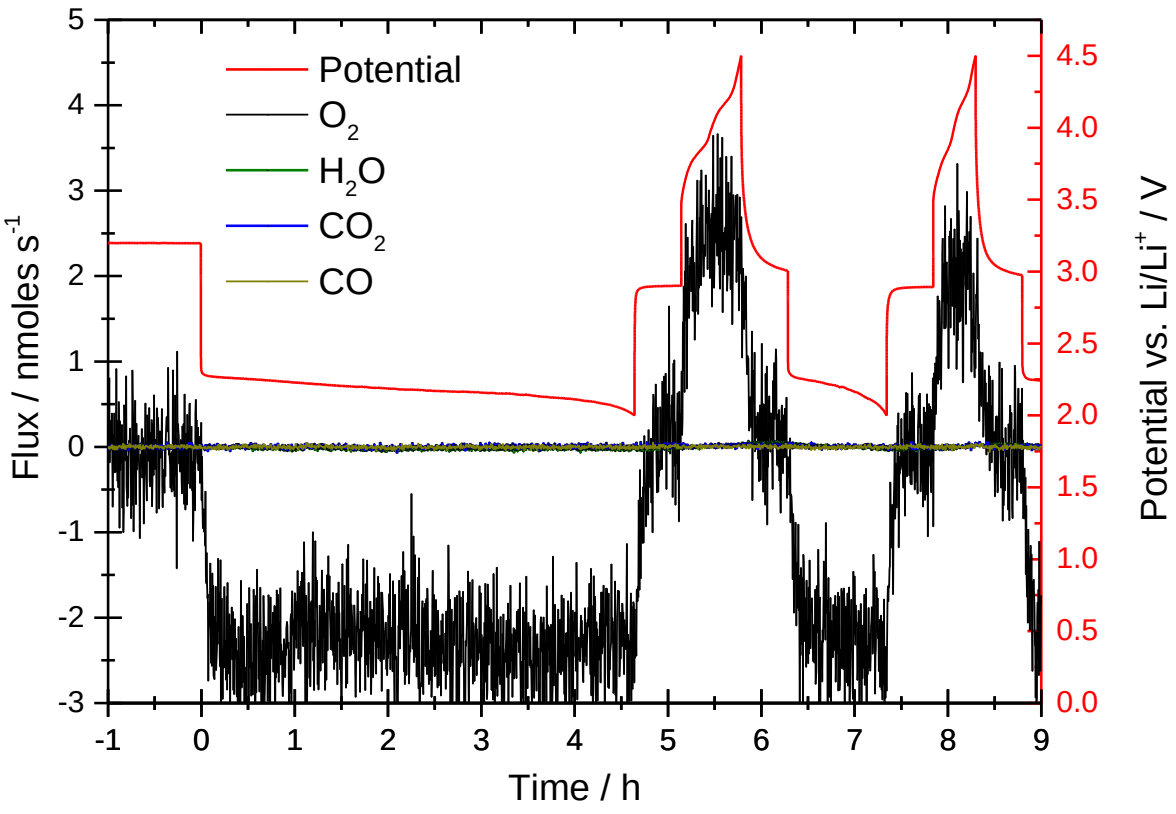

Figure 6.3.7 Galvanostatic cycles of a carbon electrode in an oxygen saturated 0.2 M LiTFSI diglyme electrolyte containing 1 mM tetrabromo-1,4-benzoquinone at 500 mA g^{-1}. The cell contents were monitored by DEMS using an argon/ oxygen 50:50 carrier gas flow at 1 mL min^{-1}.

In an attempt to provide a better measurement for the charge reaction this experiment was repeated using a larger carbon electrode with a greater carbon loading. This would allow for a lower rate to be applied while evolving the same moles per second of products. In addition to this the concentration of quinone was increased from 1 mM to 10 mM. The results are shown in Figure 6.3.8. The charge step now has an identical capacity to the discharge step indicating the peroxide is fully oxidised from the surface. The change in oxygen flux during the discharge reaction remains unaffected by the increased quinone concentration. However, during the charge step the usual 2 electron per mole of oxygen relationship was not observed. Instead a dip in evolved oxygen can be seen once the potential reaches 3.5 V vs. Li/Li^+. This dip continues until 3.8 V vs. Li/Li^+ where the onset of carbon dioxide evolution was observed, similar to what is observed in other electrolyte systems.[37,38,67] The dip in oxygen evolution is most likely due to the formation of lithium carbonate at the electrode surface which is subsequently oxidised at the electrode at higher potentials leading to the evolution of carbon dioxide. The size of the CO_2 peak indicates that at high positive potentials all of the current is going towards CO_2 evolution and there is no oxygen evolution. On the second cycle the total CO_2 evolved is larger than the first indicating a trend favouring the lithium carbonate formation and subsequent decomposition. Water was evolved at approximately 3.6 V vs. Li/Li^+ and continues to be purged by the system after the charge step has finished. A possible explanation for this could be the combustion of the electrolyte resulting in the evolution of both water and CO_2. Water accumulating in the electrolyte could also affect the quinone electrochemistry. A plot including the half current for comparison is included as Figure 6.3.9. This illustrates how the dominant reaction product changes from oxygen to CO_2 as the charge moves to higher potentials. In this figure the data has been smoothed for clarity.

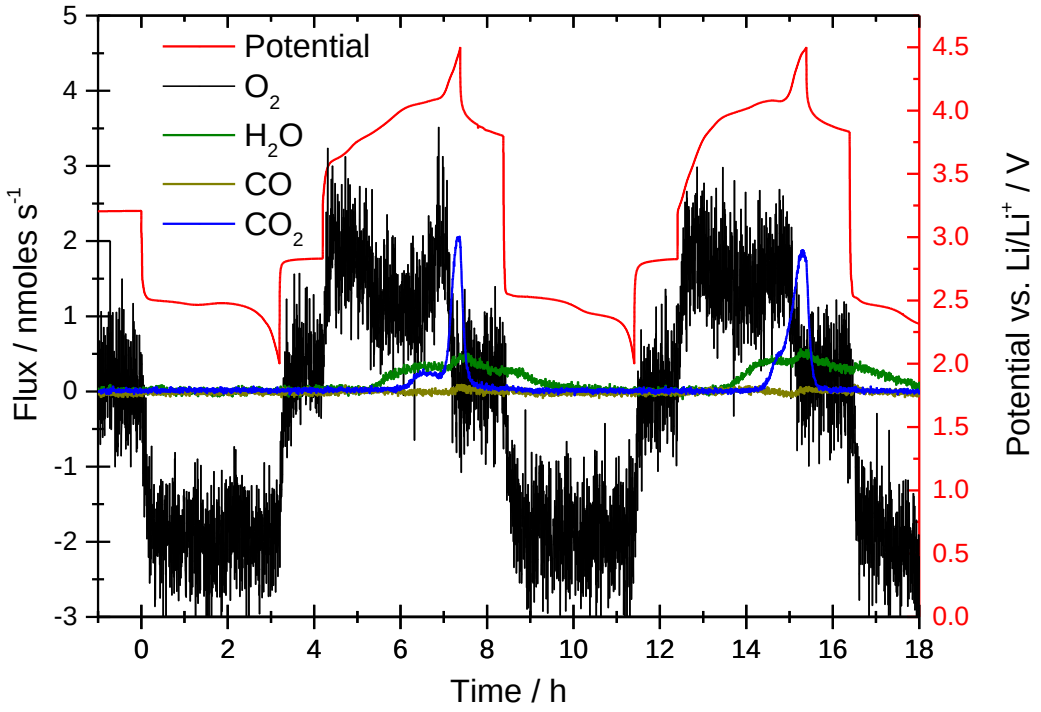

Figure 6.3.8 Galvanostatic cycles of a carbon electrode in an oxygen saturated 0.2 M LiTFSI diglyme electrolyte containing 10 mM tetrabromo-1,4-benzoquinone at 500 mA g^{-1}. The cell contents were monitored by DEMS using an argon/ oxygen 50:50 carrier gas flow at 1 mL min^{-1}.

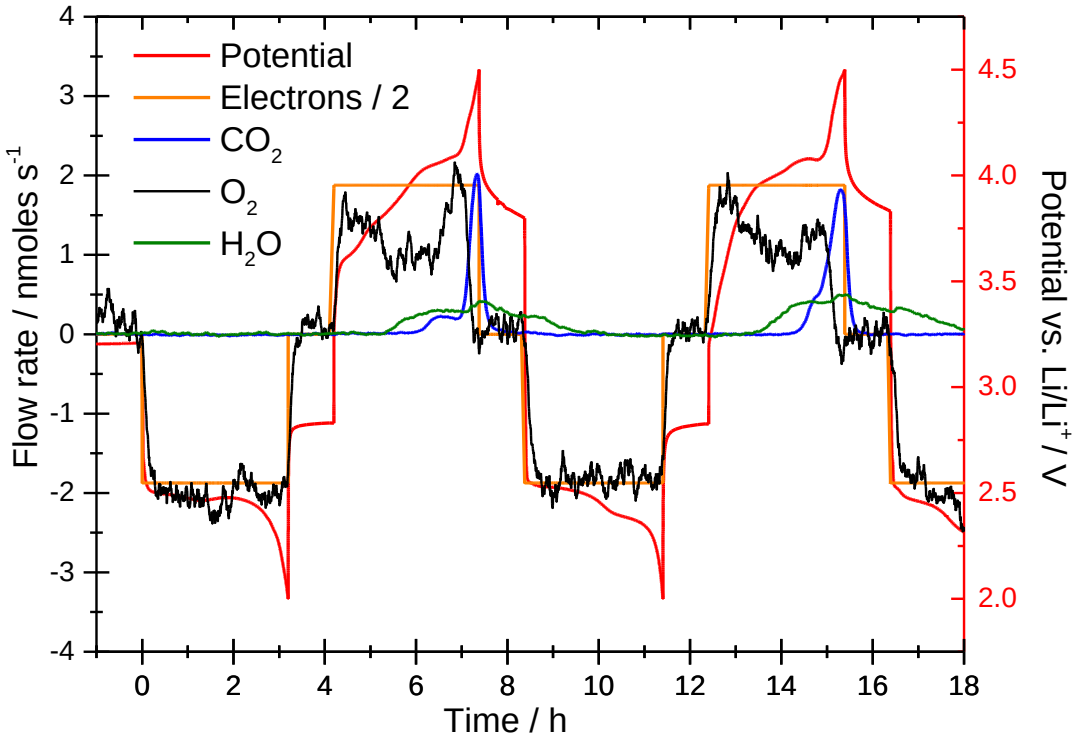

Figure 6.3.9 Galvanostatic cycles of a carbon electrode in an oxygen saturated 0.2 M LiTFSI diglyme electrolyte containing 10 mM tetrabromo-1,4-benzoquinone at 500 mA g^{-1}. The applied current has been converted to an electron flux and divided by two. The cell contents were monitored by DEMS using an argon/ oxygen 50:50 carrier gas flow at 1 mL min^{-1}.

6.4 Conclusions and Further Work

The use of differential electrochemical mass spectrometry has demonstrated that in this system the discharge reaction is dominantly the two electron reduction of oxygen to form lithium peroxide. The incorporation of quinones into the electrolyte has been shown to enhance the discharge capacity while the overall product of the discharge reaction does not change. Looking at the charge reaction, no decomposition of the quinone mediators is observed. Initially the charge step is dominantly the two electron decomposition of lithium peroxide to yield oxygen. However, it has been shown that if the charge step is able to go to completion the formation of lithium carbonate takes over at 3.5 V vs. Li/Li^+ which eventually gives rise to the evolution of carbon dioxide at 3.8 V vs. Li/Li^+ as the major reaction product.

Based on this result it would be interesting to hold the potential just below 3.5 V vs. Li/Li^+ to see if the formation of lithium carbonate could be prevented. This could avoid the decomposition of the carbon electrode and the formation of water, while allowing the charge step to go to completion albeit at a slower rate. In order to monitor the charging reaction at lower rates, larger more carbon dense electrodes could be produced allowing for a similar absolute current to be applied but at a much lower current per given carbon mass. Alternatively the flow rate could be decreased. Changing the concentration of the tetrabromo-1,4-benzoquinone in the electrolyte had a significant effect on the charging performance of the cell. Continuing to vary the concentration may enable the charging reaction to be improved further allowing the cell to be cycled at lower overpotentials. Combining both the charge and discharge quinones together in one cell could yield a far greater discharge capacity and enhanced reversibility.

Chapter 7: Summary

The electrochemical behaviour of oxygen in a non-aqueous lithium salt containing electrolyte has been examined by cyclic voltammetry. The formal potential of oxygen reduction and evolution was determined to be 2.97 V vs. Li/Li^+ with each reaction requiring an overpotential of 750 mV. The electrochemistry of a wide range of substituted quinones was then studied as these compounds possess many of the desirable characteristics of redox mediators. The first electron transfer was demonstrated to be fast and reversible in the presence of a lithium salt for some of the quinone compounds while the second electron transfer is consistently less reversible than the first. Of the compounds tested quinones with formal potentials between 2.33 and 2.75 V vs. Li/Li^+ were shown to enhance the rate of the oxygen reduction reaction at significantly lower overpotentials. Using cyclic voltammetry a peak current enhancement of 67% with an overpotential of 350 mV was achieved when using a 1 mM concentration of methyl-1,4-benzoquinone.

Galvanostatic measurements were performed demonstrating that the discharge product was predominately lithium peroxide both with and without the quinones present in the electrolyte. When charging the cell this lithium peroxide was also shown to be removed. When discharging a lithium-oxygen cell both methyl-1,4-benzoquinone and 1,4-napthoquinone were shown to provide an improved discharge capacity a higher potentials. This extra capacity was also shown to far exceed that of simply reducing the quinone indicating that there is a mediation effect enabling the formation of lithium peroxide clusters at the electrode surface. Improvements in the charging potential were also demonstrated though these were less significant. This could be due to relatively low quinone concentration of 1 mM.

Differential electrochemical mass spectroscopy (DEMS) was also used to identify the reactions taking place at different potentials. In the absence of quinones the reduction reaction was found to require two electrons per mole of oxygen consumed. This combined with the X-ray diffraction results is good evidence that lithium peroxide is the dominant product formed. When using quinones to enhance the discharge reaction the same result was observed. The use of 10 mM tetrabromo-1,4-benzoquinone made it possible to observe the charging step a high rates. Below 3.5 V vs. Li/Li^+ oxygen evolution was the dominant reaction. However, above 3.5 V vs. Li/Li^+ the rate of oxygen evolution decreases with no new volatile product evolved. At 3.8 V vs. Li/Li^+ carbon dioxide is evolved from the cell and at 4.0 V vs. Li/Li^+ accounting for most all the current passing through the cell. This suggests that lithium carbonate is formed at the electrode between 3.5 and 3.8 V vs. Li/Li^+ by reactions with the electrolyte or the carbon electrode itself.

Studying electrodes at different stages during the charging process could help to confirm this lithium carbonate formation. The use of X-ray diffraction and Raman spectroscopy would allow both crystalline and amorphous products to be detected at the electrode surface. Holding the charging voltage at 3.5 V vs. Li/Li^+ may allow the dominant reaction to remain as oxygen evolution, albeit at a much lower rate of charge. This could be overcome by combining both the discharge and charge quinones in a single cell. While limiting the discharge capacity of a lithium-oxygen cell would ensure portions of the electrode surface remain clear of lithium peroxide to enable the charge mediators to function. The use of mediators continues to receive significant attention from the battery research community and it is likely they will play an important role if there is to be a successful lithium-oxygen battery in the future.

Chapter 8: References

1 McGraw-Hill, *Handbook of Batteries*, McGraw-Hill Companies, Inc., 3rd edn., **2002**.

2 M. S. Whittingham, *Chem. Rev.*, **2004**, 104, 4271–4301.

3 M. S. Whittingham and F. Gamble, *Mater. Res. Bull.*, **1975**, 10, 363–371.

4 E. Peled, *J. Power Sources*, **1983**, 9, 253–266.

5 E. Peled, D. Golodnitsky, G. Ardel and V. Eshkenazy, *Electrochim. Acta*, **1995**, 40, 2197–2204.

6 D. Aurbach, E. Zinigrad, Y. Cohen and H. Teller, *Solid State Ionics*, **2002**, 148, 405–416.

7 J. R. Owen, *Chem. Soc. Rev.*, **1997**, 26, 259–267.

8 *Y. Nishi , H. Azuma, A. Omaru, Non aqueous electrolyte cell, US4959281*, **1989**.

9 M. Mizushima, P. Jones, P. Wiseman and J. B. Goodenough, *Mater. Res. Bull.*, **1980**, 15, 783–789.

10 K. Ozawa, *Solid State Ionics*, **1994**, 69, 212–221.

11 M. Holzapfel, H. Buqa, W. Scheifele, P. Novak and F.-M. Petrat, *Chem. Commun.*, **2005**, 0, 1566.

12 S. H. Ng, J. Wang, D. Wexler, K. Konstantinov, Z. P. Guo and H. K. Liu, *Angew. Chemie - Int. Ed.*, **2006**, 45, 6896–6899.

13 V. Etacheri, R. Marom, R. Elazari, G. Salitra and D. Aurbach, *Int. J. Electrochem. Sci.*, **2011**, 4, 3243–3262.

14 P. G. Bruce and S. A. Freunberger, *Nature*, **2011**, 11, 19–30.

15 Y. Li and H. Dai, *Chem. Soc. Rev.*, **2014**, 43, 5257–5275.

16 J. Goldstein and B. Koretz, *Proc. Intersoc. Energy Convers. Eng. Conf.*, **1993**, 28, 279.

17 H. Yadegari, Q. Sun and X. Sun, *Adv. Mater.*, **2016**, 28, 7065–7093.

18 C. L. Bender, D. Schröder, R. Pinedo, P. Adelhelm and J. Janek, *Angew. Chemie - Int. Ed.*, **2016**, 55, 4640–4649.

19 B. L. Ellis and L. F. Nazar, *Curr. Opin. Solid State Mater. Sci.*, **2012**, 16, 168–177.

20 E. Peled, D. Golodnitsky, H. Mazor, M. Goor and S. Avshalomov, *J. Power Sources*, **2011**, 196, 6835–6840.

21 X. Ji, K. T. Lee and L. F. Nazar, *Nat. Mater.*, **2009**, 8, 500–506.

22 G. Girishkumar, B. D. McCloskey, a. C. Luntz, S. Swanson and W. Wilcke, *J. Phys. Chem. Lett.*, **2010**, 1, 2193–2203.

23 Y. X. Yin, S. Xin, Y. G. Guo and L. J. Wan, *Angew. Chemie - Int. Ed.*, **2013**, 52, 13186–13200.

24 J. Hassoun and B. Scrosati, *Adv. Mater.*, **2010**, 22, 5198–5201.

25 J. Hassoun, H.-G. Jung, D.-J. Lee, J.-B. Park, K. Amine, Y.-K. Sun and B. Scrosati, *Nano Lett.*, **2012**, 12, 5775–5779.

26 J. Christensen, P. Albertus, R. S. Sanchez-Carrera, T. Lohmann, B. Kozinsky, R. Liedtke, J. Ahmed and A. Kojic, *J. Electrochem. Soc.*, **2012**, 159, R1–R30.

27 S. S. Zhang, D. Foster and J. Read, *J. Power Sources*, **2010**, 195, 1235–1240.

28 C. O. Laoire, S. Mukerjee, K. M. Abraham, E. J. Plichta and M. a Hendrickson, *J. Phys.*

Chem. C, **2009**, 113, 20127–20134.

29 C. O. Laoire, S. Mukerjee, K. M. Abraham, E. J. Plichta and M. a Hendrickson, *J. Phys. Chem. C*, **2010**, 114, 9178–9186.

30 Z. Peng, S. A. Freunberger, L. J. Hardwick, Y. Chen, V. Giordani, F. Barde, P. Novak, D. Graham, J.-M. M. Tarascon and P. G. Bruce, *Angew. Chemie - Int. Ed.*, **2011**, 50, 6351–6355.

31 B. D. McCloskey, R. Scheffler, A. Speidel, G. Girishkumar and A. Luntz, *J. Phys. Chem. C*, **2012**, 116, 23897–23905.

32 S. Meini, M. Piana, N. Tsiouvaras, A. Garsuch and H. A. Gasteiger, *Electrochem. Solid-State Lett.*, **2012**, 15, A45–A48.

33 O. Li, N. B. Aetukuri, B. D. Mccloskey, J. M. García, L. E. Krupp, V. Viswanathan and A. C. Luntz, *Nat. Chem.*, **2015**, 7, 50–56.

34 S. A. Freunberger, Y. Chen, Z. Peng, J. M. Griffin, L. J. Hardwick, F. Bardé, P. Novák and P. G. Bruce, *J. Am. Chem. Soc.*, **2011**, 133, 8040–8047.

35 B. Gallant and R. Mitchell, *J. Phys. Chem.*, **2012**, 116, 20800–20805.

36 K. U. Schwenke, M. Metzger, T. Restle, M. Piana and H. A. Gasteiger, *ECS*, **2015**, 162, 573–584.

37 M. M. Ottakam Thotiyl, S. A. Freunberger, Z. Peng and P. G. Bruce, *J. Am. Chem. Soc.*, **2012**, 135, 494–500.

38 B. D. McCloskey, A. Speidel, R. Scheffler, D. C. Miller, V. V Viswanathan, J. S. Hummelshøj, J. K. Nørskov and A. C. Luntz, *J. Phys. Chem. Lett.*, **2012**, 3, 997–1001.

39 W. Xu, J. Hu, M. H. Engelhard, S. a Towne, J. S. Hardy, J. Xiao, J. Feng, M. Y. Hu, J. Zhang, F. Ding, M. E. Gross and J.-G. Zhang, *J. Power Sources*, **2012**, 215, 240–247.

40 M. Amarilla, M. Olivares-mar and D. Tonti, *J. Mater. Chem. A*, **2013**, 1, 14270–14279.

41 M. Olivares-mar, P. Palomino, E. Enciso and D. Tonti, *J. Phys. Chem. C*, **2014**, 118, 20772–20783.

42 F. Soavi and M. Mastragostino, *J. Phys. Chem. Lett.*, **2013**, 4, 1379–1382.

43 M. M. Ottakam Thotiyl, S. A. Freunberger, Z. Peng, Y. Chen, Z. Liu and P. G. Bruce, *Nat. Mater.*, **2013**, 12, 1–7.

44 T. Momma, H. Nara, S. Yamagami, C. Tatsumi and T. Osaka, *J. Power Sources*, **2011**, 196, 6483–6487.

45 D. Aurbach, *J. Electrochem. Soc.*, **1989**, 136, 3198–3205.

46 T. Osaka, *J. Electrochem. Soc.*, **1997**, 144, 1709–1713.

47 C. J. Allen and S. Mukerjee, *J. Phys. Chem. Lett.*, **2011**, 2, 2420–2424.

48 Y. Shao, S. Park, J. Xiao, J.-G. Zhang, Y. Wang and J. Liu, *ACS Catal.*, **2012**, 2, 844–857.

49 C. O. Laoire, S. Mukerjee and K. M. Abraham, *J. Phys. Chem.*, **2010**, 114, 9178–9186.

50 X. Gao, Y. Chen, L. Johnson and P. G. Bruce, *Nat. Mater.*, **2016**, 15, 882–888.

51 Z. Peng, S. A. Freunberger, Y. Chen and P. G. Bruce, *Science*, **2012**, 337, 563–566.

52 Y. Chen, S. A. Freunberger and Z. Peng, *Nature*, **2013**, 5–7.

53 M. Roberts, R. Younesi, W. Richardson, J. Liu, T. Gustafsson, J. Zhu and K. Edström, *ECS Electrochem. Lett.*, **2014**, 3, A62–A65.

54 R. Younesi, M. Hahlin, M. Roberts and K. Edström, *J. Power Sources*, **2012**, 225, 40–45.

55 L. Grande, E. Paillard, G.-T. Kim, S. Monaco and S. Passerini, *Int. J. Mol. Sci.*, **2014**, 15, 8122–8137.

56 H. Nakamoto, Y. Suzuki, T. Shiotsuki, F. Mizuno, S. Higashi, K. Takechi, T. Asaoka, H. Nishikoori and H. Iba, *J. Power Sources*, **2013**, 243, 19–23.

57 S. Higashi, Y. Kato, K. Takechi, H. Nakamoto, F. Mizuno, H. Nishikoori, H. Iba and T. Asaoka, *J. Power Sources*, **2013**, 240, 14–17.

58 A. W. Lodge, M. J. Lacey, M. Fitt, N. Garcia-Araez and J. R. Owen, *Electrochim. Acta*, **2014**, 140, 168–173.

59 S. Monaco, A. M. Arangio, F. Soavi, M. Mastragostino, E. Paillard and S. Passerini, *Electrochim. Acta*, **2012**, 83, 94–104.

60 F. Soavi, S. Monaco and M. Mastragostino, *J. Power Sources*, **2013**, 224, 115–119.

61 C. J. Allen, J. Hwang, R. Kautz, S. Mukerjee, E. J. Plichta, M. a Hendrickson and K. M. Abraham, *J. Phys. Chem. C*, **2012**, 116, 20755–20764.

62 R. G. Evans, O. V. Klymenko, S. a. Saddoughi, C. Hardacre and R. G. Compton, *J. Phys. Chem. B*, **2004**, 108, 7878–7886.

63 T. Kuboki, T. Okuyama, T. Ohsaki and N. Takami, *J. Power Sources*, **2005**, 146, 766–769.

64 J. T. Frith, A. E. Russell, N. Garcia-Araez and J. R. Owen, *Electrochem. commun.*, **2014**, 46, 33–35.

65 S. A. Freunberger, Y. Chen, N. E. Drewett, L. J. Hardwick, F. Bardé and P. G. Bruce, *Angew. Chem. Int. Ed. Engl.*, **2011**, 50, 8609–8613.

66 Y.-C. Lu, D. G. Kwabi, K. P. C. Yao, J. R. Harding, J. Zhou, L. Zuin and Y. Shao-Horn, *Energy Environ. Sci.*, **2011**, 4, 2999–3007.

67 B. D. McCloskey, D. S. Bethune, R. M. Shelby, G. Girishkumar and A. C. Luntz, **2011**, 1161–1166.

68 S. Meini, M. Piana, H. Beyer, J. Schwammlein and H. A. Gasteiger, *J. Electrochem. Soc.*, **2012**, 159, A2135–A2142.

69 N. Tsiouvaras, S. Meini, I. Buchberger and H. A. Gasteiger, *J. Electrochem. Soc.*, **2013**, 160, A471–A477.

70 C. O. Laoire, S. Mukerjee, E. J. Plichta, M. A. Hendrickson and K. M. Abraham, *J. Electrochem. Soc.*, **2011**, 158, A302–A308.

71 C. O. Laoire, S. Mukerjee, K. M. Abraham, E. J. Plichta and M. A. Hendrickson, *J. Phys. Chem. C*, **2010**, 114, 9178–9186.

72 F. Barrière, Y. Ferry, D. Rochefort and D. Leech, *Electrochem. commun.*, **2004**, 6, 237–241.

73 B. W. Carlson and L. L. Miller, *J. Am. Chem. Soc.*, **1985**, 107, 479–485.

74 K. Ben Aribia, T. Moehl and S. M. Zakeeruddin, *Chem. Sci.*, **2013**, 4, 454–459.

75 T. J. Ohara, R. Rajagopalan and A. Heller, *Anal. Chem.*, **1993**, 65, 5970–5975.

76 A. Pinczewska and M. Sosna, *J. Am. Chem. Soc.*, **2012**, 134, 18022–18033.

77 G. Tojo and M. Fernández, *Oxidation of Primary Alcohols to Carboxylic Acids*,

Springer, 1st edn., **2006**.

78 L. Zhang, Z. Zhang and K. Amine, *Lithium Ion Batteries*, InTech, 1st edn., **2012**.

79 W. K. Behl and D. Chin, *J. Electrochem. Soc.*, **1988**, 135, 16–21.

80 A. Odom, S, S. Ergun, P. P. Poudel and S. R. Parkin, *Energy Environ. Sci.*, **2014**, 7, 760–767.

81 *G. Chase, S. Zecevi, W. Walker, J. Uddin, K. Sasaki, V. Giordani, V. Bryantsev, M. Blanco, D. Addison, Soluble Oxyg. Evol. Catal. Recharg. Met. Batter. WO 2011/133982 A1*, **2011**.

82 M. J. Lacey, J. T. Frith and J. R. Owen, *Electrochem. commun.*, **2013**, 26, 74–76.

83 L. Yang, J. T. Frith and J. R. Owen, *Chem. Commun.*, **2015**, 51, 1705–1708.

84 J. Read, *J. Electrochem. Soc.*, **2002**, 149, A1190–A1195.

85 T. Ogasawara, A. Débart, M. Holzapfel, P. Novák and P. G. Bruce, *J. Am. Chem. Soc.*, **2006**, 128, 1390–1393.

86 B. J. Bergner, A. Schurmann, K. Peppler, A. Garsuch and J. Janek, *JACS*, **2014**, 136, 15054–15064.

87 D. Sun, Y. Shen, W. Zhang, L. Yu, Z. Yi, W. Yin, D. Wang, Y. Huang, J. Wang, D. Wang and J. B. Goodenough, *J. Am. Chem. Soc.*, **2014**, 136, 8941–8946.

88 A. Y. Tesio, D. Blasi, I. Ratera, D. Tonti and J. Veciana, *Chem. Commun.*, **2015**, 51, 17623–17626.

89 I. Landa-medrano, M. Olivares-marín, R. Pinedo, I. R. De Larramendi, T. Rojo and D. Tonti, *Electrochem. commun.*, **2015**, 59, 24–27.

90 C. M. Burke, R. Black, I. R. Kochetkov, V. Giordani, D. Addison, L. F. Nazar and B. D. McCloskey, *ACS Energy Lett.*, **2016**, 1, 747–756.

91 I. Landa-Medrano, M. Olivares-Marín, B. J. Bergner, R. Pinedo, A. Sorrentino, E. Pereiro, I. Ruiz de Larramendi, J. Janek, T. Rojo and D. Tonti, *J. Phys. Chem. C*, **2017**, 121, 3822–3829.

92 Y. Zhao, L. Wang and H. R. Byon, *Nat. Commun.*, **2013**, 4, 1–7.

93 T. Liu, M. Leskes, W. Yu, A. J. Moore, L. Zhou, P. M. Bayley, G. Kim and C. P. Grey, *Science*, **2015**, 350, 530–533.

94 Y. G. Zhu, Q. Liu, Y. Rong, H. Chen, J. Yang, C. Jia, L.-J. Yu, A. Karton, Y. Ren, X. Xu, S. Adams and Q. Wang, *Nat. Commun.*, **2017**, 8, 1–7.

95 Y. Shen, W. Zhang, S. Chou and S. Dou, *Science*, **2016**, 352, 3–5.

96 T. Liu, G. Kim, J. Carretero-González, E. Castillo-Martínez and C. P. Grey, *Science*, **2016**, 352, 667–668.

97 Z. Liang and Y. C. Lu, *J. Am. Chem. Soc.*, **2016**, 138, 7574–7583.

98 D. Kundu, R. Black, B. Adams and L. F. Nazar, *ACS Cent. Sci.*, **2015**, 1, 510–515.

99 K. P. C. Yao, J. T. Frith, S. Y. Sayed, F. Barde, J. R. Owen, Y. Shao-Horn and N. Garcia-Araez, *J. Phys. Chem. C*, **2016**, 120, 16290–16297.

100 M. W. Lehmann and D. H. Evans, *J. Electroanal. Chem.*, **2001**, 500, 12–20.

101 M. Namazian and P. Norouzi, *J. Electroanal. Chem.*, **2004**, 573, 49–53.

102 X. Guo, H. Zipse and H. Mayr, *J. Am. Chem. Soc.*, **2014**, 136, 13863–13873.

103 K. Sasaki, T. Kashimura and M. Ohura, *J. Electrochem. Soc.*, **1990**, 137, 2437–2443.

104 P. S. Guin, S. Das and P. C. Mandal, *Int. J. Electrochem.*, **2011**, 2011, 1–22.

105 F. Mirkhalaf, K. Tammeveski and D. J. Schiffrin, *Phys. Chem. Chem. Phys.*, **2004**, 6, 1321–1327.

106 S. Matsuda, K. Hashimoto and S. Nakanishi, *J. Phys. Chem. C*, **2014**, 118, 18397–18400.

107 R. Younesi, S. Urbonaite, F. Björefors and K. Edström, *J. Power Sources*, **2011**, 196, 9835–9838.

108 C. Tran, X. Q. Yang and D. Qu, *J. Power Sources*, **2010**, 195, 2057–2063.

109 X. H. Yang, P. He and Y. Y. Xia, *Electrochem. commun.*, **2009**, 11, 1127–1130.

110 M. Mirzaeian and P. J. Hall, *Electrochim. Acta*, **2009**, 54, 7444–7451.

111 W. Xu, V. V Viswanathan, D. Wang, S. a. Towne, J. Xiao, Z. Nie, D. Hu and J.-G. Zhang, *J. Power Sources*, **2011**, 196, 3894–3899.

112 W. Xu, K. Xu, V. V Viswanathan, S. a Towne, J. S. Hardy, J. Xiao, Z. Nie, D. Hu, D. Wang and J.-G. Zhang, *J. Power Sources*, **2011**, 196, 9631–9639.

113 G. M. Veith, N. J. Dudney, J. Howe and J. Nanda, *J. Phys. Chem. C*, **2011**, 115, 14325–14333.

114 F. Mizuno, S. Nakanishi, Y. Kotani, S. Yokoishi and H. Iba, *Electrochemistry*, **2010**, 5, 403–405.

115 H. Baltruschat, *J. Am. Soc. Mass Spectrom.*, **2004**, 15, 1693–706.

116 C. Hammond, *The Basics of Crystallography*, Oxford Science Publications, 3rd edn., **2009**.

117 V. V Viswanathan, K. S. Thygesen, J. S. Hummelshøj, J. K. Nørskov, G. Girishkumar, B. D. McCloskey and a C. Luntz, *J. Chem. Phys.*, **2011**, 135, 214704–214710.

118 J. Read, K. Mutolo, M. Ervin, W. Behl, J. Wolfenstine and A. Driedger, *ECS*, **2003**, 150, 1351–1356.

119 J. Read, *ECS*, **2006**, 153, 96–100.

120 M. Leskes, N. E. Drewett, L. J. Hardwick, P. G. Bruce, G. R. Goward and C. P. Grey, *Angew. Chem. Int. Ed. Engl.*, **2012**, 51, 8560–8563.

121 L. J. Hardwick and P. G. Bruce, *Curr. Opin. Solid State Mater. Sci.*, **2012**, 16, 178–185.

122 W. A. Henderson, *J. Phys. Chem.*, **2006**, 110, 13177–13183.

123 F. Mohazabrad, F. Wang and X. Li, *ECS*, **2016**, 163, 2623–2627.

124 N. Garcia-Araez and P. Novák, *J. Solid State Electrochem.*, **2013**, 17, 1793–1807.

125 B. Huskinson, M. P. Marshak, C. Suh, S. Er, M. R. Gerhardt, C. J. Galvin, X. Chen, A. Aspuru-Guzik, R. G. Gordon and M. J. Aziz, *Nature*, **2014**, 505, 195–198.

126 Y. Hanyu, Y. Ganbe and I. Honma, *J. Power Sources*, **2013**, 221, 186–190.

127 D. Sharon, V. Etacheri, A. Garsuch, M. Afri, A. a Frimer and D. Aurbach, *J. Phys. Chem. Lett.*, **2013**, 4, 127–131.

128 K. M. Abraham and Z. Jiang, *J. Electrochem. Soc.*, **1996**, 143, 1–5.

129 B. D. McCloskey, D. S. Bethune, R. M. Shelby, T. Mori, R. Scheffler, A. Speidel, M.

Sherwood and A. C. Luntz, *J. Phys. Chem. Lett.*, **2012**, 3, 3043–3047.

Chapter 9: Appendices

9.1 Appendix A

This section provides additional information for Chapter 3: Cyclic Voltammetry of Oxygen Reduction and Evolution.

A value of 2300 Ω was obtained for the internal resistance of the cell using impedance spectroscopy. The Nyquist and Bode impedance plots are shown below in Figure 9.1.1.

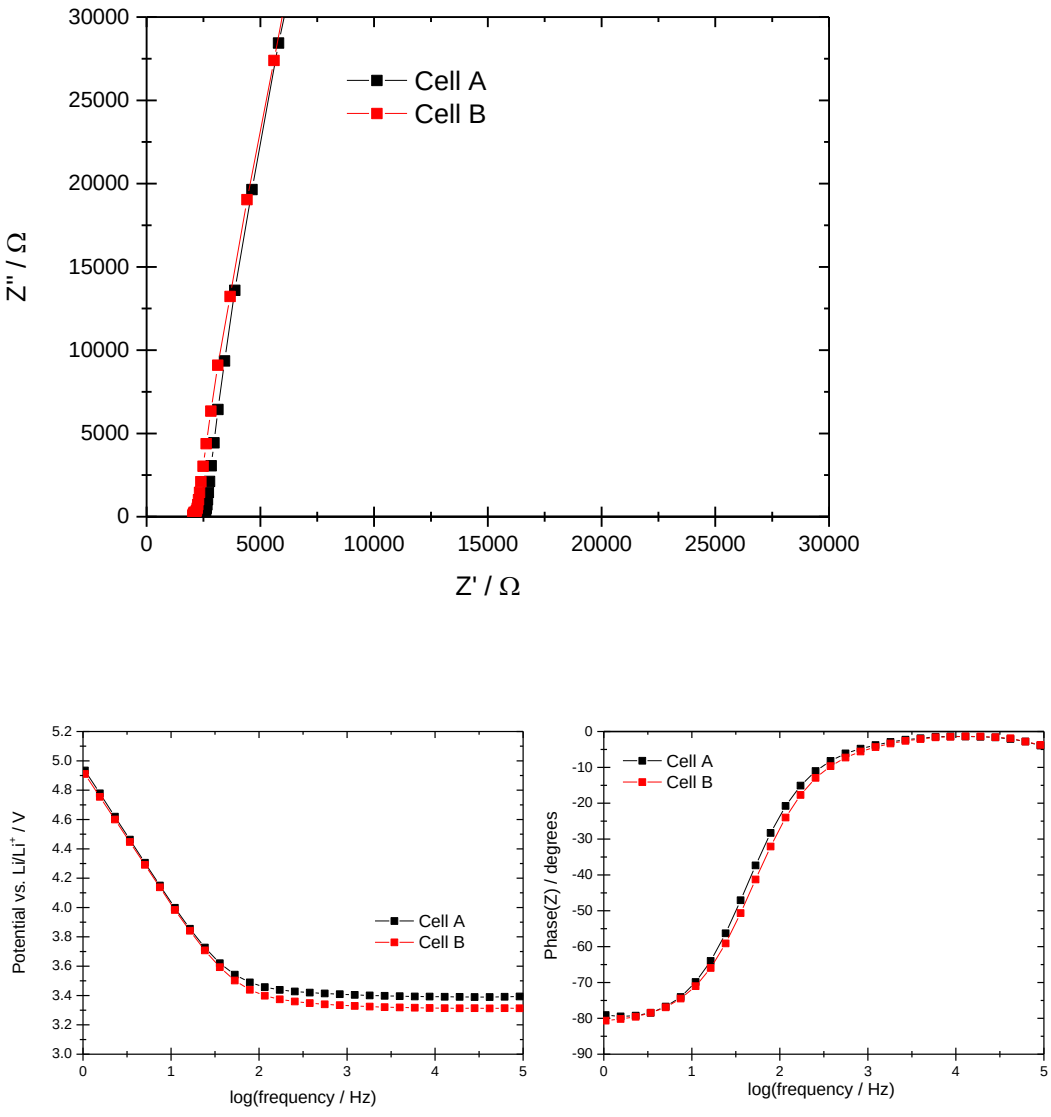

Figure 9.1.1 AC Impedance plots from a glassy carbon electrode (Ø = 3 mm) in argon saturated 0.2 M LiTFSI in diglyme electrolyte. A lithium metal electrode was used as both the counter and reference using the U-Cell geometry described in Chapter 2.

The conductivity of 0.2 M LiTFSI in tetraglyme is reported to be 1.5 mS cm^{-1}.[1] A solution resistance can therefore be calculated by using the following equation.

$$R_u = \frac{1}{4\sigma a}$$

Equation 9.1.1

Where:

a = Disk electrode radius (0.15 cm)

R_u = Uncompensated solution resistance

σ = Conductivity

From these equations a resistance of 1100 Ω is calculated for the electrolyte which is significantly lower than the 2300 Ω determined experimentally. However, this 1100 Ω value does not take into account the porous glass frit which greatly reduces the area available to the electrolyte thereby lowering its conductivity and increasing the overall resistance.

9.2 Appendix B

This section provides additional information for Chapter 4: Cyclic Voltammetry of Substituted Quinones.

Calculating the diffusion coefficient using a graph of the peak current vs. the scan rate.

This method is based upon the use of the Randles Sevcik equation as shown below.

$$j_p = 2.69 \cdot 10^5 \cdot n^{3/2} D^{1/2} c v^{1/2}$$

Equation 9.2.1

Where:

j_p = Current density (A cm^{-2})

n = Number of moles of electrons transferred (1)

c = Concentration of species (1 x 10^{-6} mol cm^{-3})

v = Scan rate (V s^{-1})

D = Diffusion coefficient (cm^2 s^{-1})

Plotting a graph of j_p on the y-axis and $v^{1/2}$ on the x-axis yields a gradient (m) equal to the following.

$$m = 2.69 \cdot 10^5 \cdot n^{3/2} D^{1/2} c$$

Equation 9.2.2

Rearranging this equation and substituting in the gradient yields a diffusion coefficient in units of cm^2 s^{-1}.

$$D = \left(\frac{m}{2.69 \cdot 10^5 \cdot n^{3/2} c} \right)^2$$

Equation 9.2.3

Plots to determine the diffusion coefficient, formal potential and peak separation of various quinones are shown below. As the quinone electrochemistry is not completely reversible and subject to IR drop these values are likely to contain some error.

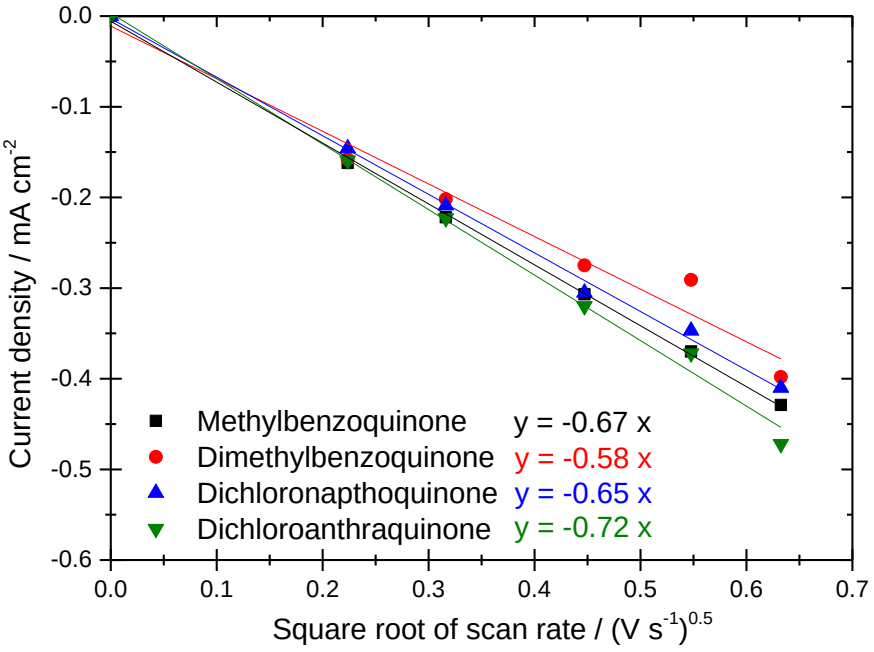

Figure 9.2.1 Determination of the diffusion coefficients of several substituted quinones.

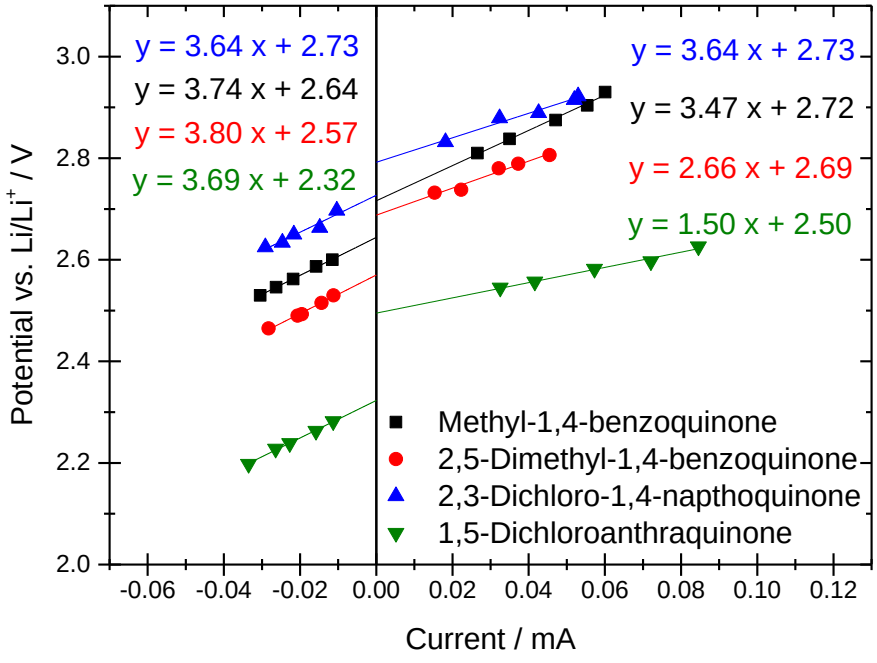

Figure 9.2.2 Peak potential vs. peak current plot to determine the formal potential and the peak separation of several functionalised quinones.

Cyclic voltammograms of each of these quinones were recorded in oxygen at different scan rates. For reference these plots, including the corresponding quinone structures are included below.

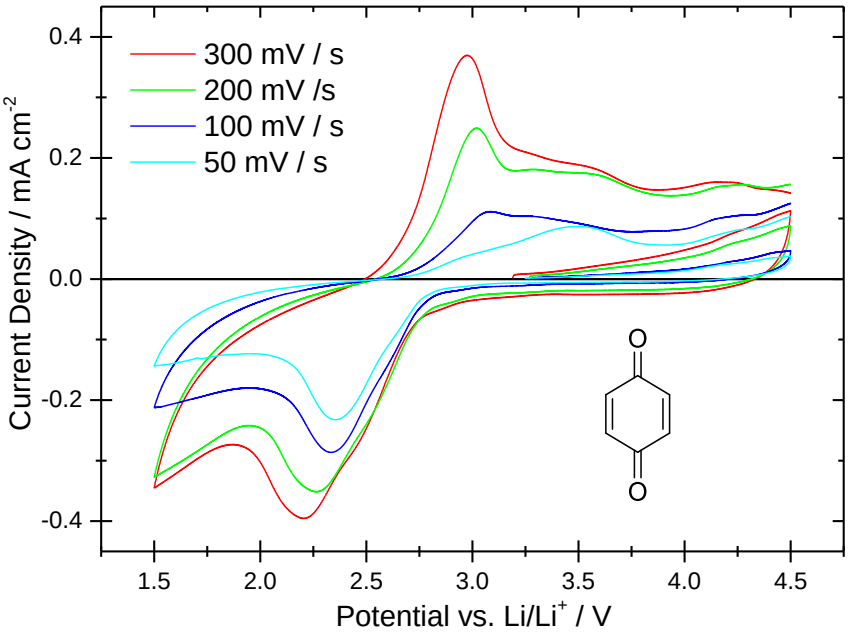

Figure 9.2.3 Cyclic voltammograms of a glassy carbon electrode (Ø = 3 mm) in an oxygen saturated 0.2 M LiTFSI in diglyme electrolyte. The electrolyte also contained 1 mM of 1,4-benzoquinone (structure shown). Scans were conducted at various sweep rates vs. a lithium metal counter/reference electrode.

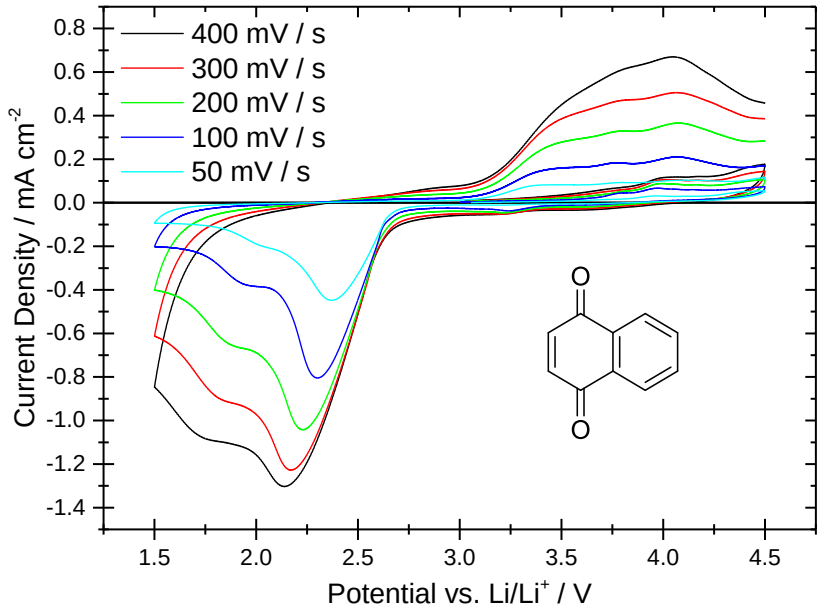

Figure 9.2.4 Cyclic voltammograms of a glassy carbon electrode (Ø = 3 mm) in an oxygen saturated 0.2 M LiTFSI in diglyme electrolyte. The electrolyte also contained 1 mM of 1,4-napthoquinone (structure shown). Scans were conducted at various sweep rates vs. a lithium metal counter/reference electrode.

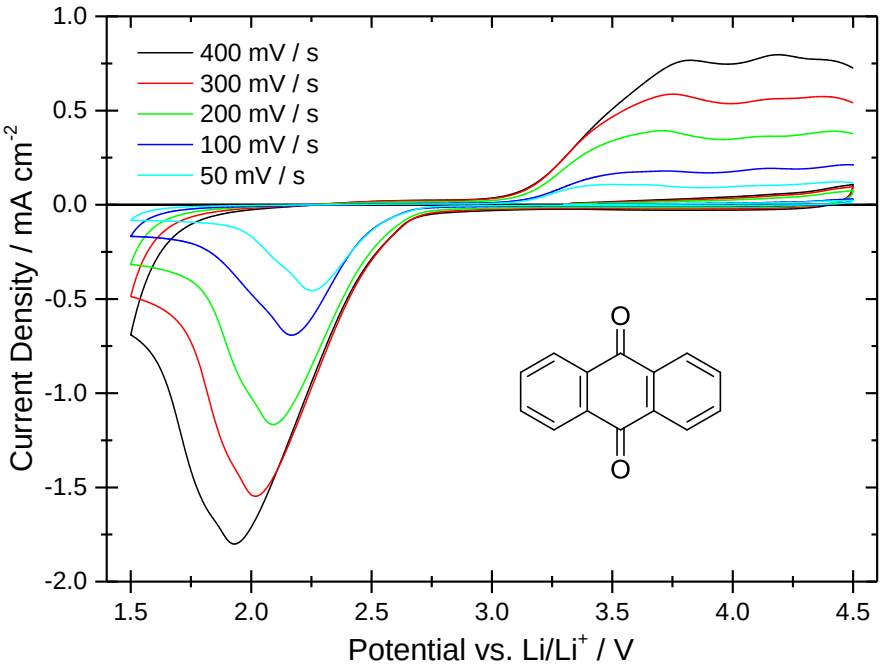

Figure 9.2.5 Cyclic voltammograms of a glassy carbon electrode (Ø = 3 mm) in an oxygen saturated 0.2 M LiTFSI in diglyme electrolyte. The electrolyte also contained 1 mM of anthraquinone (structure shown). Scans were conducted at various sweep rates vs. a lithium metal counter/reference electrode.

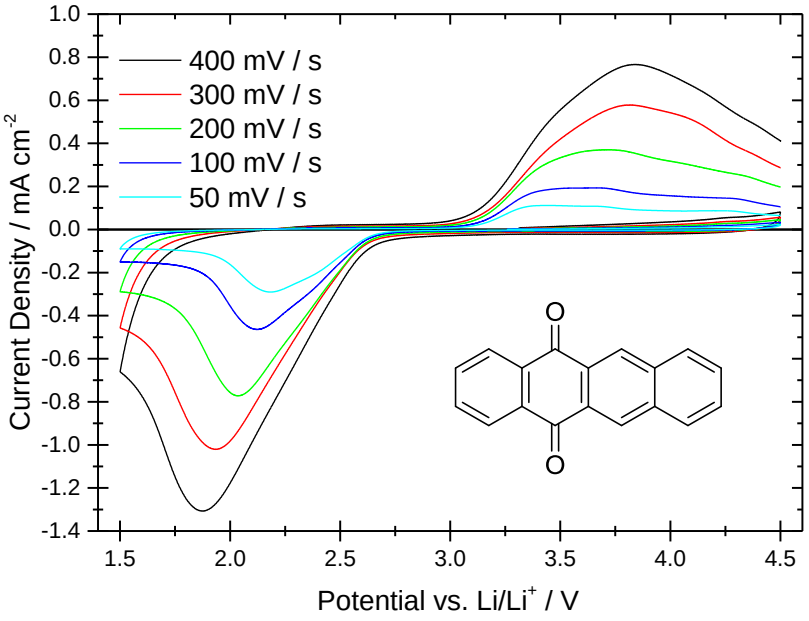

Figure 9.2.6 Cyclic voltammograms of a glassy carbon electrode (Ø = 3 mm) in an oxygen saturated 0.2 M LiTFSI in diglyme electrolyte. The electrolyte also contained 1 mM of 5,12-napthacenequinone (structure shown). Scans were conducted at various sweep rates vs. a lithium metal counter/reference electrode.

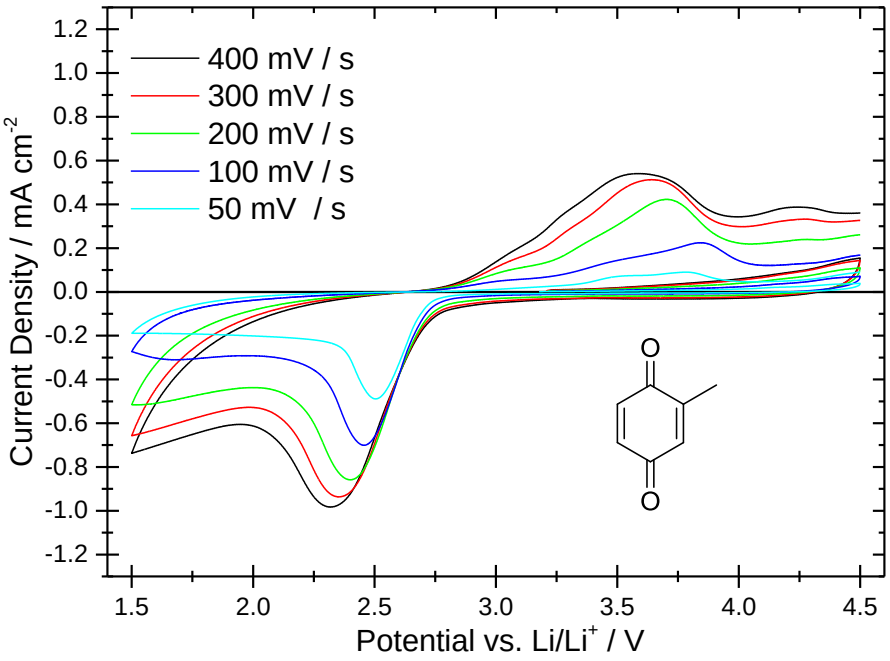

Figure 9.2.7 Cyclic voltammograms of a glassy carbon electrode (Ø = 3 mm) in an oxygen saturated 0.2 M LiTFSI in diglyme electrolyte. The electrolyte also contained 1 mM of methyl-1,4-benzoquinone (structure shown). Scans were conducted at various sweep rates vs. a lithium metal counter/reference electrode.

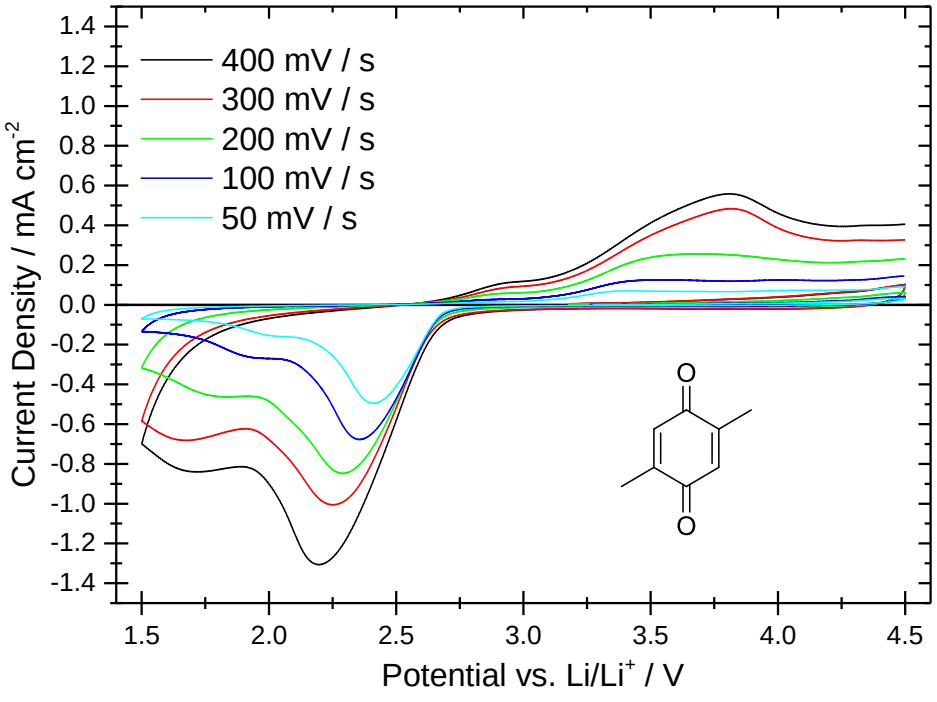

Figure 9.2.8 Cyclic voltammograms of a glassy carbon electrode (Ø = 3 mm) in an oxygen saturated 0.2 M LiTFSI in diglyme electrolyte. The electrolyte also contained 1 mM of 2,5-dimethyl-1,4-benzoquinone (structure shown). Scans were conducted at various sweep rates vs. a lithium metal counter/reference electrode.

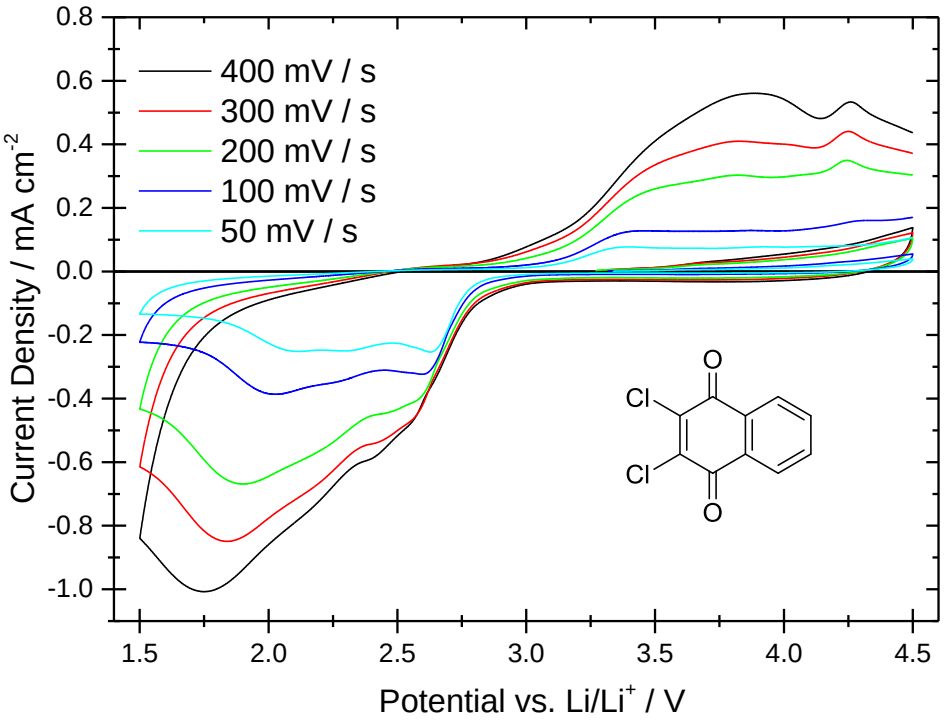

Figure 9.2.9 Cyclic voltammograms of a glassy carbon electrode (Ø = 3 mm) in an oxygen saturated 0.2 M LiTFSI in diglyme electrolyte. The electrolyte also contained 1 mM of 2,3-dichloro-1,4-napthoquinone (structure shown). Scans were conducted at various sweep rates vs. a lithium metal counter/reference electrode.

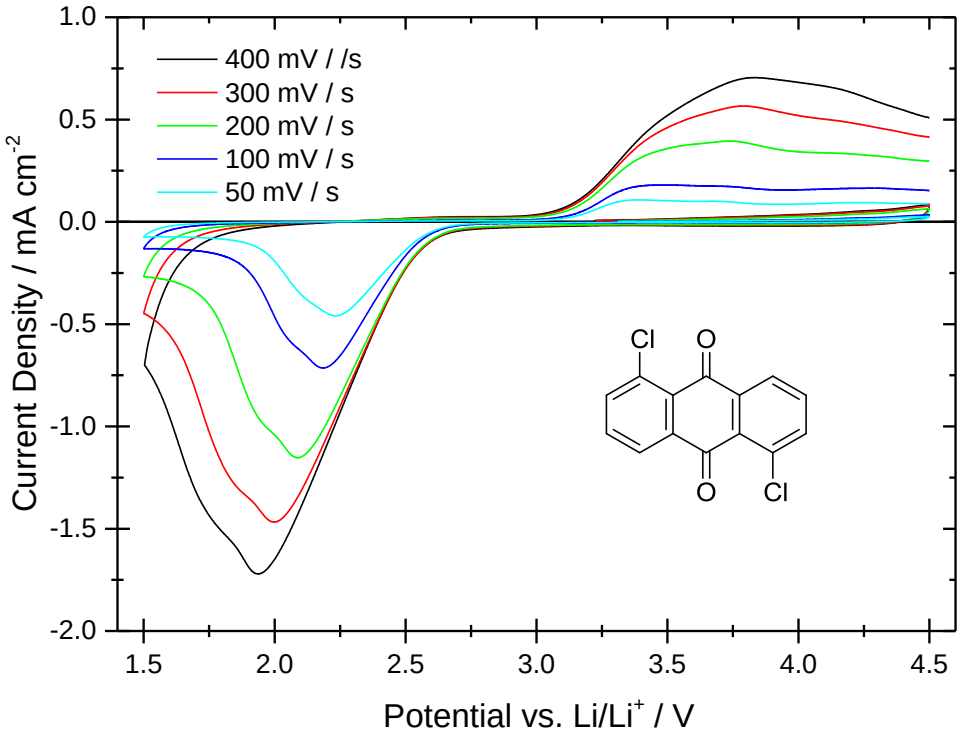

Figure 9.2.10 Cyclic voltammograms of a glassy carbon electrode (Ø = 3 mm) in an oxygen saturated 0.2 M LiTFSI in diglyme electrolyte. The electrolyte also contained 1 mM of 1,5-dichloroanthraquinone (structure shown). Scans were conducted at various sweep rates vs. a lithium metal counter/reference electrode .

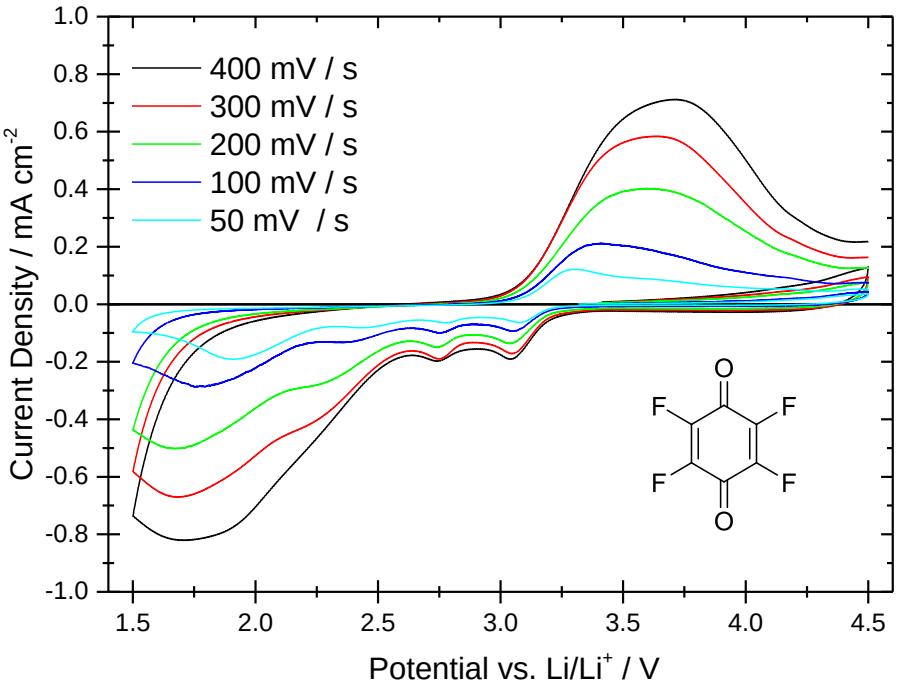

Figure 9.2.11 Cyclic voltammograms of a glassy carbon electrode (Ø = 3 mm) in an oxygen saturated 0.2 M LiTFSI in diglyme electrolyte. The electrolyte also contained 1 mM of tetrafluoro-1,4-benzoquinone (structure shown). Scans were conducted at various sweep rates vs. a lithium metal counter/reference electrode.

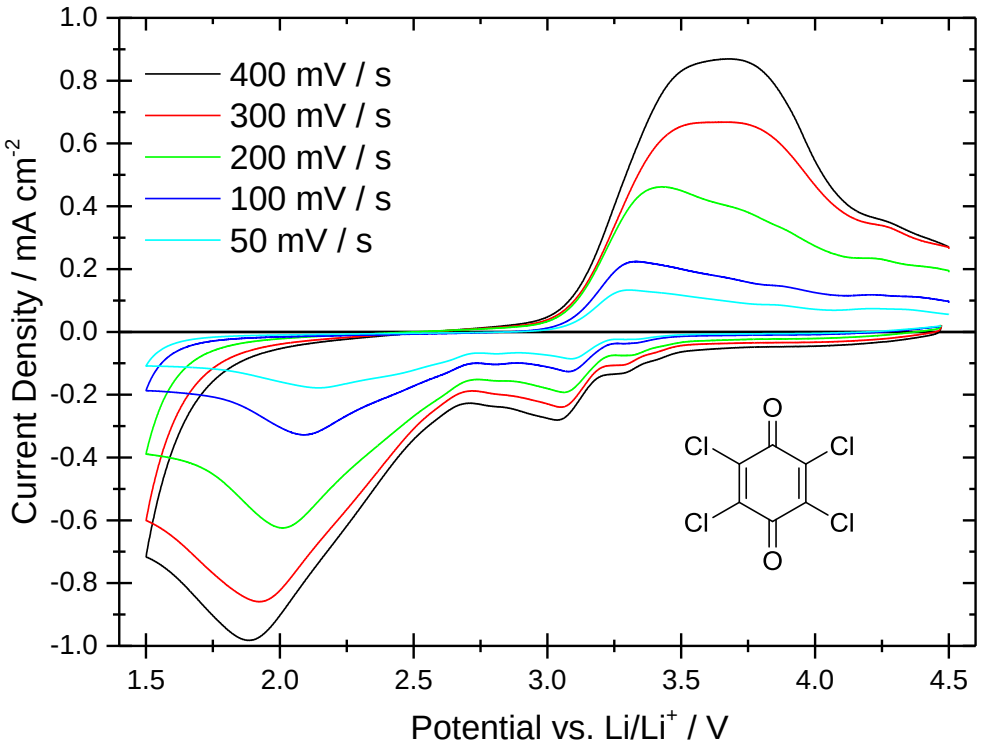

Figure 9.2.12 Cyclic voltammograms of a glassy carbon electrode (Ø = 3 mm) in an oxygen saturated 0.2 M LiTFSI in diglyme electrolyte. The electrolyte also contained 1 mM of tetrachloro-1,4-benzoquinone (structure shown). Scans were conducted at various sweep rates vs. a lithium metal counter/reference electrode.

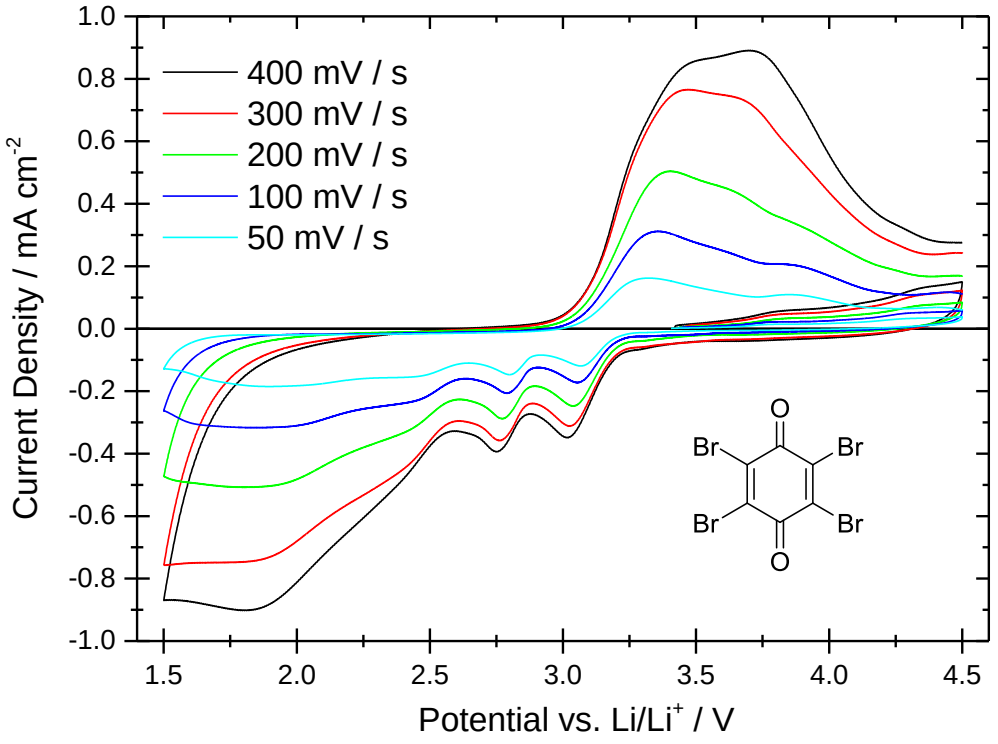

Figure 9.2.13 Cyclic voltammograms of a glassy carbon electrode (Ø = 3 mm) in an oxygen saturated 0.2 M LiTFSI in diglyme electrolyte. The electrolyte also contained 1 mM of tetrabromo-1,4-benzoquinone (structure shown). Scans were conducted at various sweep rates vs. a lithium metal counter/reference electrode.

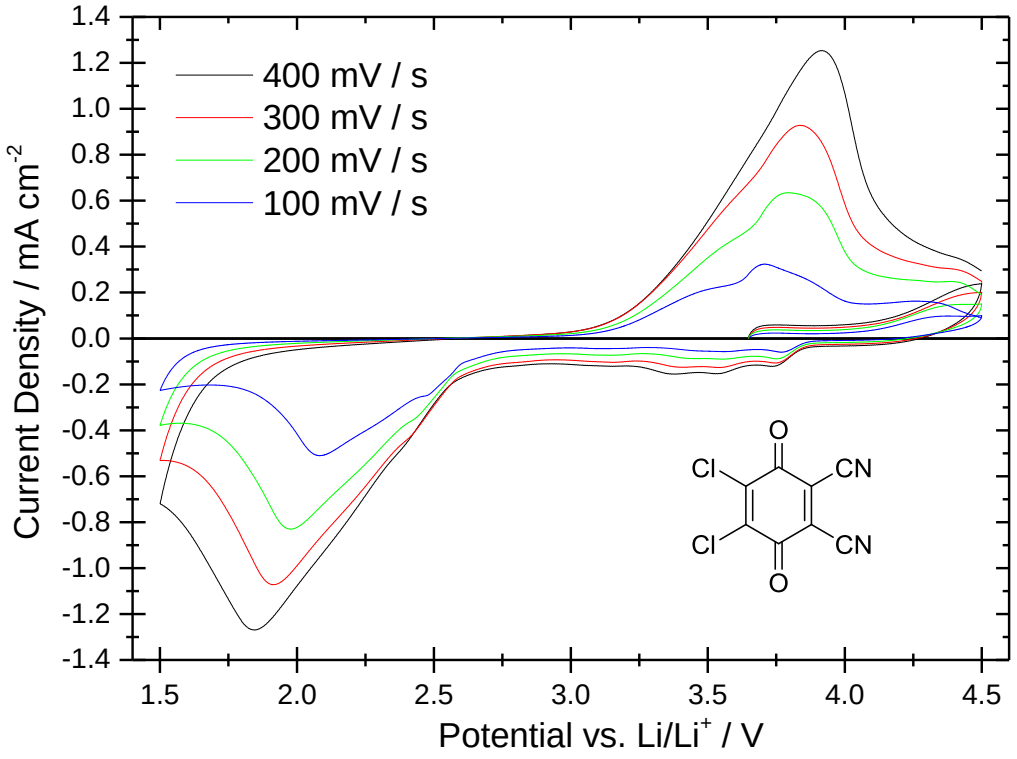

Figure 9.2.14 Cyclic voltammograms of a glassy carbon electrode (Ø = 3 mm) in an oxygen saturated 0.2 M LiTFSI in diglyme electrolyte. The electrolyte also contained 1 mM of 2,3-dichloro-5,6-dicyano-1,4-benzoquinone (structure shown). Scans were conducted at various sweep rates vs. a lithium metal counter/reference electrode.